

Copyright is owned by the Author of the thesis. Permission is given for a copy to be downloaded by an individual for the purpose of research and private study only. The thesis may not be reproduced elsewhere without the permission of the Author.

# **DYNAMIC RESPONSE OF ROTATIONALLY PERIODIC STRUCTURES**

**RANA NOMAN MUBARAK**

Thesis Submitted in fulfillment of the degree of Doctor of Philosophy

in

Engineering

**MASSEY UNIVERSITY**

**SCHOOL OF ENGINEERING AND TECHNOLOGY**

February 2014

## ABSTRACT

Due to their structural dynamics, rotationally periodic structures (RPS) have always been an area of interest for engineers and scientists. RPS is found in almost all industries and could be as large as jet turbines to as small as hard disk drives. We come across with RPS on daily routine like washing machine tub, small gears in home appliances and brakes in automobile etc. With such an influence in our life, an RPS dynamic response to the environment is crucial to keep them working and hence is the focus of the thesis. The research involves three major responses on rotationally periodic structures (RPS) namely vibration, thermal and shock. Hard disk drives and integrally bladed rotors (IBR) has been selected as research models.

On vibratory response in rotationally periodic structures, effects on structural designs and free vibrations of integrated bladed rotor (IBR) have been investigated in this research. The migration of natural frequencies is characterized through parametric studies considering changes in blade angle and blade thickness of an underlying uniform axis-symmetric rotor. Recurring coupled repeated doublet modes, defined as replica modes, have been observed in this study by characterizing blade vibrations in-phase or out-of-phase to disk vibrations. Veering and clustering of replica modes' natural frequencies are observed with respect to the blade design parameters. Existence of replica modes has been verified via experimental studies. Fourier content for the low frequency replica component is found to be sensitive and tuneable to blade angle design.

For the thermal response of RPS, structural thermal analysis of spindle disk assembly used in hard disk drives (HDDs) was adopted. With the view toward understanding the underlying physics and to minimize the corresponding repeatable run-out (RRO) of track following position error signal (PES) in high track per inch (TPI) magnetic disk drives, analytical representations of thermal expansion mismatch between disk and spindle hub structure formulated in form of operators and finite element analysis (FEA) are employed. Parametric studies with analysis taken at different operational temperatures suggested that RRO can be minimized significantly when location of spindle notch is properly located. RRO harmonics resulted from the thermal expansion mismatch and structure misalignments are studied and concluded with simple algebraic expression related to number of fasteners used in the disk-spindle assembly.

On shock response of RPS, head gimbal assembly (HGA) in HDD was analysed. Experimental observation of de-bonding phenomena between head gimbal assembly (HGA) and suspension for a commercial 3.5-inch enterprise HDD under non-operational 250G shock test was performed. In this research the experimental observation and numerical finite element studies were conducted to understand the effect on the mechanical failure of HGA when it is subjected to non-operational shock in the parked position on the ramp. Different design modifications were adapted to withstand shock waves. It was observed that by changing flexure angle in HGA, shock stress can be reduced. FEA simulation results have been presented to verify the findings.

The research findings in this thesis can be implemented in the industry where RPS has been widely used, as for example the new replica modes discovery in bladed rotors can also be applied on small scales like as on hard drive, where no. of blades can be replaced by no. of fasteners and the spinning hard drive will be benefited by studying its vibrations with concentration on replica modes. Furthermore, the serendipitous finding of HDD platters expansion under thermal stress can be beneficial in actually storing more data per inch as it has been recently used in TAMR (thermally assisted magnetic recording) technology. Gears, brakes, washing machines to name a few can get supported from the findings in the thesis where controlling vibrations, shock and heat is crucial.

# TABLE OF CONTENTS

<b>Table of Contents</b>	<b>Vi</b>
<b>List of Figures</b>	<b>V</b>
<b>List of Tables</b>	<b>X</b>
<b>List of Abbreviations</b>	<b>Xi</b>
<b>Acknowledgement</b>	<b>Xii</b>
<b>Chapter 1 Introduction</b>	<b>1</b>
1.1 What is a Rotationally Periodic Structure?	1
1.2 Topological Affinity of Rotationally Periodic Structures	2
1.3 Motivations and Model Selections	3
1.3.1 Vibrational Response on Rotationally Periodic Structures	4
1.3.2 Thermal Response on Rotationally Periodic Structures	5
1.3.3 Shock Response on Rotationally Periodic Structures	5
1.4 Aim and Objectives	6
1.5 Scope and Contributions	7
1.6 Thesis Organization	7
<b>Chapter 2 Literature Review</b>	<b>10</b>
2.1 Rotationally Periodic Structures	10
2.2 Applications of Rotationally Periodic Structures	11
2.2.1 Brakes	11
2.2.2 Gears	12
2.2.3 Hard Disk Spindle System	13
2.2.4 Turbines	14
2.2.4.1 Discrete to Continuous Models	16
2.2.4.2 Point Stiffness Considerations	16
2.2.4.3 Coupled Bladed Disk to Integrally Bladed Rotors	17

2.4	Conclusion	17
<b>Chapter 3</b>	<b>Free Vibration Response of Rotationally Periodic Structures</b>	<b>19</b>
3.1	Introduction	19
3.2	Finite Element Model	20
3.2.1	Convergence Study	21
3.3	Replica Modes	23
3.4	Lumped Mass Model Approach	26
3.4.1	Equivalent IBR Model	27
3.4.2	Equation of Motion (EOM)	28
3.5	Parametric Study	30
3.5.1	Replica Modes with Varying Blade Angles	30
3.5.2	Replica Modes with Varying Blade Thickness	34
3.6	Modulated Stiffness Analysis	36
3.7	Experimental Modal Analysis	41
3.7.1	Experimental Setup	42
3.7.2	Experimental Investigation	44
3.8	Chladni's Pattern	49
3.8.1	Experimental Setup	50
3.9	Conclusion	51
<b>Chapter 4</b>	<b>Thermal Response of Rotationally Periodic Structures</b>	<b>53</b>
4.1	Introduction	54
4.2	Experimental Observations	56
4.3	Finite Element Model	60
4.3.1	Modification in Finite Element Model	61
4.3.2	Interrelation at Increased Temperatures	63
4.4	Perturbation Study	65
4.5	Reduction of 2X RRO	68

<b>Chapter 5</b>	<b>Shock Wave Response of Rotationally Periodic Structures</b>	<b>71</b>
5.1	Introduction	72
5.2	Experimental Observations	73
5.3	Finite Element Model	78
5.4	Minimization of Shock Effect	79
5.5	Conclusion	82
<b>Chapter 6</b>	<b>Conclusion</b>	<b>84</b>
6.1	Summary	84
6.2	Limitations	86
6.3	Future Work	87
6.3.1	Forced Vibration Response on Replica Modes	87
6.3.2	Damping of Replica Modes	87
6.3.3	Mistuning Effects on Replica Modes	88
<b>References</b>		<b>89</b>
<b>Appendices</b>		<b>98</b>
Appendix A		99
Appendix B		102
Appendix C		104
<b>List of Publications</b>		<b>111</b>

# LIST OF FIGURES

## Chapter 1

Fig. 1.1	Rotationally periodic structure example (Integrated bladed rotor)	2
Fig. 1.2	Frequency analysis on (a) IBR (c) DSA and (b) its corresponding modeshape (0,3) at outer edge of disk near blades (d) and outer edge of DSA near Screw locations respectively	3
Fig. 1.3	Graphical hierarchy of Thesis organization	9

## Chapter 2

Fig. 2.1	Typical bladed section of a reaction turbine rotor	10
Fig. 2.2	Slotted Brake Rotors (source: <a href="http://www.turnermotorsport.com">www.turnermotorsport.com</a> )	11
Fig. 2.3	A typical spur and bevel gears (source: <a href="http://www.gearsandstuff.com">www.gearsandstuff.com</a> )	12
Fig. 2.4	Hard disk drive spindle system (Source: <a href="http://www.hdddoctor.net">www.hdddoctor.net</a> )	14
Fig. 2.5	Schematic of a gas turbine engine	15
Fig. 2.6	Integrated bladed rotor ( IBR )	17

## Chapter 3

Fig. 3.1	Schematics of rapid prototyped model of an integrally bladed rotor	20
Fig. 3.2	Convergence of frequency modes of the present IBR model at $N_b = 19, \beta = 30^\circ$	22
Fig. 3.3	Example of (a) = in-phase ( $\uparrow\uparrow$ ) and (b) = out-of-phase ( $\uparrow\downarrow$ ) replica mode components of the IBR at $N_b = 19, \beta = 30^\circ$	24
Fig. 3.4	Finite Element Analysis pictures of in-phase ( $\uparrow\uparrow$ ) and out-of-phase ( $\uparrow\downarrow$ ) replica mode components of the IBR at $N_b = 19, \beta = 30^\circ$	25
Fig. 3.5	Lumped mass model with flexible disk approach	26
Fig. 3.6	Lumped mass model with interbladed connectors	26
Fig. 3.7	Sophisticated Lumped mass model with interblade connectors	27
Fig. 3.8	Equivalent Integrally Bladed Disk (IBR) lumped mass model	28
Fig. 3.9	J <sup>th</sup> sector of Integrally bladed disk (IBR)	28
Fig. 3.10	Schematics of different blade angle at (a) $30^\circ$ , (b) $0^\circ$ , (c) $15^\circ$ , and (d) $50^\circ$	31
Fig. 3.11	Migration of replica modes as a function of blade angle; $N_b = 19$ and $T_b = 5\text{mm}$ .	31
Fig. 3.12	Fourier amplitudes of replica (a) $P(0, 4)_L$ and (b) $P(0, 4)_H$ mode of the model IBR with different blade angles	33
Fig. 3.13	Schematic illustrations of different blade thickness, $T_b$ at (a) 14mm, (b) 11mm, (c) 8mm, and (d) 5mm	35
Fig. 3.14	Migration of replica modes as a function of blade thickness; $\beta = 30^\circ$	36
Fig. 3.15	Fourier amplitude of IBR at 1000N force with different blade angles ( $\beta$ )	37
Fig. 3.16	1 <sup>st</sup> modulated wavenumber trend at different forces	38
Fig. 3.17	(a) 1 <sup>st</sup> harmonic trend with linear fitting (b) 2 <sup>nd</sup> harmonic trend with second order polynomial fitting (c) 3 <sup>rd</sup> harmonic trend with third order polynomial fitting	40
Fig. 3.18	Actual 3D prototype IBR developed for EMA	42
Fig. 3.19	Schematic of Experimental Modal Testing	42
Fig. 3.20	Input-output Measurement Locations for FRF	43
Fig. 3.21	Selection of Hammer tips for required FRF	45



Fig. 3.22	Frequency response function plot at different Input-output measuring locations	46
Fig. 3.23	Comparison b/w filtered and non-filtered frequency plot at 60Hz DC hum	46
Fig. 3.24	Frequency and phase angle plot of replica mode through Experimental modal analysis	47
Fig. 3.25	Schematic of Chladni's pattern experiment	49
Fig. 3.26	Series of PZTs glued at IBR Prototype	49
Fig. 3.27	Mode (0, 2) <sub>H</sub> depicted by Chladni's	50

## Chapter 4

Fig. 4.1	(a) Mechanical components in a commercial HDD (b) Servo and data sectors on magnetic disk	53
Fig. 4.2(a)	HDD deformed as a saucer against a disk flatness measurement	55
Fig. 4.2(b)	The subsequent displacement plot at outer diameter (OD) of spindle assembly	56
Fig. 4.3	RRO PES spectra examples as seen on disk (a) OD, (b) MD , and (c) ID	57
Fig. 4.4	Repeatable Run-out Diagrams from disk OD to ID for (a) 2X, (b) 4X, (c) 5X, and (d) 6X RRO harmonics	58
Fig. 4.5	Finite Element Model of the Disk Spindle Assembly (DSA) of a HDD	59
Fig. 4.6	Comparison of (a) rotationally periodic and (b) non-periodic spindle assembly models and the corresponding disk radial deformation in (c) and (d), respectively. The resultant harmonics are shown in (e) and (f).	61
Fig. 4.7	Side view of (a) Original and (b) deformed spindle hub structure at 80°C and (c) Original and (d) deformed DSA at 80°C	62
Fig. 4.8	FEA results of interrelationship of 2X with 4X and 8X RRO scales at disk internal and Outer Dia. in (a) and (c), respectively; Interrelationship of 1X with 5X and 7X RRO scales at disk internal and outer diameter, in (b) and (d), respectively. [45]	64
Fig. 4.9	Elastic constrains of a disk clamped by six fasteners	65
Fig. 4.10	Spindle hub designs with different slot angles	67
Fig. 4.11	FEA nodal displacement plots at Disk OD at 80° C on (a) 0° slot angle (b) 15 slot angle (c) 30° slot angle and (d) 45° slot angle.	68
Fig. 4.1	RRO harmonics of OD radial displacement (mm) at different temperature and slot angle designs	69

## Chapter 5

Fig. 5.1	Experimental setup for drop test analysis	73
Fig. 5.2	Sanity check of drop fixture	73
Fig. 5.3	Independent and tester accelerometer stability diagram	74
Fig. 5.4	De-bonding of flexure @250G and 2ms	75
Fig. 5.5	Photograph of small and large de-bonding resulting mechanical failure	76
Fig. 5.6	Photograph of dismantled enterprise HDD (a) and the corresponding finite element model in (b)	77
Fig. 5.7	Fig. 5.7 HGA designs with different flexure angle, $\alpha$ at (a) 1°, (b) 2°, (c) 3°, and (d) 4°	78

Fig. 5.8	Fig. 5.8 HGA impact stress history plot of four critical vertex points with flexure angle at $\alpha=1^\circ$	79
Fig. 5.9	Maximum impact stress around HGA critical vertex points as function of drop heights with $\alpha=1^\circ$	80
Fig. 5.10	Maximum impact stress around HGA critical vertex points as function of flexure angles at 200G/2m drop height	80
Fig. 5.11	Fig. 5.11 Simulated HGA with Stress concentration regions	81

## **LIST OF TABLES**

3.1	Design parameters of the IBR	17
3.2	Natural Frequency Comparison of Replica Modes Through FEA, EMA and Chladni	44
5.1	(a) Drop Test Statistics & (b) Qualitative observation of Flexure De-bond	70

## LIST OF ABBREVIATIONS

( $\uparrow\uparrow$ )	In-phase Mode
( $\uparrow\downarrow$ )	Out-of-Phase Mode
D.S.A	Dynamic Signal Analyzer
DSA	Disk Spindle Assembly
EMA	Experimental Modal Analysis
EOM	Equation of Motion
FCA	Flexible Cable Assembly
FEA	Finite Element Analysis
FFT	Fast Fourier Transform
FRF	Frequency Response Function
HAS	Hard-disk Spindle Assembly
HCF	High Cycle Fatigue
HDD	Hard Disk Drive
HGA	Head Gimbal Assembly
IBR	Integrated Bladed Rotor
$K_g$	Structural Stiffness
$K_\beta$	Spatial modulated stiffness
LCF	Low Cycle Fatigue
$N_b$	No. of Blades
NF	No. of Fasteners
NVH	Noise Vibration Harness
PES	Position Error Signal
RPS	Rotationally Periodic Structures
RRO	Repeatable Run-out
$T_b$	Blade Thickness
TMR	Track Mis-Registration
TPI	Track per Inch
$U_{(k)n}$	Displacement
VCM	Voice Coil Motor
$\beta$	Blade Angle

## ACKNOWLEDGEMENTS

The work done during the last four years for the doctoral studies could have not been brought about without the support of others. Firstly, I would like to thank my former supervisor, Dr. Jen-Yuan (James) Chang. His encouragement and advice facilitated me to achieve the research goals. Secondly, I would like to express my deepest thanks to my two supervisors, Associate Professor Johan Potgieter and Dr. Loulin Huang.

Dr. Johan has been my supervisor and guiding beacon through four years of PhD research. I am truly thankful for his steadfast integrity and selfless dedication to both my personal and academic development. His thorough and excellent feedbacks and academic corrections on an earlier version of this thesis have been immensely appreciable.

The privilege of having Dr. Loulin as my co-supervisor was also of great assistance, from whom I have learnt the vital skill of disciplined critical thinking. His technical advice on my thesis has been invaluable.

I would also like to thank the staff at the School of Engineering and Technology (SEAT) especially Professor Stephen Marsland for his continuous cooperation in dealing with the issues arising during my studies. His forensic scrutiny of my academic writing has been invaluable. He has always found the time to propose consistently excellent improvements. I owe a great debt of gratitude to Dr. Johan, Dr. Loulin and Prof. Stephen.

I cannot overlook the support of my fellow students and friends at the University. Specially, I wish to thank M. Khurruam for his sincere and timely suggestions when I needed them. I am indebted to my parents for their love for me and continuous prayers for my success. My success belongs to them as much as it belongs to me. I am thankful to my lovely wife Warda for her tremendous patience, understanding and support.

I would also like to offer my gratitude to National Tsing Hua University, Hsinchu Taiwan, for letting me perform experiments in their state-of-the-art mechatronics and vibration lab.

I would like to thank Hitachi Global Storage Technologies for the donation of the enterprise hard disk drives used in the research.

# CHAPTER 1

## INTRODUCTION

### 1.1 WHAT IS A ROTATIONALLY PERIODIC STRUCTURE?

An object or an assembly with certain arrangement of features that repeat itself around the center of its own axis are known as rotationally periodic structures (RPS) or cyclic symmetric structures. There are varieties of different RPS in the market like gears, washing machine tubs, bladed disks, hard disk drives assemblies, brakes, pumps etc. All of these structures plays vital role in modern industries. Research has been carried out on different responses on these structures to minimize the errors related to RPS and their responses. Responses like free or forced vibrational, gravitational, centripetal, centrifugal, aerodynamical, thermal, shock etc. all are critical in the design and assemblies of such structures. For example a washing machine tub's centrifugal and vibrational response is quite critical in making the tub stable and to make it perform properly. In a hard disk drive, thermal response is critical to avoid the overheating and damaging of the data stored on the memory sectors. Similarly, thermal and vibratory response of jet turbine bladed disks must be understood in order to reduce very harmful effects to the rotating system as well as passenger's safety. All in all, rotationally periodic structures and their different responses are very important in the engineering world.

To analyze different response on RPS, a partial model can be considered with proper load and boundary conditions to determine properties of the full structure. This is the advantage of an RPS. For example, a turbine blade portion 'A to B' as shown in figure 1.1 can be modelled by segmenting the full model in equal portions with given distributed load to save time for analysis of a specific response. The given model with highlighted section can be repeated 18 times around its axis to give the complete structure and can be analyzed to produce predicted results.

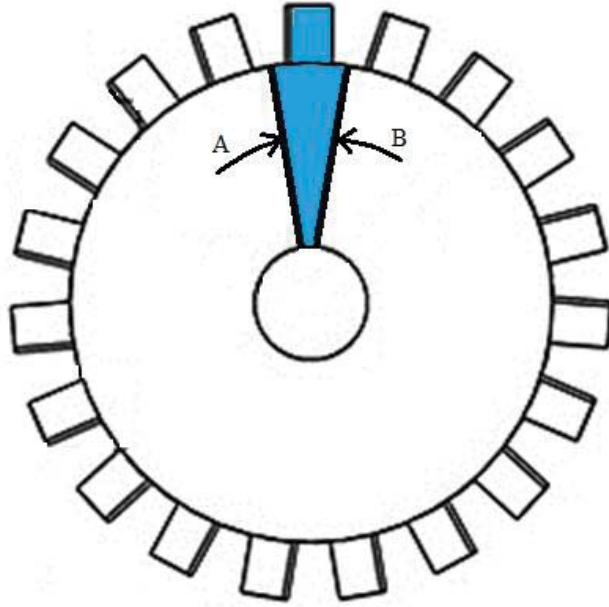


*Fig. 1.1 Rotationally periodic structure example (Integrated bladed rotor)*

## **1.2 TOPOLOGICAL AFFINITY OF ROTATIONALLY PERIODIC STRUCTURES (RPS)**

A group of identical sub-structures when assembled in a proper way form a cyclic symmetric or in other words a rotationally periodic structure (RPS). These structures are commonly used in natural and engineering world. They possess similarities in terms of their geometric shapes, boundary conditions, physical properties and connection with other substructures. Generally the modes and natural frequency of a structure are determined by whole structure but in case of rotationally periodic structures, by virtue of its periodicity, the natural frequency can be determined from those of its single substructure. Periodicity on a rotationally periodic structure can either be in the form of screws which act as point stiffness in a hard drive spindle assembly or turbine blades in a jet turbine rotor that can modulate the natural frequency. The advantage of RPS is that no matter how big or small the structure is or where it is applicable in engineering industries, it inhabits almost the same modulated results regardless of its size or design. Fig. 1.2 (a) and (b) show topological affinity of a prototypical integrally bladed rotor (IBR) and a disk spindle system (DSA) in a hard drive respectively and their corresponding frequency analysis in (b) and (d). A free vibration analysis on both the structures depicts their natural frequencies have been modulated with extra harmonics but with almost same results. These extra

harmonics have been formed because of periodic blades in case of IBR and screw locations in case of DSA.

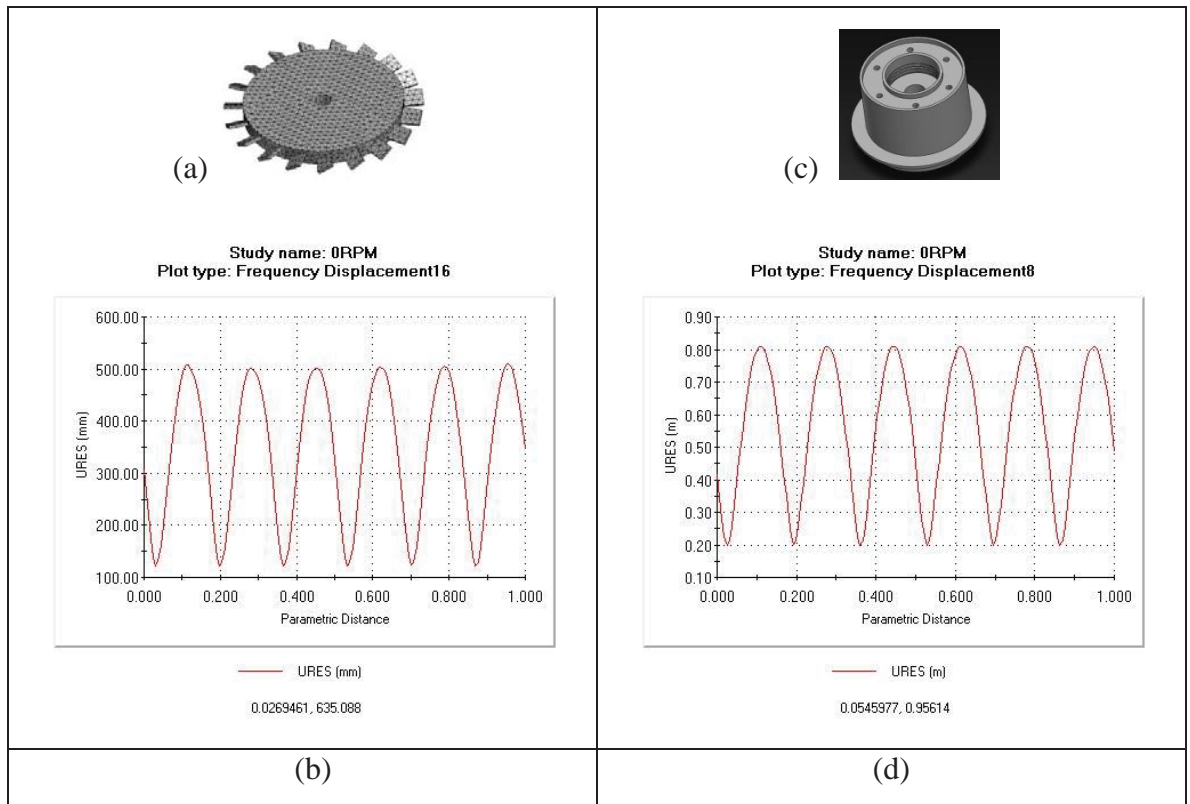


*Fig. 1.2 Frequency analysis on (a) IBR (c) DSA and (b) its corresponding mode-shape (0,3) at outer edge of disk near blades (d) and outer edge of DSA near Screw locations respectively*

The advantage of topological affinity in RPS and their vast implication in industries and engineering research motivated the theme of this thesis and is defined as under.

### 1.3 MOTIVATIONS AND MODEL SELECTIONS

Out of variety of models of rotationally periodic structures, research models were selected after thorough investigation and literature survey to carry out in this thesis. Out of hundreds of RPS available in the engineering market two of the most ongoing researched models have been selected namely integrated bladed rotor (IBR) and hard disk drive (HDD) as the focus of the thesis. Also from numerous different responses 3 major responses namely vibratory, thermal and shock has been selected by carefully examining literature



loopholes that required further investigation. For free vibrations response the newly designed integrally bladed rotors (IBR) were selected and is the focus as the first objective of the research ; a Hard Disk Drive Spindle Assembly (HSA) and Head Gimbal Assembly (HGA) were taken into account for thermal and shock analysis on rotationally periodic structures as second and third objectives of the thesis respectively. To bear in mind, different responses on research models are a demonstration which can be applied on any rotationally periodic structure as they follow the same topology as briefed in previous section. The motivation for selection of these models and responses are provided in the subsection that follows.

### **1.3.1 VIBRATIONAL RESPONSE ON ROTATIONALLY PERIODIC STRUCTURES**

Localized vibrations are commonly observed in rotationally periodic structures or cyclic symmetric structure such as the integrated bladed rotors (IBR). The localized vibrations can potentially contribute to large dynamic responses which are locked on to the structures when they are subjected to engine order and external shock and vibration excitations. As a result, excessive fatigue loading from the localized vibrations can be very harmful to the rotating system as well as to jet engine's health, and pilot and passengers' safety. Therefore, careful dynamic engineering research on the subject area through natural vibration modes is of great importance and is critical to the dynamic design of cyclic symmetric rotor structure systems. As opposed to periodically packing blades on to rigid rotors and taking out for maintenance in jet engines and power generation turbine applications, IBRs blades are integrated to the underlying disk rotor during manufacturing process. When blades are packed to a rotor, due to mechanical and handling tolerance, unexpected and uncontrolled structural dynamics can occur. In the literature, direct contact friction dampers are reported to be effective in moderating the vibrations. Motivated by the aforementioned engineering concerns and demand to reduce engine size for unmanned aerial vehicle, iterates that IBR free vibrations becomes essential and is the focus in vibrational response research on RPS.

### **1.3.2 THERMAL RESPONSE ON ROTATIONALLY PERIODIC STRUCTURES**

In the last few decades, the hard disk drive (HDD) has emerged as key technological product of the computer age beginning. It consists of the main, magnetic disk-spindle assembly (DSA) system which greatly influences the dynamics of the performance of the HDD. Hard disk spindle is one of the most important mechanical parts of hard disk drive. Its dynamic characteristics have great influence on HDD's performance. With such a wide usage of HDD, operating temperature of the HDD can have a critical effect on the performance and lifetime of HDD. Such temperature variations cause repeatable run-out errors. Run-out error is defined as a separation from perfectly circular motion of spindle hub. The components of run-out errors that repeat itself at an integral multiple of spindle rotational frequency regarded as repeatable run-out (RRO). To eliminate these off track errors and head crashes and to provide performance improvement, operation of hard disk drives in safe temperature range is critically important and hence is the motivation and focus as thermal response on RPS.

### **1.3.3 SHOCK RESPONSE ON ROTATIONALLY PERIODIC STRUCTURES**

Hard disk drives (HDD) are composed of tiny components that hold an immense degree of sensitivity. Increasing demands of HDD with shrinkage of data track widths requires precision in design, with consideration of all aspects of possible failures either physically or logically. Major drive failure most likely is caused by shock impulse.

All shocks carry the potential of causing the drive to fail or data loss. The most disruptive events are those with high shock levels and short duration. Hence the study to overcome these errors is eminent in the design of HDD and was the motivation to carry out further research in HDD critical sub-assemblies mainly in head gimbal assembly (HGA) which is more susceptible to shock impulses, and hence is the focus of the shock stress response on RPS.

## **1.4 AIM AND OBJECTIVES**

The aim and objectives of this research is to investigate three main responses namely vibration, thermal and shock on commercially available rotationally periodic structures (RPS). Primarily the research focused around newly developed integrally bladed rotors and later on enhancements of hard disk drive technologies as selective models of RPS. The areas of investigation have been carefully selected from the literature survey in model's respective fields and thus follow the steps as:

### **Objective 1:**

For vibration response, have a detailed investigation on free vibration of newly developed integrated bladed rotors (IBR)

### **Objective 2:**

For thermal response, find a methodology to optimize and reduce the repeatable run-out error (RRO) of track following position error signal (PES) in high track per inch (TPI) hard disk drives caused by thermal expansion of Disk Spindle Assembly (DSA) of HDD.

### **Objective 3:**

For shock response, investigate the de-bonding phenomena between head gimbal assembly (HGA) and suspension of commercial hard disk drive under non-operational shock analysis with objective placed on withstanding shock stress waves between head slider and suspension.

## 1.5 SCOPE AND CONTRIBUTIONS

The thesis presents the free vibratory response of integrally bladed rotors (IBR) and the thermal and shock response of hard disk drive spindle and head gimbal system respectively. All these systems have rotationally periodic structures. The main contributions of this thesis are therefore in these three areas and can be summarized as follows:

**Contribution 1:** Discovery of new replica modes in integrated bladed rotors with certain properties.

**Contribution 2:** Development of perturbation model for Disk Spindle Assembly (DSA) of a hard disk drive concluding 2X repeatable run-out errors can be eliminated by proper design.

**Contribution 3:** Discovery of flexure angle has a significant impact on the amount of shock stress on Head Gimbal Assembly (HSA) of a Hard Disk Drive (HDD).

## 1.6 THESIS ORGANIZATION

This thesis provides insight into the response of rotationally periodic or cyclic symmetric structures and the contribution of the author in the thesis is mainly on the topic of “Free Vibrations in Integrally bladed rotors” and “thermal and shock response in Hard disk drive technology”.

Chapter 2 provides an overview of different applications of rotationally periodic structures and draws the attention on the vast research areas and very briefly presents the work done by different researchers in this field. The same chapter describes the selection of RPS model to carry out the research in this thesis from the vast list of rotationally periodic structures and also highlight open ended research areas.

In chapter 3 of this thesis, free vibration analysis on Integrated Bladed Rotor (IBR) as the main selection of research model is discussed in detail with the help of the prototypical designed model. Firstly, a fully populated finite element model was generated and its equation of motion has been established. The same chapter further demonstrated new finding of replica modes through frequency analysis and analyzed its trend with parametric study and modulated stiffness analysis. Furthermore, experimental model analysis and Chladni's pattern technique was employed on the rapid prototypical model of IBR to prove the existence of replica modes in integrally bladed rotors. All the results were also presented in the same chapter.

In chapter 4, thermal response was carried out on rotationally periodic structures. As for the reason of limitations with IBR and same topological affinity of RPS, hard disk drive spindle was taken as a research model selection. Experimental observations were taken to analyze the repeatable run-out (RRO) error of track following position error signal (PES) in high track per inch (TPI) disk drives. System models for disk-spindle assembly were constructed by considering realistic conditions of alignment eccentricity and structure imperfection. Thermal –elastic finite element analyses were performed for the system at elevated temperatures. New spindle design approach was introduced to reduce 2X and 1XRRO. Perturbation analysis was performed for the verification of RRO. All the results were also presented in the same chapter.

In the light of the model selections presented in chapter 3 and chapter 4, shock analysis was performed on RPS with HDD as model selection in chapter 5. Following the experimental observation of de-bonding phenomena between Head Gimbal Assembly (HGA) and suspension for a commercial 3.5-inch enterprise HDD under non-operational shock test, Finite Element – Drop test study was carried out with objective placed on withstanding shocks between the head slider and the suspension. New designs of HGA were suggested to withstand stress waves in non-operational conditions and to ensure the mechanical integrity of HGA.

Chapter 6 concludes the thesis with the summary of the contributions made by the author in the research following with list of published material. Future work suggestions are also included in the end of the last chapter.

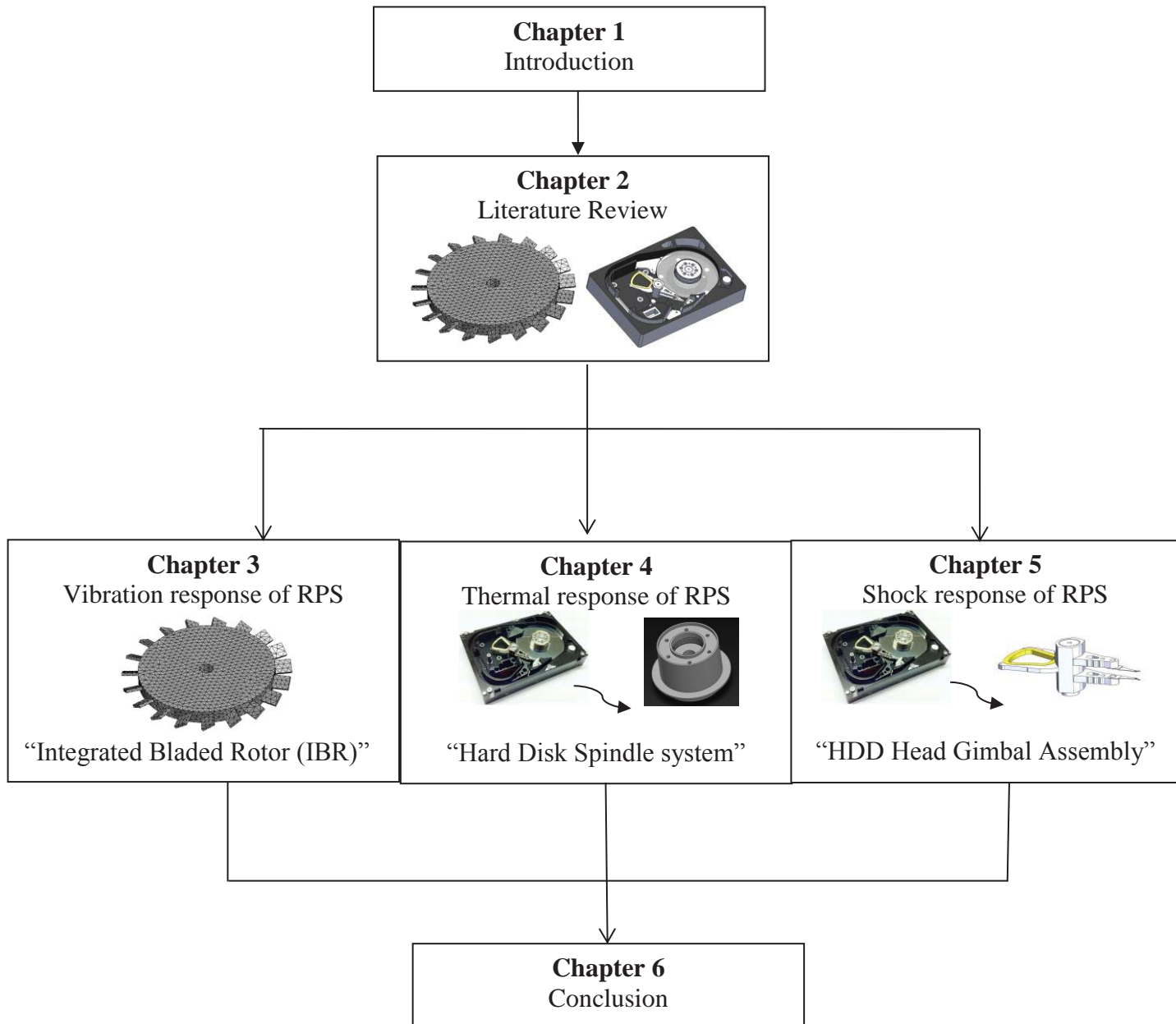


*Fig. 1.3 Graphical hierarchy of Thesis organization*

## CHAPTER 2

### LITERATURE REVIEW

#### 2.1 ROTATIONALLY PERIODIC STRUCTURES

Cyclic symmetric or rotationally periodic structures are very common both in engineering and in natural world. A structure can be defined as repetitive when it is assembled in a proper way by a group of identical substructures. These substructures are identical in terms of geometric shape, physical properties, boundary conditions and connections with other substructures [4]. Rotationally periodic structures are composed of a number  $N_b$  of identical substructures, periodically arranged around an axis, so that the original shape is recovered upon rotations of an angle of  $2\pi / N_b$ . This topology of structures plays an important role in many engineering applications, such as turbines, washing machines, hard disk drives, stator-rotor assemblies of electrical machineries, disk brakes of automobiles etc. and so on [5]. Fig. 2.1 shows an example of a cyclic symmetric structure.

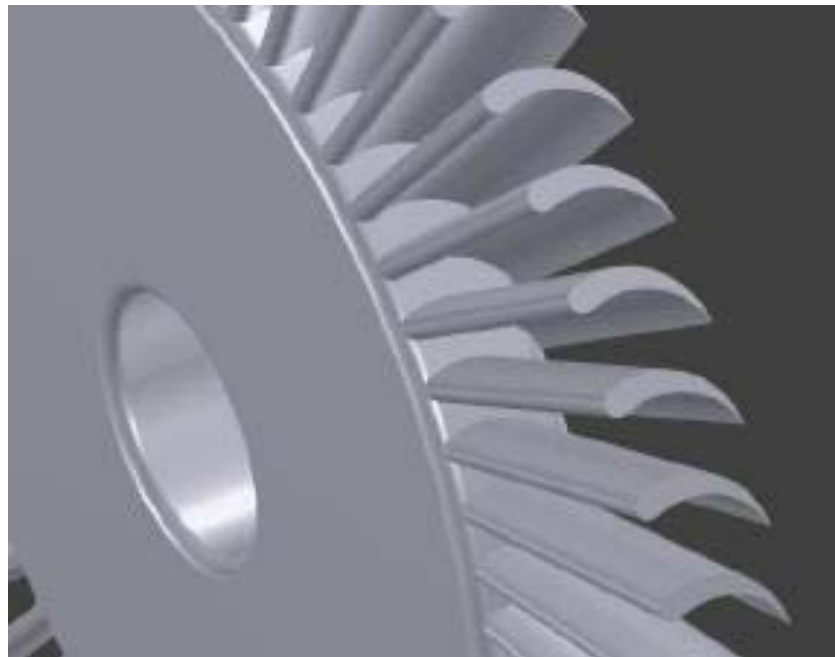


*Fig. 2.1 Typical bladed section of a reaction turbine rotor (Source: [www.Seabirdadventure.com/tesla-turbine](http://www.Seabirdadventure.com/tesla-turbine))*

## 2.2 APPLICATIONS OF ROTATIONALLY PERIODIC STRUCTURES

There are numbers of technological applications for rotationally periodic structures spread throughout the market. All of these structures have common axis-symmetrical base with periodic features either in shape of evenly spaced bolts, clamping or additional built-in features. With such periodic features the vibratory response becomes contaminated and produces additional wavenumber in the structure's circumference. Extreme vibration may cause fractures, blade breakdown and lastly the total collapse of structures. Therefore, monitoring vibratory effects is of great significance. Following are some examples given of rotationally periodic structures where vibratory and thermal response acts as a vital benefactor.

### 2.2.1 BRAKES

A key example of rotationally periodic structures is disc brake rotor system. Fig. 2.2 shows slotted brake rotors used in sports cars. A brake rotor is mounted on a flange by evenly spaced bolts subjected to thermal stress and excitation force generated by the interaction between brake pad and rotor.



*Fig. 2.2 Slotted Brake Rotors (Source: [www.turnermotorsport.com](http://www.turnermotorsport.com))*

There are numerous publications available dealing with high frequency vibrations, such as brake squeal, brake judder including mathematical models for analysis and



simulation [ 25- 28]. Most brake squeal is produced by vibration (resonance instability) of the brake components, especially the pads and discs known as force-coupled excitation [33].

Also, brake judder is usually perceived by the driver as minor to severe vibrations transferred through the chassis during braking. These vibrations are the result of uneven thermal distributions, or *hot spots*. Hot spots are classified as concentrated thermal regions that alternate between both sides of a disc that distort it in such a way that produces a sinusoidal waviness around its edges. Once the brake pads (friction material/brake lining) come in contact with the sinusoidal surface during braking, severe vibrations are induced, and can produce hazardous conditions for the person driving the vehicle [25-28, 33]. Noise, vibration, and harshness (NVH) are among the most important priorities for today's vehicle manufacturers [33]. A combined effort of vibratory and thermal stress analysis is mandatory in this application of cyclic symmetric structure.

### 2.2.2 GEARS

Gears are the most common means of transmitting power in mechanical engineering and a good illustration of cyclic symmetric structures. An example of spur and bevel gear are shown in figure 2.3.



Fig. 2.3 Typical spur and bevel gears (source: [www.Howstuffworks.com/transport/engines-equipment](http://www.Howstuffworks.com/transport/engines-equipment))

The most important components in gear vibration spectra are the tooth meshing frequency and its harmonics, together with sidebands due to modulation phenomena. The increment in the number and amplitude of such sidebands may indicate a fault condition [22-27]. Cepstral analysis has been widely applied to gear monitoring. The cepstrum is well suited for the detection of sidebands in vibration spectra and for the estimation of their evolution during gear life. In addition, since the cepstrum estimates the average sideband spacing over a wide frequency range, it allows very accurate measurement of the sideband periodicity. It is therefore applicable to both detection and diagnosis of gear faults [27-32].

The amplitude and phase demodulation of one of the tooth meshing harmonics is a well-known gear monitoring technique [23-24]. This technique requires the time synchronous averaging of the vibration signal in order to remove any periodic events not exactly synchronous with the gear of interest and to reduce the effects of noise and vibration sources other than gear pairs [22, 23, 32]. The literature indicates significant research in gear applications. Most published articles on gear vibration discuss the torsional resonances of the shaft supporting the gear. Analyses that model continuous system elastic vibration typically focus on either the spindle (with any attached disks modelled as rigid) or the disk (supported by a rigid structure). For example, the dominant excitation in gears is at the tooth mesh, but unacceptable noise is radiated primarily from the housing. The vibratory response is a coupled one involving the disk, spindle, bearings, and housing. There is not much literature found in continuous vibration [25].

### **2.2.3 HARD DISK SPINDLE SYSTEM**

Hard disk spindle system is also a key technological application of rotationally periodic structures. Figure 2.4 shows a typical hard disk spindle system. The fast growth of digital data is pushing the continued rapid increases in hard disk drive capacity and its area density. One key challenge of them is to detect and reduce various vibrations such as, the disk flutter of high speed-spinning media disk platters within an air filled enclosure space. There are many researches on FEA simulation and analysis of the disk flutter, including the prediction of the natural frequencies and amplitudes of vibration mode shapes [30, 31].



Fig. 2.4 Hard disk drive spindle system (Source: [www.hddoctor.net](http://www.hddoctor.net))

Continuous vibration in a typically elastic system focus on either the spindle (with any attached disks modeled as rigid) or the disk (supported by a rigid structure) but the reverse path occurs in disk drives where bearing forces and support structure motion drives disk vibration. While focusing on disk drive spindle system, the existing literature also emphasizes free vibration and stability investigations with considerably less attention to operating condition response [25].

#### 2.2.4 TURBINES

In a multi stage jet turbine shown in figure 2.5, evenly spaced blades coupled on axis symmetric disk form cyclic symmetric structure results in modulating vibration modes. Structures key vibration parameters are its natural frequencies. It's critically important that all the modes natural frequencies should be placed far apart to avoid resonance from the excitations frequency. A rich literature exists in the field of free and forced vibrations of bladed rotors [1-6, 13-17]. The effects of mistuning and mode localization are also critical concerns when analyzing the free and forced vibrations of bladed disks structures as

certain part of these structures have higher response amplitude than other parts due to the fact that the blades are not uniform [29,30].

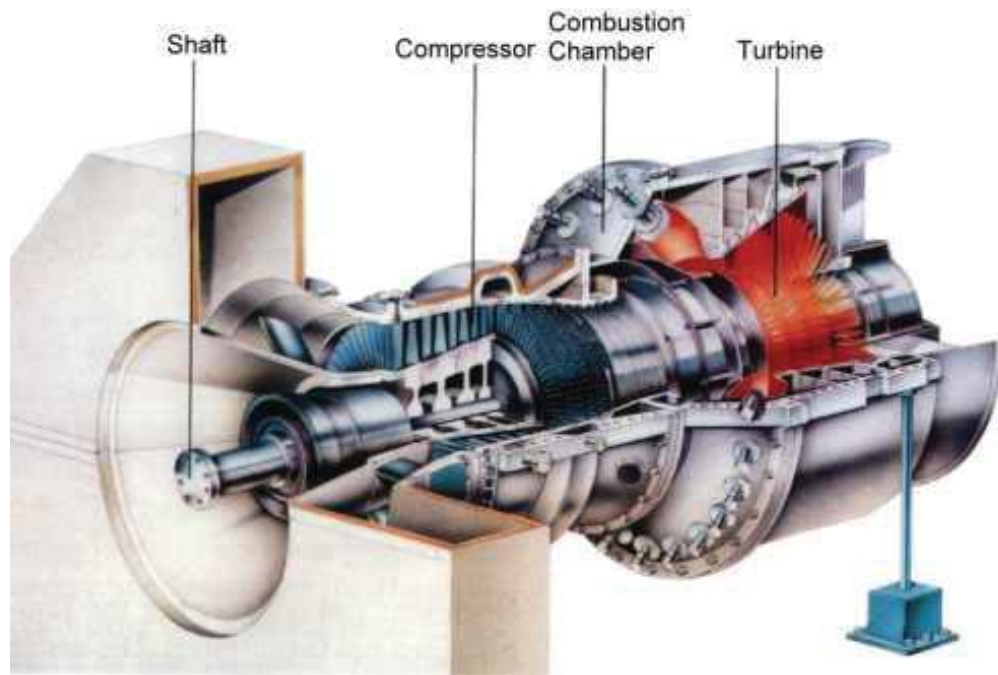


*Fig. 2.5 Schematic of a gas turbine engine (source: [www.wartsila.com/gas-turbine-for-power-generation](http://www.wartsila.com/gas-turbine-for-power-generation))*

Extreme vibrations may cause fractures, blade breakdown and lastly the total collapse of the jet turbines. Therefore, monitoring vibratory effects is of great significance. It prevents damage and it is likely to foresee the stability and the life of bladed disk under different operating conditions. Changes in blade airfoil dimensions will affect the blade natural frequency. Damage or material loss occurring at the blade tip will increase the natural frequency. On the other hand, damage occurring at or near the blade root weakens the blade structurally and decrease the blade natural frequency. Blades natural frequencies are above the normal running speed of jet turbine. However, in reduction of blades natural frequency could move it closer to the turbine normal running speed [9]. An engineer must decide whether the excitation source can be reduced or eliminated, or whether the dynamics of the structure must be altered to control the problem. Many times, it is simply not possible to reduce the level of excitation or alter its frequency content. Therefore the problem must be solved by altering the dynamics of the structure [9].

In case of bladed disk rotors, when a structure deviates from axis-symmetry because of circumferentially varying modal features, significant changes can occur to its natural frequencies and modes, particularly for the doublet modes that have non-zero nodal diameters and repeated natural frequencies in the limit of axis-symmetry. Much of this research is based on finite element methods [1-4, 8-14] in order to study the free and forced vibration of rotationally periodic structures and some analytical mode summation approaches have been investigated. In addition, some more of the downsides of bladed disk rotors research have been discussed in the subsection that follows.

#### **2.2.4.1 DISCRETE TO CONTINUOUS MODELS**

Because of the complications of design, continuous models are less developed in the literature. For Example, Wagner LF and Griffin JH [33] considered a bladed disk which composed of grouped blades mounted on a flexible disk; the analogy uses a series of transversely vibrating, continuous string segments that are arranged in a rotationally periodic pattern, with coupling between the segments accomplished by discrete springs [33]. In reality, each blade is coupled to all the other blades mounted on the flexible disk through the disk itself, and this feature should be taken into account for an accurate evaluation of the structural eigen modes and eigen frequencies [31].

#### **2.2.4.2 POINT STIFFNESS CONSIDERATIONS**

Mediocre thickness level between disk and blades were less developed in literature, mostly it was taken as either the disk was too thick with thin blades or the disks were too thin with thick blades and with such setup a general idea about eigen value and eigen functions were reported. For example, Hyunchul Kim and I.Y.Shen [31] focuses on vibration measurements of spinning disk carrying four pairs of evenly spaced brackets (considered as point stiffness on disk itself) mounted on a high-speed air bearing spindle. With this setup, they reported the presence of gyroscopic force and centrifugal stiffening could cause the repeated modes to split into two modes with distinct frequencies and also resonance branches in waterfall plot [31]. Yet again the model itself was away from reality as the brackets were too thick considering the disk.



#### 2.2.4.3 COUPLED BLADED DISKS TO INTEGRATED BLADED ROTORS

In literature, mostly jet turbines research is on coupled bladed disks vibration analysis. As currently, integrated bladed disk model approach have obsoletes coupled bladed disks in small jet turbines and gives an open end of research in free and forced vibrations. Figure 2.6 depicts a newly designed integrated bladed rotor (IBR).

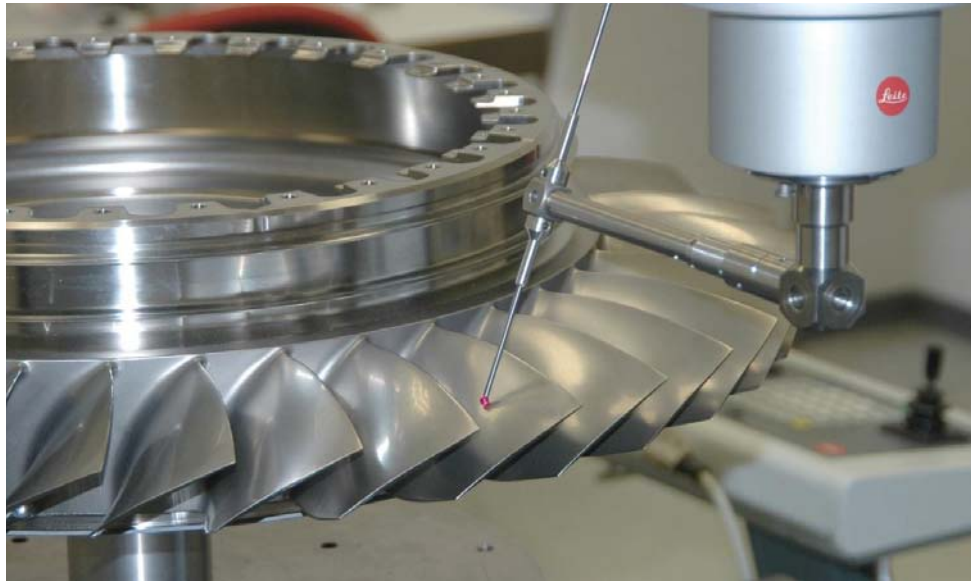


*Fig. 2.6 Integrated bladed rotor (IBR) (source: [www.hexagonmetrology.com](http://www.hexagonmetrology.com))*

IBR – are rotor blades for aircraft engines. They are manufactured in one piece instead of being assembled from several pieces as with older technologies. Currently, there is not much literature available in IBR on free or forced vibration analysis.

## 2.4 CONCLUSION

All technological application of rotationally periodic structures has been under a thorough on-going research. It has been observed from the literature that there are still some open ended research areas available in field of vibratory, thermal and shock response. For example, the dominant excitation in gears is at the tooth mesh, but unacceptable noise is radiated primarily from the housing [25]. In hard disk spindle system, different operational

conditions cause track mis-registration (TMR) problems to drive. Non-operational shock stress over HDD because head damage in HDDs. Therefore, further improvement is inevitable in field of vibration and thermal response of HDD spindle system.

In case of jet turbines, most research has been done on discrete vibration; because of complications less literature is available on continuous vibration. In disk bladed system of turbines, previous studies have focused on coupled bladed systems, their effects on the structure's frequencies and mode shapes have thoroughly examined but very little literature, however, address integrated bladed systems with continuous vibration analysis.

Motivated by the aforementioned engineering concerns and demand to reduce engine size for unmanned aerial vehicle, iterates that IBR free vibrations becomes essential and integrated bladed rotor (IBR) model as a typical cyclic symmetric structure has been selected and is focus of the next chapter. Design focus of the present study is placed on ensuring the mechanical integrity of a prototypical bladed disk, or blisk, and its natural modes through experimental, numerical and finite element parameter studies. Free vibration response on integrally bladed rotor (IBR) as a key example on rotationally periodic structure is discussed thoroughly in the next chapter.

## CHAPTER 3

# FREE VIBRATION RESPONSE OF ROTATIONALLY PERIODIC STRUCTURES

### PRÉCIS

<b>Response selection:</b>	Free vibrations
<b>Model selection:</b>	Integrated bladed rotor
<b>Problem statement:</b>	Investigation on free vibrations on newly designed IBR's as RPS

### 3.1 INTRODUCTION

Localized vibrations are commonly observed in rotationally periodic structures or cyclic symmetric structures [1-4] such as the integrated bladed rotors (IBR) exemplified in Fig. 2.6. The localized vibrations can potentially contribute to large dynamic responses which are locked on to the structures when they are subjected to engine order and external shock and vibration excitations. Therefore, careful dynamic engineering research on the subject area through natural vibration modes is of great importance and is critical to the dynamic design of cyclic symmetric rotor structure systems.

As opposed to periodically packing blades on to rigid rotors and taking out for maintenance in jet engines and power generation turbine applications, in IBRs blades are integrated to the underlying disk rotor during manufacturing process. When blades are packed to a rotor, due to mechanical and handling tolerance, unexpected and uncontrolled structural dynamics can occur. In the literature, direct contact friction dampers [7-9] are reported to be effective in moderating the vibrations. Motivated by the aforementioned engineering concerns and demand to reduce engine size for unmanned aerial vehicle, iterates that IBR free vibrations becomes essential and is the focus of this research. Design focus of the present study is placed on ensuring the mechanical integrity of a prototypical bladed disk, or blisk, and its natural modes through numerical, experimental and finite element parameter studies.



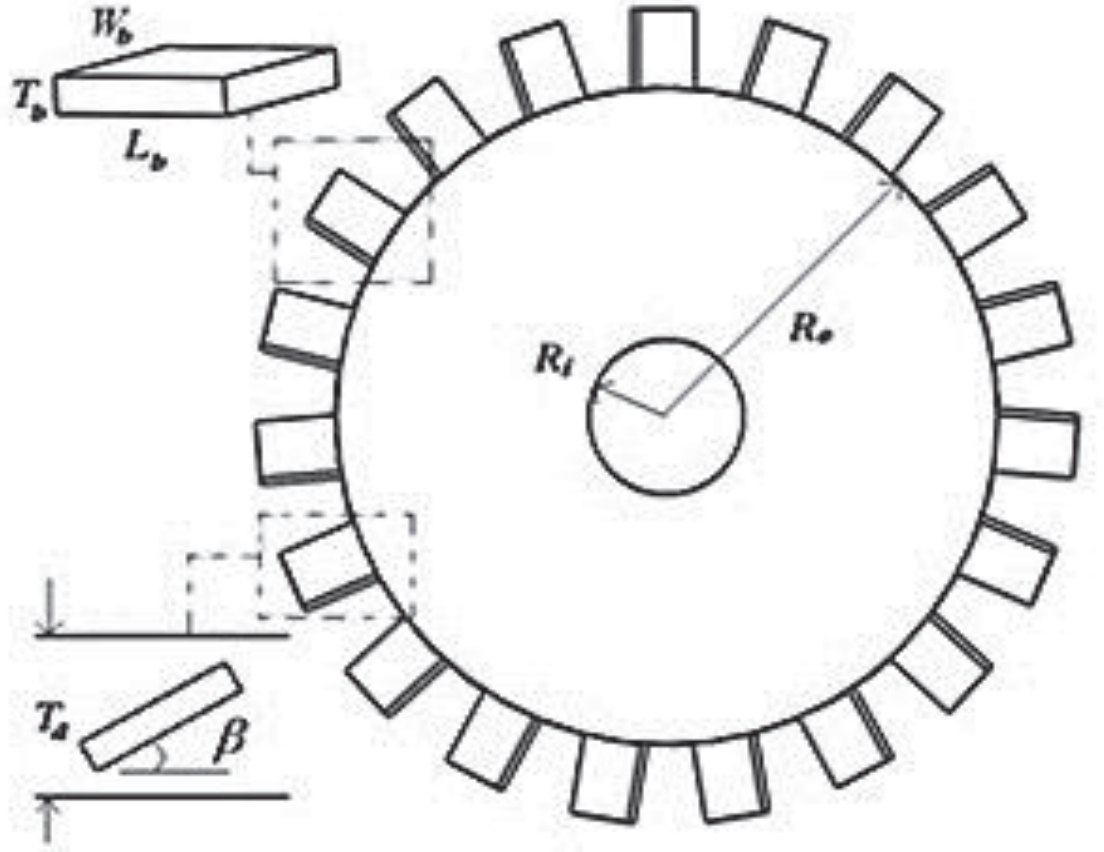


*Fig. 3.1 Schematics of rapid prototyped model of an integrally bladed rotor*

### 3.2 FINITE ELEMENT MODEL

An integrated bladed rotor having  $N_b = 19$  identical plate-like blades superimposed on underlying uniform circular plate as depicted in Fig.3.1 is constructed by using commercial finite-element package. Tetrahedral three-dimensional elements with linear shape functions were used in constructing the model which is axis-symmetrically clamped at inner radius  $R_i$  and free of constraints elsewhere. Plastic type ABS is assumed and its material properties are applied homogeneously in the IBR finite element model. Fixed structural parameters listed in Table 3.1 form the basis of the present free vibration study in which vibrations and dynamics of the underlying disk and blades are intentionally set to be comparable. Effects of the blade angle,  $\beta$ , and blade thickness,  $T_b$  as listed in Table 3.1 on

morphing of natural frequencies and mode shapes of the thermal stress-free IBR are the engineering focus of this study which has design implications in jet engine industry.

Table 3.1: Design parameters of the IBR

Fix structural parameters	Symbols	Values
Number of blades	$N_b$	19
Disk thickness	$T_d$	12.5 mm
Disk outer radius	$R_o$	62.5 mm
Disk inner radius	$R_i$	6.25 mm
Blade width	$W_b$	12.5 mm
Blade length	$L_b$	15 mm
Variable structural parameter		
Blade angle	$\beta$	$0^\circ - 60^\circ$
Blade thickness	$T_b$	1 - 7 mm

### 3.2.1 CONVERGENCE STUDY

Convergence of the structure's natural frequencies was first examined by increasing number of meshing elements globally in the IBR model. Natural frequencies of the lowest couple of natural modes of the IBR model are plotted as a function of number of element in Fig.3.2 in which convergence with 2% of allowable error can be declared when roughly 12000 elements are used. Natural frequencies for all the modes are observed to be within 0.5% error when 40000 elements are used. To save computation time, 12000 elements were adopted in all finite element models with focus given to understanding effect of blade angle,  $\beta$ , and blade thickness,  $T_b$ , on the IBR's free vibration natural frequencies and modes.

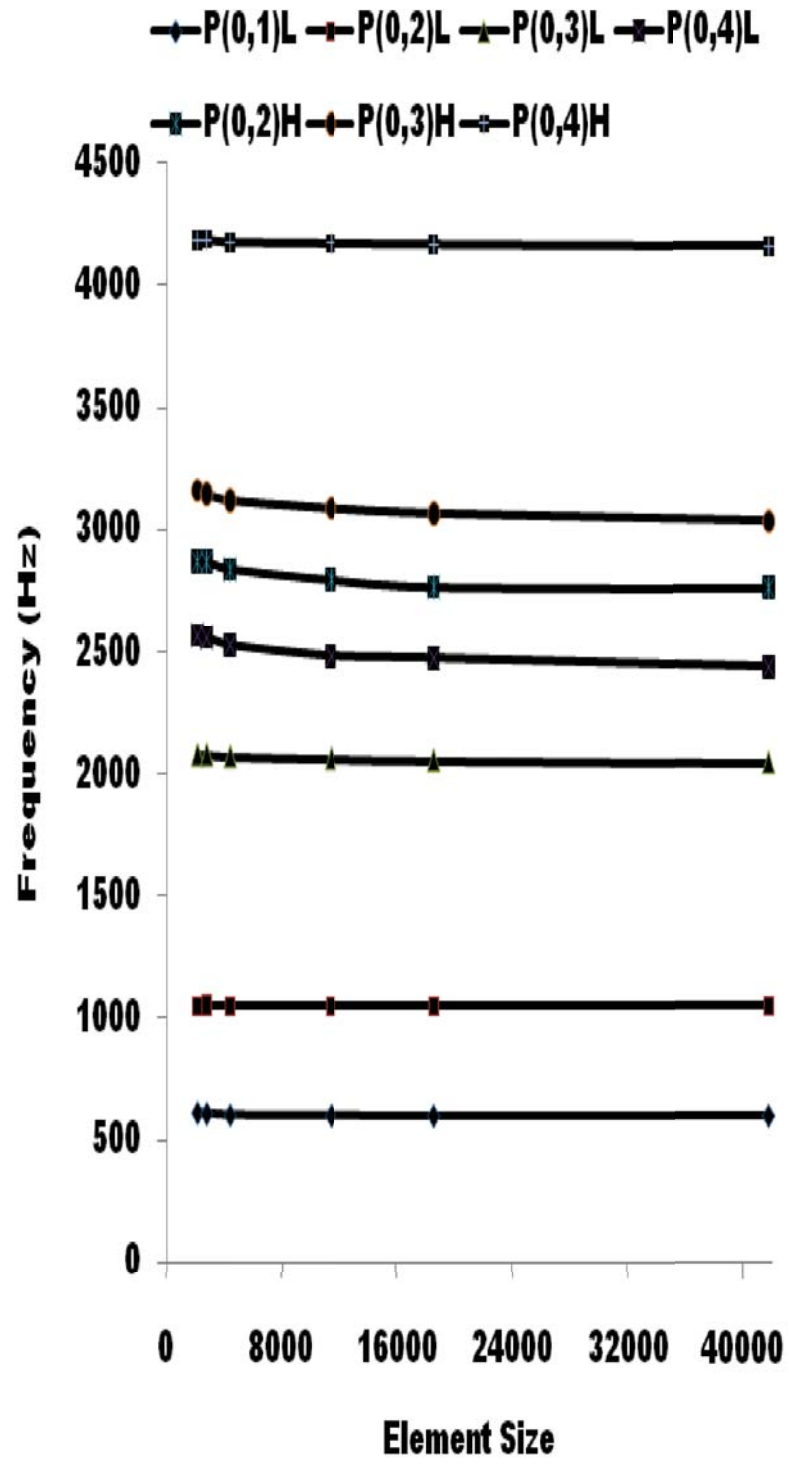


Fig. 3.2 Convergence of frequency modes of the present IBR model at  $N_b = 19$ ,  $\beta = 30^\circ$ .

### 3.3 REPLICA MODES

Following nomenclature and mode structure characterized in references [1-2], letter P is given to distinguish the IBR's vibration modes from those modes denoted as  $(m, n)$  in axis-symmetric case, where  $m$  represents number of nodal circles and  $n$  is the number nodal diameters, respectively. For instance,  $P(0, 1)$  stands for the IBR's vibration mode having zero nodal circle and one "nodal line" while  $(0, 1)$  implies vibration mode of zero nodal circle and one "nodal diameter" in axis-symmetric disk case. As stated in the literature, for nonzero  $n$ , sine,  $S$ , and cosine,  $C$ , modes repeat in frequency for each  $P(m, n)$  and  $(m, n)$  modes. When vibrating kinetic energies stored in blade- and disk-subsystem of an IBR are comparable, replica modes are observed. Replica modes denoted as  $R(m, n)$  is mathematically defined as:

$$R(m, n) \in \{P(m, n)_L, P(m, n)_H\}, \quad (1)$$

Where subscripts 'L' stands for lower frequency pair and 'H' stands for higher frequency repeated pair, respectively. For the lower frequency pair, repeated frequency sine mode,  $P(m, n)S$  and cosine mode  $P(m, n)C$  constitute to the replica mode  $R(m, n)$  having blade vibrations in-phase to disk vibrations whereas for higher frequency pair, blades are vibrating out-of-phase to disk vibrations. As illustrative examples, mode shapes of several replica modes are shown in Fig. 3.3 and Fig. 3.4 when the model IBR is with  $N_b = 19$ ,  $\beta = 30^\circ$ . Note that  $(\uparrow\uparrow)$  and  $(\uparrow\downarrow)$  are given to indicate in-phase and out-of-phase blade to disk vibrations for each replica mode component having natural frequency  $\omega_L$  and  $\omega_H$ , respectively.

In literature [1-6], addition of blades to the baseline axis-symmetric disk has been commonly assumed to be point stiffness and inertia perturbations. Although modulated modes  $P(m, n)$  have been theoretically and experimentally proven in reference [1-2] for rotationally periodic structures, which provide physical explanation of dispersive traveling wave components commonly observed in real engineering practice, little has been focused on substructure interaction on the vibration modes in IBR case. On the other hand, to give

quick dynamics estimation in wind turbine or gas turbine rotors, blades are frequently modelled as flexible beams attached rigid rotors [7-9].

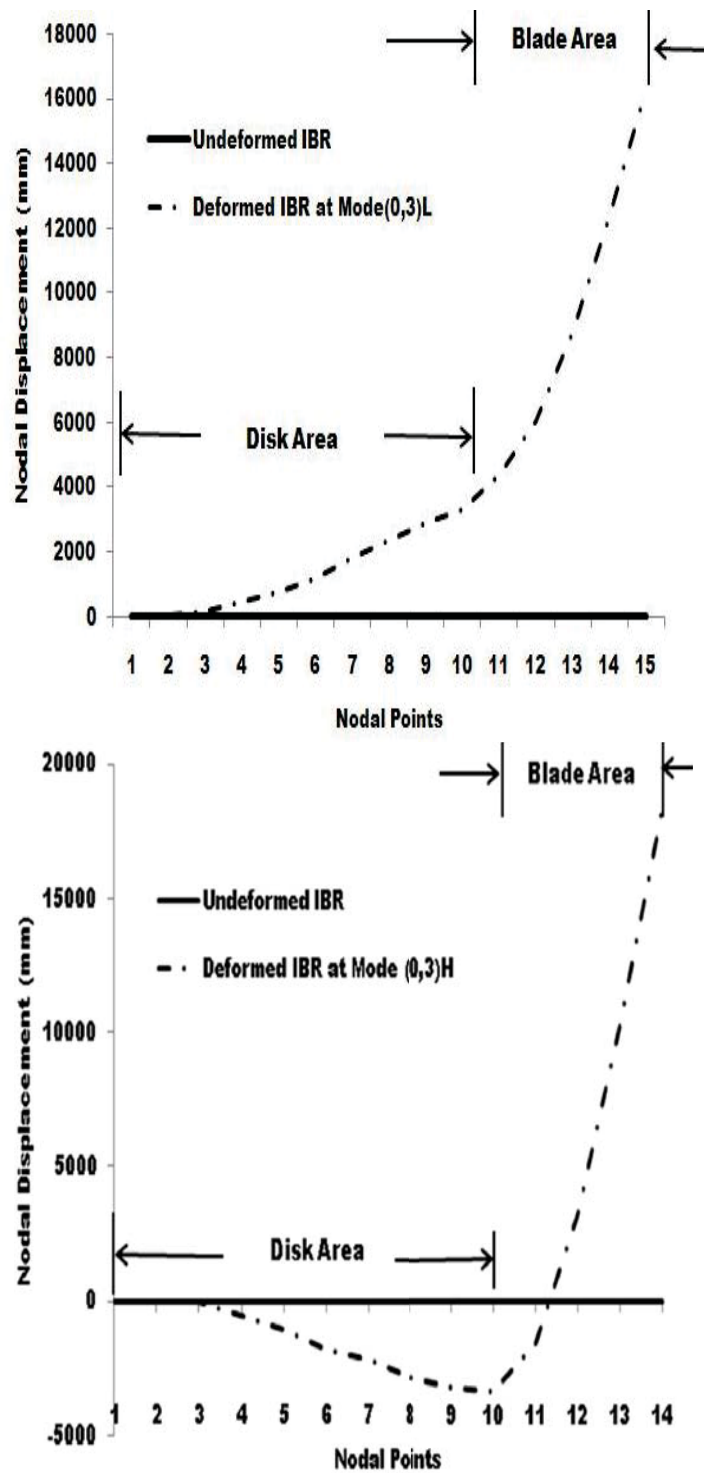


Fig. 3.3 Example of (a) = in-phase ( $\uparrow\uparrow$ ) and (b) = out-of-phase ( $\uparrow\downarrow$ ) replica mode components of the IBR at  $N_b = 19, \beta = 30^\circ$ .







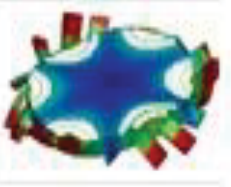

Mode	$P(0, 1)_L$	$P(0, 2)_L$	$P(0, 3)_L$	$P(0, 4)_L$
$(\uparrow\uparrow)$ $P(m, n)_L$				
$\omega_L$	603 Hz	1050 Hz	2055 Hz	2502 Hz
	$P(0, 1)_H$	$P(0, 2)_H$	$P(0, 3)_H$	$P(0, 4)_H$
$(\uparrow\downarrow)$ $P(m, n)_H$				
$\omega_H$	2778 Hz	2822 Hz	3140 Hz	4453 Hz

Fig. 3.4 Finite Element Analysis pictures of in-phase ( $\uparrow\uparrow$ ) and out-of-phase ( $\uparrow\downarrow$ ) replica mode components of the IBR at

### 3.4 LUMPED MASS MODEL APPROACH

The prediction of natural frequencies, mode shapes, and free and forced response analysis is essential part of bladed disk designs. Although more powerful and expensive techniques are available, it is still worthwhile of adapting lumped mass parameter models which help determining some invariant properties in cost effective and simple ways. For the reason of their reduced order size and simplicity, this approach has been adapted by many researchers, and the methods of finding natural frequencies, mode shapes and their responses have been well established. J.T Wagner [45] was the first to proposed a lumped mass model in which he included an elastic foundation of the massless disk to take care of reduction of blade alone frequencies as shown in fig. 3.5

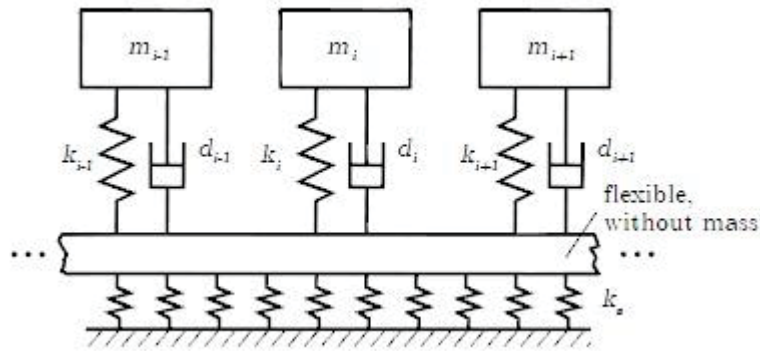


Fig. 3.5 Lumped mass model with flexible disk approach [45]

Sinha [46] also considered the mechanical coupling by spring elements while the each blades structural parameter were adjusted by dashpots and spring connections with the ground as depicted in figure 3.6. Similar approaches have been carried out by Kenyon [36], mignolet [46], Wei and Perrie [49].

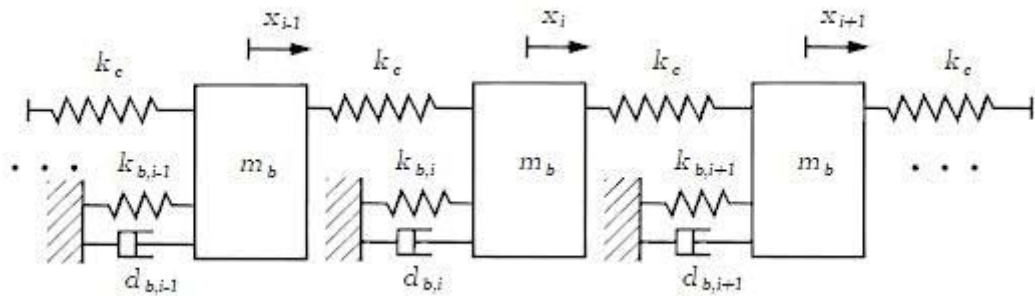


Fig. 3.6 Lumped mass model with interbladed connectors [46]

A slightly different and more sophisticated model has been adapted by Griffin [30] who employed two or three degree of freedoms per sector as shown in fig.3.7.

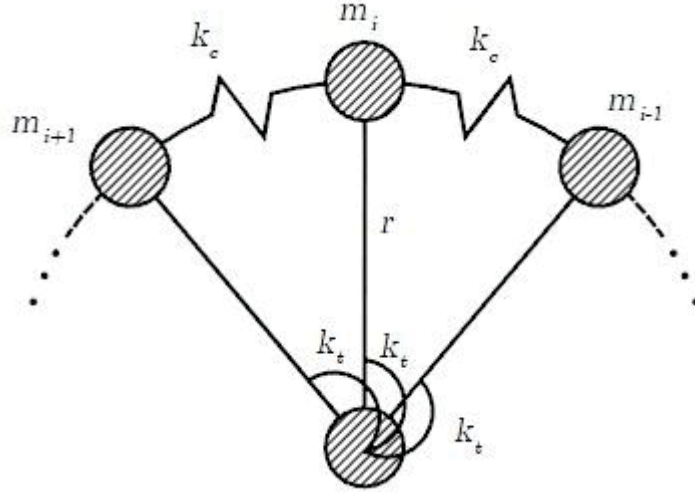


Fig. 3.7 Sophisticated Lumped mass model with inter-blade connectors [30]

Concisely, the use of lumped mass models is a common method for the analysis of blisks which has been mainly restricted to research purposes. Their ability to give reasonable results has been approved by many researchers. Hence, a lumped mass model was chosen for establishing an IBR model and its free vibration behavior without damping and structural stiffness effects.

### 3.4.1 EQUIVALENT IBR MODEL

On the basis of the aforementioned range of lumped mass models, an equivalent IBR model has been developed which comprises two degrees of freedom per disk sector as shown in fig 3.8. Here the spring and mass with the index  $d$  represent the disk part of the sector. Additionally,  $K_g$  is added as structural stiffness with which the assembly is attached to the ground, it may be thought as the stiffness of the shaft with which the disk is attached. In current free vibration analysis and interest in the outer ring of integrally bladed disk, the value of  $K_g$  has been taken as zero. And finally the elements with index  $b$  are used to adapt the blades properties to measured data.



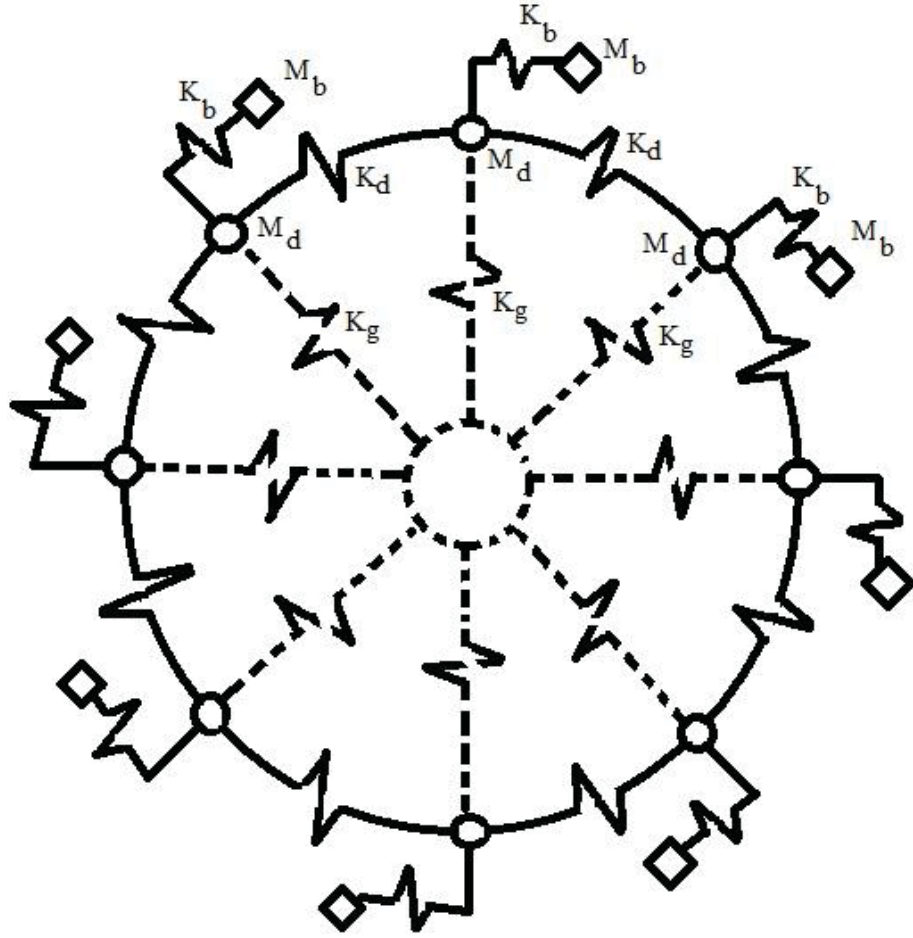


Fig. 3.8 Equivalent Integrally Bladed Disk (IBR) lumped mass model

### 3.4.2 EQUATION OF MOTION (EOM)

To establish the equation of motion for the predicted lumped mass model, a  $j^{\text{th}}$  sector has been taken as shown in fig. 3.9

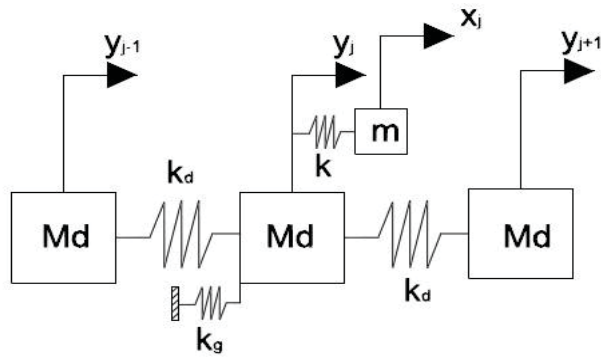


Fig. 3.9  $J^{\text{th}}$  sector of designed integrally bladed disk (IBR)

The figure shown represent  $j^{\text{th}}$  sector of the disk. The kinetic and potential energy for this sector can be written as:

$$\begin{aligned} KE &= \frac{1}{2}M_d\dot{y}_j^2 + \frac{1}{2}m\dot{x}_j^2 \\ PE &= \frac{1}{2}k_g\dot{y}_j^2 + \frac{1}{2}k_d(y_j - y_{j-1})^2 + \frac{1}{2}k_d(y_j - y_{j+1})^2 + \frac{1}{2}k(y_j - x_j)^2 \end{aligned} \quad (1)$$

Using the Lagrange equation, the equations of motion (EOM) for the  $j^{\text{th}}$  sector can be written as:

$$\begin{aligned} m\ddot{x}_j + k(x_j - y_j) &= 0 \\ M_d\ddot{y}_j + k(y_j - x_j) + k_g y_j + k_d(2y_j - y_{j-1} - y_{j+1}) &= 0 \end{aligned} \quad (2)$$

Using this general form, the EOMs for all sectors can easily be written. Let say we have  $n$  number of sectors then, due to the cyclic symmetry it is noted that for the 1st sector  $y_{j-1}$  is  $y_n$ , whereas for the last ( $n^{\text{th}}$ ) sector  $y_{j+1}$  will be  $y_1$ .

For example for the case of three sectors the equations are:

$$\begin{aligned} m\ddot{x}_1 + k(x_1 - y_1) &= 0 \\ M_d\ddot{y}_1 + k(y_1 - x_1) + k_g y_1 + k_d(2y_1 - y_3 - y_2) &= 0 \\ m\ddot{x}_2 + k(x_2 - y_2) &= 0 \\ M_d\ddot{y}_2 + k(y_2 - x_2) + k_g y_2 + k_d(2y_2 - y_1 - y_3) &= 0 \\ m\ddot{x}_3 + k(x_3 - y_3) &= 0 \\ M_d\ddot{y}_3 + k(y_3 - x_3) + k_g y_3 + k_d(2y_3 - y_2 - y_1) &= 0 \end{aligned} \quad (3)$$

The coefficients of mass and stiffness matrix can easily be separated from the above equations and the general form of the equation can be written as:

$$M\ddot{X} + KX = 0 \quad (4)$$

Where  $M$  and  $K$  are  $2n \times 2n$  mass and stiffness matrices, where  $n$  is 3 in this case. The form of the generalized coordinate vector is:

$$X = [ \cdots \quad X_j \quad Y_j \quad \cdots ]^T \quad (5)$$

### 3.5 PARAMETRIC STUDY

Integrated bladed rotors are used to sustain and transform high cycle fatigue (HCF) and low cycle fatigue (LCF) loads into other energy forms in turbines engines [7-10]. Blade angle and blade thickness are found to be the two most important design parameters for airfoils to meet thermodynamics and aerodynamics performance targets in gas turbines and wind turbines [9]. In this section, transition of replica modes of the IBR as depicted in Fig. 3.4 at various blade angle and blade thickness values will be studied.

#### 3.5.1 REPLICA MODES WITH VARYING BLADE ANGLE

Parametric study of changing blade angle,  $\beta$ , as shown in Fig. 3.10 while leaving all the other parameters fixed including blade thickness  $T_b$  at 5mm is conducted. Migration of the IBR's natural frequencies as a function of blade angle is plotted in Fig. 3.11 for selected replica mode pairs of  $P(0, 2)_L$ ,  $P(0, 2)_H$ ,  $P(0, 3)_L$ ,  $P(0, 3)_H$ ,  $P(0, 4)_L$ ,  $P(0, 4)_H$  and repeated doublet mode  $P(0, 1)$ . It is found that replication doesn't exist for repeated frequency doublet mode at  $n = 1$ .

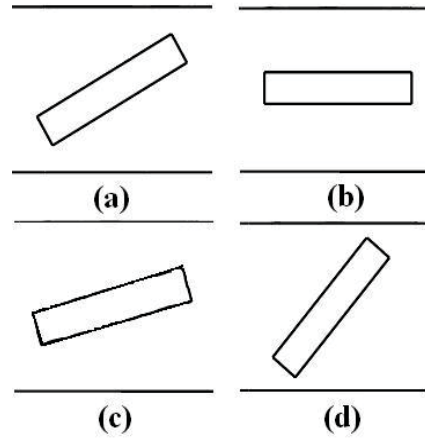


Fig. 3.10 Schematics of different blade angle at (a) 30°, (b) 0°, (c) 15°, and (d) 50°

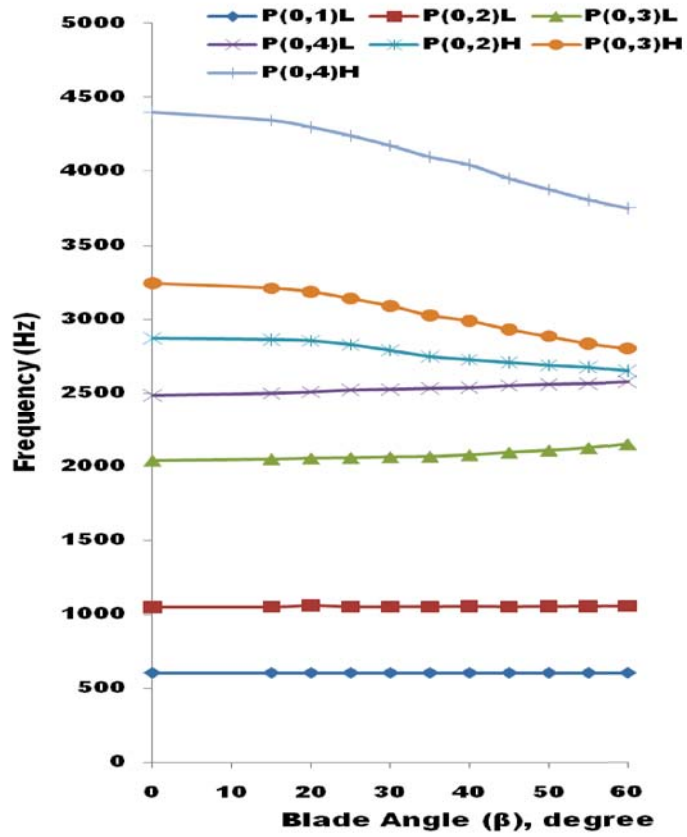


Fig. 3.11 Migration of replica modes as a function of blade angle;  $N_b = 19$  and  $T_b = 5\text{mm}$

The implication of this merging phenomenon can be explained as what follows. For low frequency component of a replica mode, blades are to vibrate in-phase with the disk. When blades have low bending rigidity value, which corresponds to small blade angle, the IBR vibrates such as blades are viewed as added masses on to the disk.

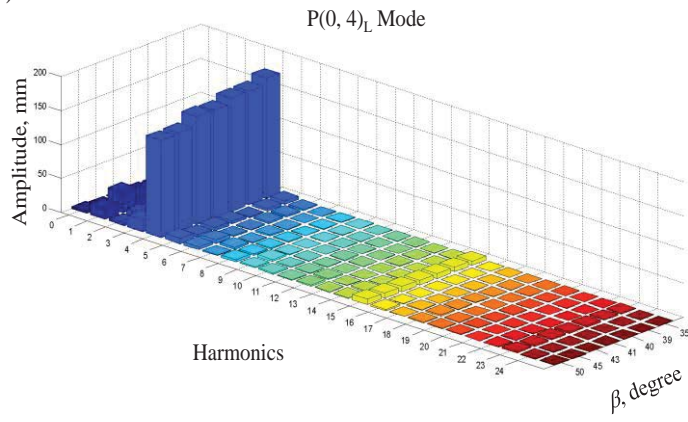
Since blades still need to be bended flexibly in-phase with the disk, so when blade angle increases, natural vibrations of the IBR can be viewed as more added stiffness components from more “rigid” blades. For high frequency component of a replica mode on the other hand, blades need to vibrate out-of-phase to the disk. When blade angle increases, the blades vibration is decreased because of higher bending rigidity from geometry. Therefore, less stiffness components as well as kinetic energy are associated with the vibration, which result in decreasing value in its natural frequency. For instance, if blades are perpendicular to the disk, that is  $\beta = 90^\circ$ , they can be viewed as point inertia to the disk, which results in lower natural frequency than viewing the blades as added kinetic energy carriers.

This phenomenon depicts a dangerous swarming of modes at a certain close range of frequencies as the blade angle increases [12-13]. Running turbine near this frequency range could be catastrophic causing resonant vibrations at multiple modal responses. On the other hand, one can use this technique of merging modes in structure design to allow wider operation range for turbines with lower risk in hitting at resonant modes. Modification of blade angle is found to cause significant change in a replica mode’s modal content. The slight increase and decrease in natural frequencies due to the blade angle change correspond to those shown in Fig. 3.11 for the  $P(0, 4)_L$  and  $P(0, 4)_H$  replica pair, respectively. Although change in natural frequencies is not phenomenal, two new phenomena are observed regarding the mode’s nodal content.

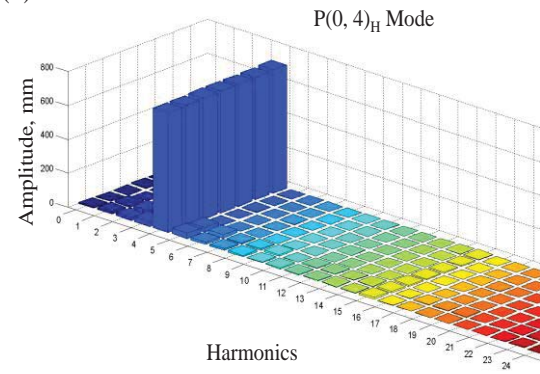
First of all, the nodal pattern is significantly distorted for the low frequency component of the replica mode, the  $P(0, 4)_L$  mode. Secondly, the nodal pattern appears to be locked on to the IBR structure for high frequency component of the same replica mode, the  $P(0, 4)_H$  as depicted in fig. 3.12. The statement holds true for all replica modes. When the blade angle increases toward  $50^\circ$ , nodal pattern of the  $P(0, 4)_L$  is completely distorted or modulated by addition of other contaminated wavenumbers,  $k$  as defined in reference [40] from which out-of-plane nodal displacement  $u$  of the IBR’s replica mode  $R(m, n)$  at  $R_o$  can be written in Fourier representation of

$$u_{R(m,n)}(R_o, \theta) = \sum_{k=0}^{\infty} A_k \cos(k\theta) + B_k \sin(k\theta) \quad (6)$$

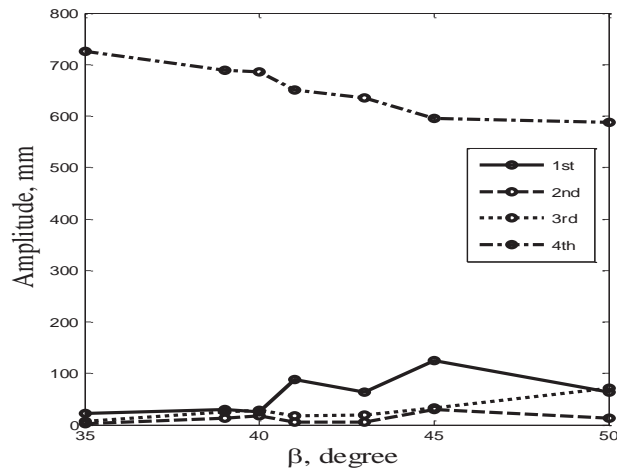
(a)



(b)



(a)



(b)

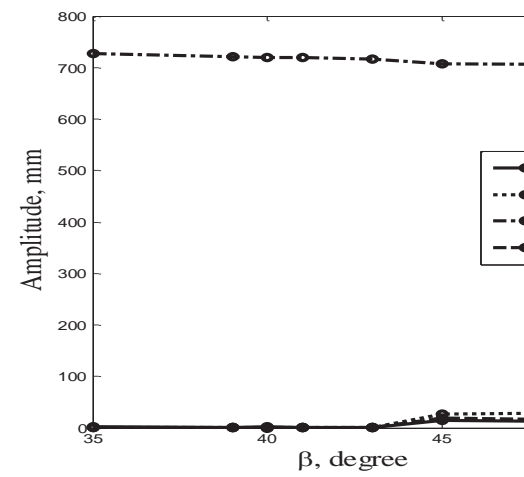


Fig. 3.12 Fourier amplitudes of replica (a)  $P(0, 4)_L$  and (b)  $P(0, 4)_H$  mode of the model IBR with different blade

where  $\theta$  is the circumferential measure starting from center of a blade. Using nodal displacement at  $R_o$  from the model IBR with blade thickness  $T_b = 5\text{mm}$ , Fourier amplitude  $C_k = \sqrt{A_k^2 + B_k^2}$  is plotted for each blade angle up to  $k = 25$  harmonic count in Fig. 3.12 (a) for  $P(0, 4)_L$  and (b) for  $P(0, 4)_H$ , respectively. Obviously  $C_4$  dominates the Fourier spectrum. This is because the mode, the  $R(0, 4)$  replica mode, being concerned has base wavenumber at  $n=4$ . If one looks closer in the Fourier spectra in Fig. 3.12, nonzero  $C_k$  can be found at  $k = 15$  and  $k = 23$ , which apparently satisfies the following modulation criteria reported by Chang and Wickert in references [1-2] when  $N_b=19$  blades are integrated to the baseline axis-symmetric disk

$$|n \pm k| = N_b, 2N_b, 3N_b \dots \quad (7)$$

Although the 4<sup>th</sup> harmonic, the  $n = 4$  base wavenumber, dominates the mode's Fourier spectra, as shown in Fig. 3.12, it is observed that  $C_4$  amplitude decrease significantly for the low frequency component, the  $P(0, 4)_L$  mode, when blade angle increases. Using the present IBR model for an example,  $C_4$  value at  $\beta = 50^\circ$  is 20% smaller than that at  $\beta = 35^\circ$ . It is also noted that the corresponding  $C_4$  amplitude is less sensitive to change of blade angle for high frequency component, the  $P(0, 4)_H$  mode, of the replica mode. This new finding has signification design implications in forced response.

For instance, if placement of external excitation frequency at or closer to  $P(0, 4)_L$ 's natural frequency is inevitable; one can simply change the blade angle to reduce its base wave's contribution, the  $C_4$ , so as to result in lower forced response amplitude. Of course, changing the blade angle for structure dynamics also needs to balance or trade off with design considerations from thermodynamic performance perspectives.

### 3.5.2 REPLICA MODES WITH VARYING BLADE THICKNESS

Parametric study by varying blade thickness,  $T_b$ , as shown in Fig. 3.13 while leaving other parameters constant including blade angle at  $30^\circ$  for the model IBR structure is conducted and discussed in this section.

With fixed blade angle, morphing of the IBR's natural frequencies for repeated doublet  $P(0, 1)$  and  $P(0, 2)_L, P(0, 2)_H, P(0, 3)_L, P(0, 3)_H, P(0, 4)_L$  and  $P(0, 4)_H$  replica mode pairs is observed in Fig. 3.14 against different blade thickness. The solid circles on vertical axis at 0 blade thickness represent natural frequencies for (0, 1)-(0, 4) nodal diameter modes of the underlying axis-symmetric annular disk. When blade thickness deviates slightly from  $T_b = 0$ , the nodal diameter modes become repeated doublet  $P(m, n)$  modes, in which nodal diameters are distorted similar to those shown in Fig. 3.12. When blade thickness continues to increase, replica mode pairs are then observed.

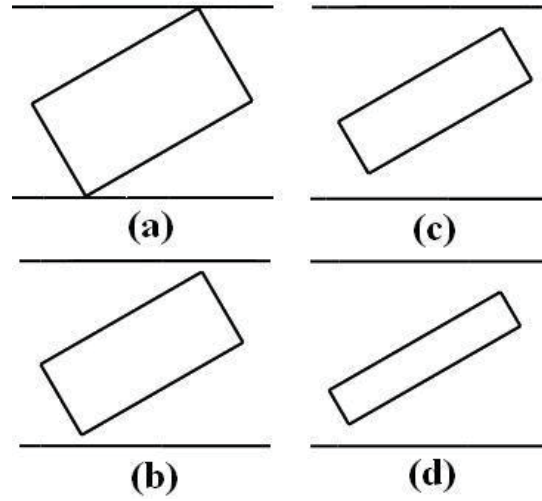


Fig. 3.13 Schematic illustrations of different blade thickness,  $T_b$  at (a) 14mm, (b) 11mm, (c) 8mm, and (d) 5mm

There are a number of interesting phenomena worth noticing in Fig. 3.14. Firstly, when the structure deviates from axis-symmetric and become cyclic symmetric, bifurcation in natural frequency is observed for replica modes at with wavenumber  $n > 1$ . For instance, the (0, 2) becomes replica pair  $P(0, 2)_L$  and  $P(0, 2)_H$ .

Secondly, veering of frequency loci is observed for high frequency replica mode components. For an example, in Fig. 3.14, when blade thickness is greater than 3 mm, frequency traces for  $P(0, 2)_H, P(0, 3)_H$  and  $P(0, 4)_H$  modes veer and cluster with each other. This clustering and veering of frequencies have implication in engine operations. One can simply vary the blade thickness to “lump” multiple modes at certain frequency ranges to allow more freedom for engine operations. On the other hand, one can conclude that by adding blade thickness the high and low frequency replica modes depart away from



each other. This divergence is important in keeping relevant natural frequencies of the IBR at running speed sufficiently far apart from the excitation frequencies.

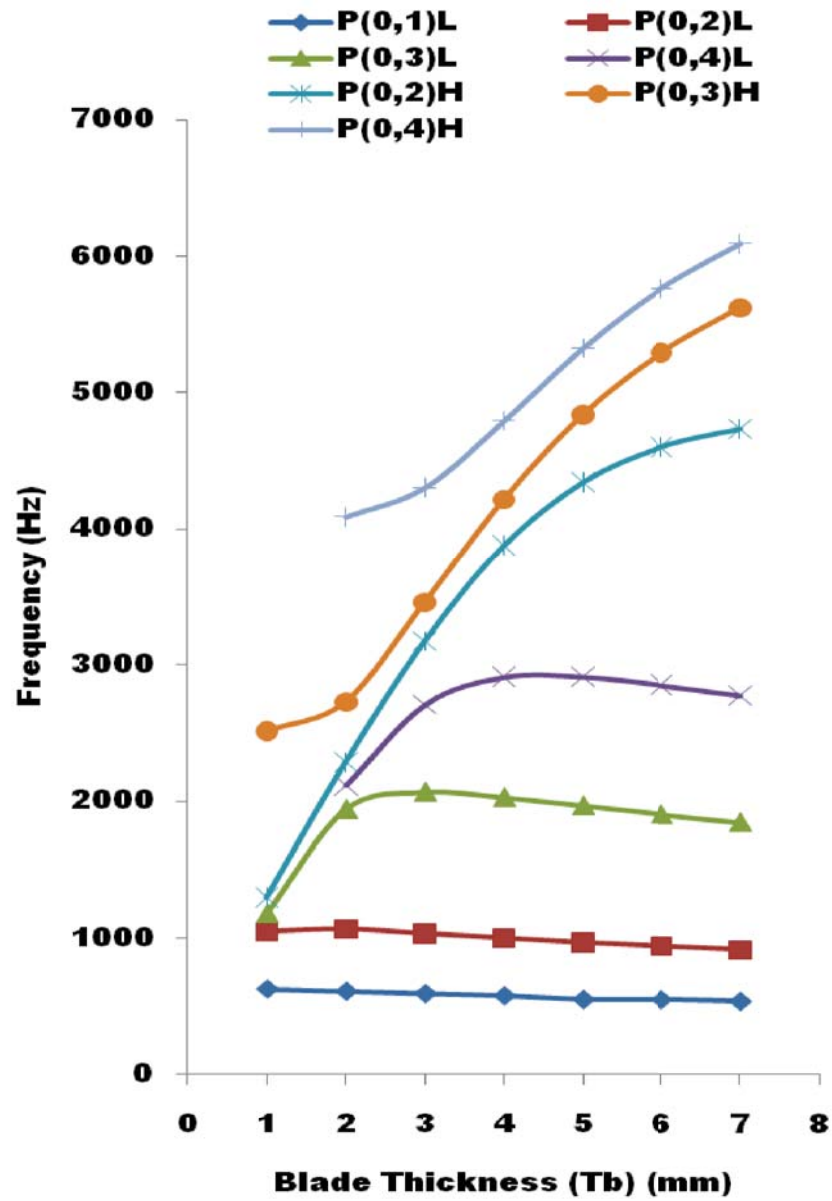


Fig. 3.14 Migration of replica modes as a function of blade thickness;  $\beta = 30^\circ$

### 3.6 MODULATED STIFFNESS ANALYSIS

Modulation of mode shape and natural frequency with respect to change in blade angle depicts that there is some hidden wave-number contaminating the current IBR model. Since no further mass was added in this parametric approach, it was assumed that

contaminating factor resides in blade stiffness. Using the present IBR model as an example different force has been imposed to determine stiffness modulation. To uncover the trend, hook's law has been applied:

$$K_{\beta} = - F_{\beta} / U_{k(n)\beta}, \quad (4)$$

where  $F_{\beta}$  is Force exerted normal to IBR,  $K_{\beta}$  is the spatial modulated stiffness with respect to blade angle and  $U_{k(n)\beta}$  is the displacement from its equilibrium position.

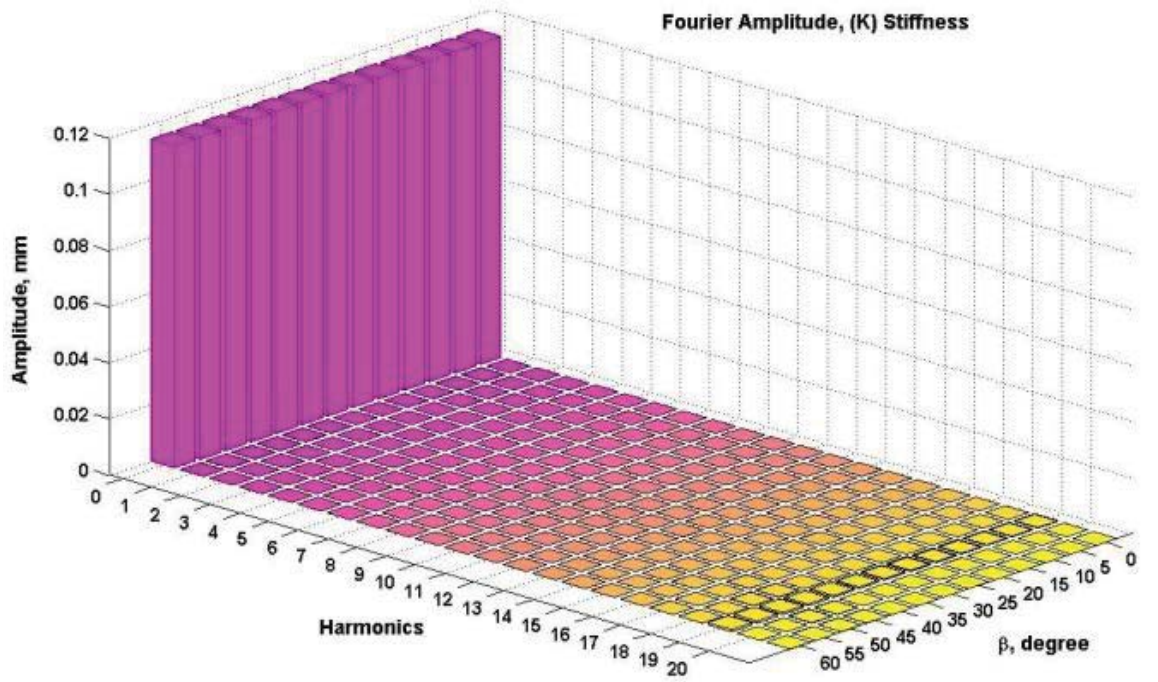


Fig. 3.15 Fourier amplitude of IBR at 1000N force with different blade angles ( $\beta$ )

Figure 3.15 shows the Fourier representation of stiffness sensitivity with change of blade angle after application of known force value. If one look closer at the fourier spectra, it was found that that there is some modulated wave-number present at 19<sup>th</sup> harmonic and varies with change in blade angle. Since present IBR study have  $N_b = 19$  , So  $K_{(n)\beta} = n(19/N_b)$  where  $n=1,2,3....$ stating that 1<sup>st</sup> modulated wave-number is at 19<sup>th</sup> harmonic and so on, which can be represented as

$$K_{\beta} = \Sigma (K_o + K_{1\beta} + K_{2\beta} + K_{3\beta} + \dots), \quad (5)$$

where  $K_\beta$  is total stiffness,  $K_o$  is stiffness of annular disk, and  $K_{1\beta}$ ,  $K_{2\beta}$  and  $K_{3\beta}$  are 1<sup>st</sup>, 2<sup>nd</sup> and 3<sup>rd</sup> harmonics.

To verify stiffness sensitivity value with respect to different force application; 500N, 1000N and 1500N force value was applied to check the contamination wave-number trend. It's been observed that different applied forces effects imperceptible change in the contaminated wave-number trend as shown in fig 3.16; which implies that any force value can be taken for observation. In the experimental analysis, 1000N slope trend has been taken for spatially modulated stiffness wave-number calculation.

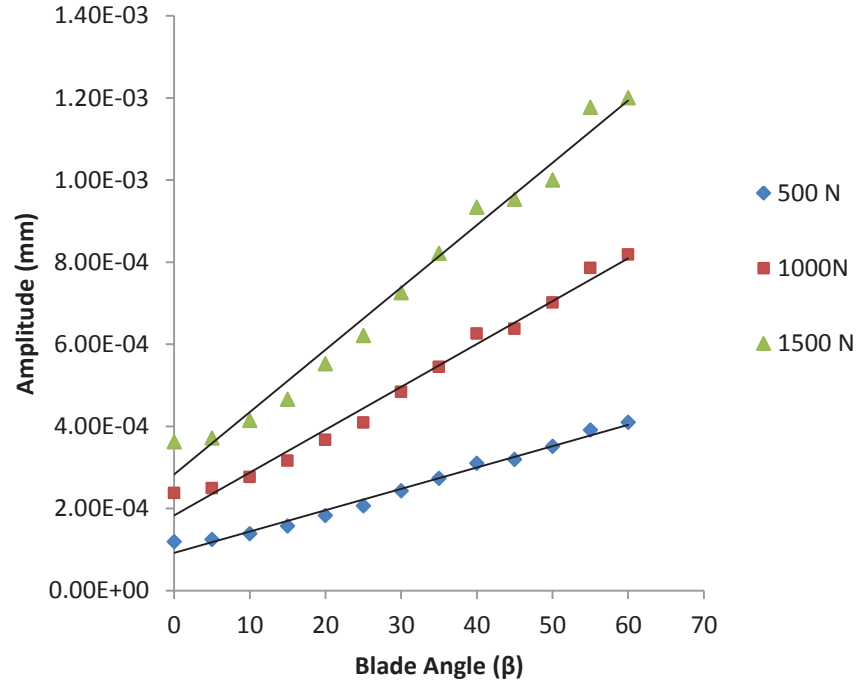


Fig. 3.16 1<sup>st</sup> modulated wavenumber trend at different forces

The task at hand involves calculating the stiffness contamination  $K_\beta$ , for that we need to find out total modulated displacement variation as stated below.

$$U_{k(n)\beta} = \Sigma(U_o + U_{1\beta} + U_{2\beta} + U_{3\beta} + \dots) \quad (6)$$

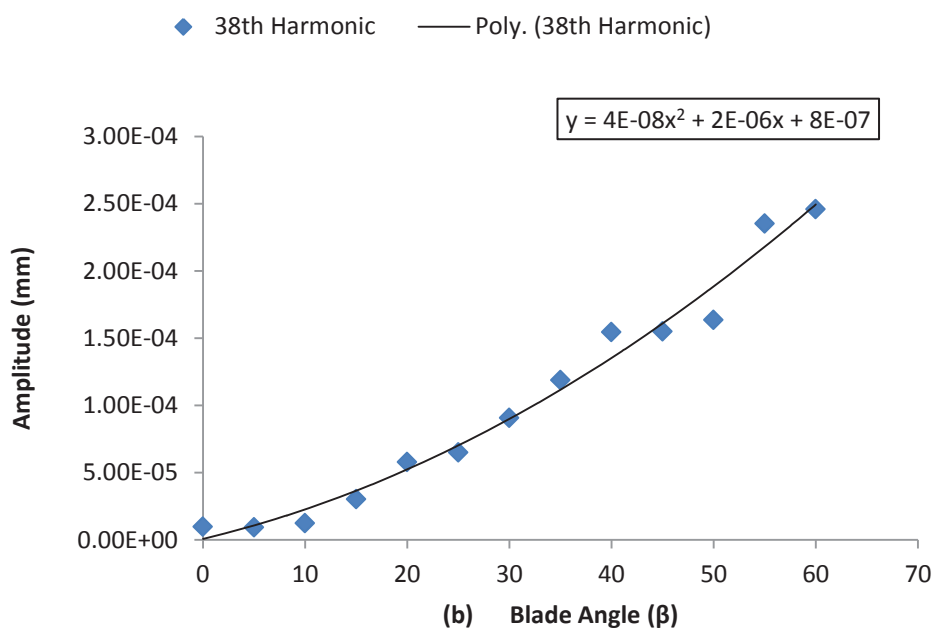
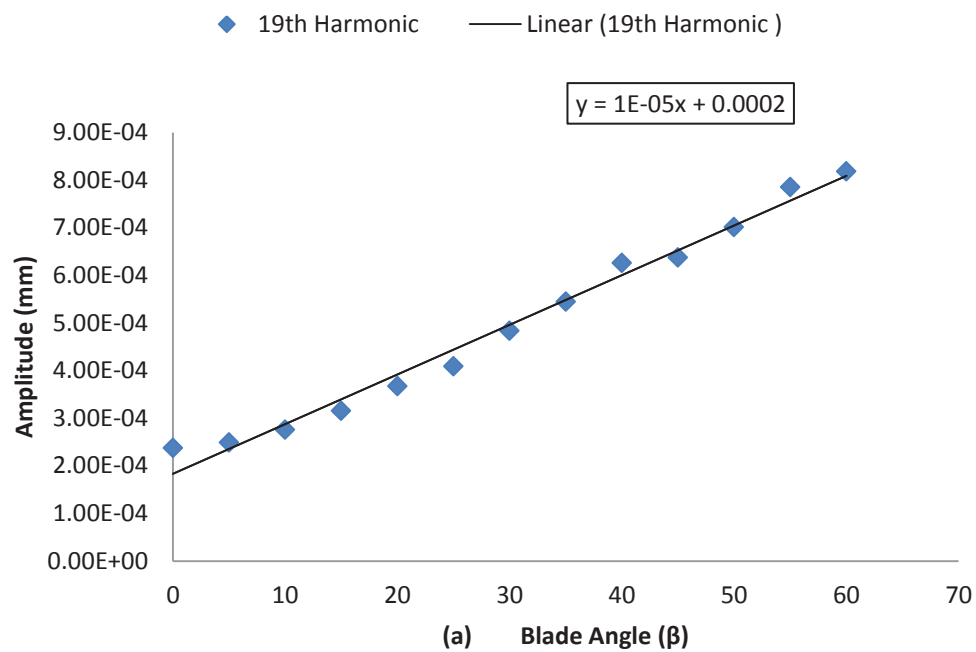
Where,  $U_{k(n)\beta}$  is the total displacement,  $U_o$  is the displacement of annular disk,  $U_o$  is amplitude of annular disk, and  $U_{1\beta}$ ,  $U_{2\beta}$  and  $U_{3\beta}$  are 1<sup>st</sup>, 2<sup>nd</sup> and 3<sup>rd</sup> Fourier harmonics. By using curve fitting technique as depicted in figure 3.17, 1<sup>st</sup> contaminated wavenumber at the 19<sup>th</sup> harmonic was found to be linear with respect to blade angle ( $\beta$ ) as shown in fig. 3.17(a) but as we gradually increase the number of harmonics it has been found that the trend of harmonics is directly proportional to the order of polynomial curve displayed in fig. 3.17(b) and 3.17(c).

In illustrated IBR model example with  $N_b = 19$ , direct substitution of these harmonic expansions into the base stiffness equation, normalizing and grouping of terms of like orders in the present IBR model lead to the following equation:

$$K_\beta = - [F_\beta / (U_{k0\beta} + U_{k1\beta} + U_{k2\beta} + U_{k3\beta} + \dots)] \quad (7)$$

$$K_\beta = - [F_\beta / (1\beta + 1.1E^{-4}\beta^2 + 3.3E^{-5}\beta^3 + \dots + \zeta)] \quad (8)$$

Where,  $\zeta$  is the error factor. The above equation indicates the modulated stiffness trend which occurs in an integrated bladed rotor with respect to change in blade angle. As discussed earlier the aforementioned modelled equation of modulated stiffness is only valid for low frequency replica modes  $P(m, n)_L$ . Since the contamination factor is very small it doesn't affect high frequency replica modes  $P(m, n)_H$ .



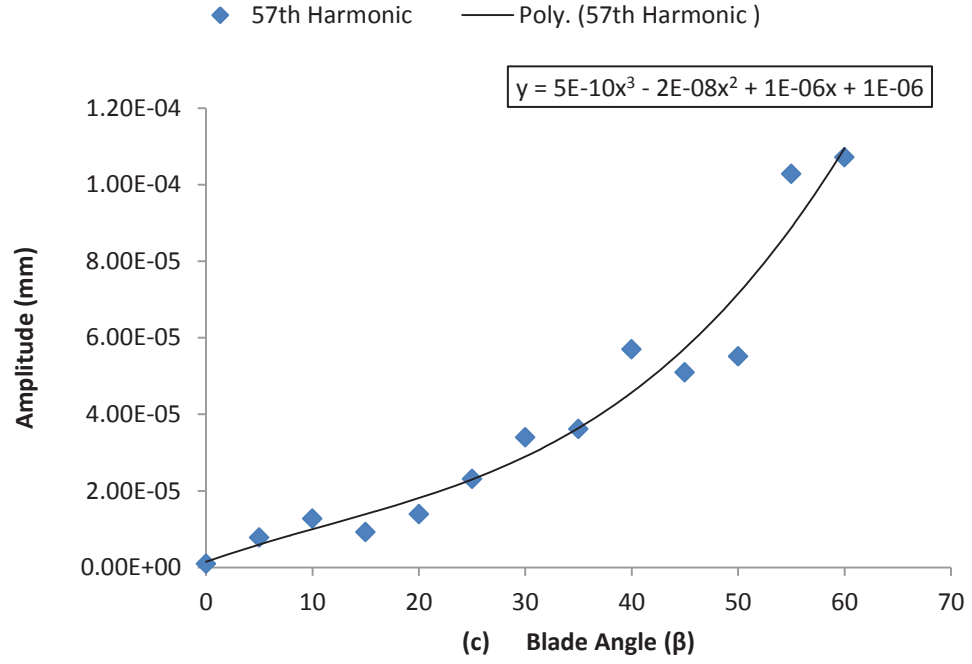


Fig. 3.17 (a) 1<sup>st</sup> harmonic trend with linear fitting (b) 2<sup>nd</sup> harmonic trend with second order polynomial fitting (c) 3<sup>rd</sup> harmonic trend with third order polynomial fitting

### 3.7 EXPERIMENTAL MODAL ANALYSIS

Experimental Modal Analysis is the study of natural characteristics of structures and has been commonly used to help design all types of structures including automotive, aircraft structures, computers, rackets etc. [3, 8-10]. In the past two decades, Modal Analysis has become a major technology in the quest for determining, improving and optimizing dynamic characteristics of engineering structures. It involves the extraction of modal parameters from measurement of dynamic response [31]. The modal parameters may be determined by analytical means, such as finite element analysis, and one of the common reasons for experimental modal analysis is the verification / correction of the results of the analytical approach. Predominately, experimental modal analysis is used to explain a dynamics problem that is not obvious from insight, analytical models, or previous similar experience. Vibration measurements are taken directly from a physical structure, without any assumptions about the structure, and that is the reason why modal testing models are

considered to be more reliable than Finite Element models. In the present study, same modal testing approach was applied on the prototyped IBR to verify the new findings of replica modes.

### 3.7.1 EXPERIMENTAL SETUP

An actual 3D model was developed using 3D printing technique to carry out the experiment as shown in figure 3.18. The model has been developed by means of finite element calculations in such a way that the Eigen frequencies of the model lie close together. Same material properties and boundary conditions were adapted to replicate the finite element model. Fig. 3.19 shows the schematic diagram of the experimental set-up used for modal testing. An excitation signal was generated by an impact hammer with a load cell attached to its head to measure the input force and was sent to dynamic signal analyzer. The vibration amplitude at the measuring locations was sensed by an accelerometer, and monitored by both dynamic signal analyzer and an oscilloscope using a BNC T-connector

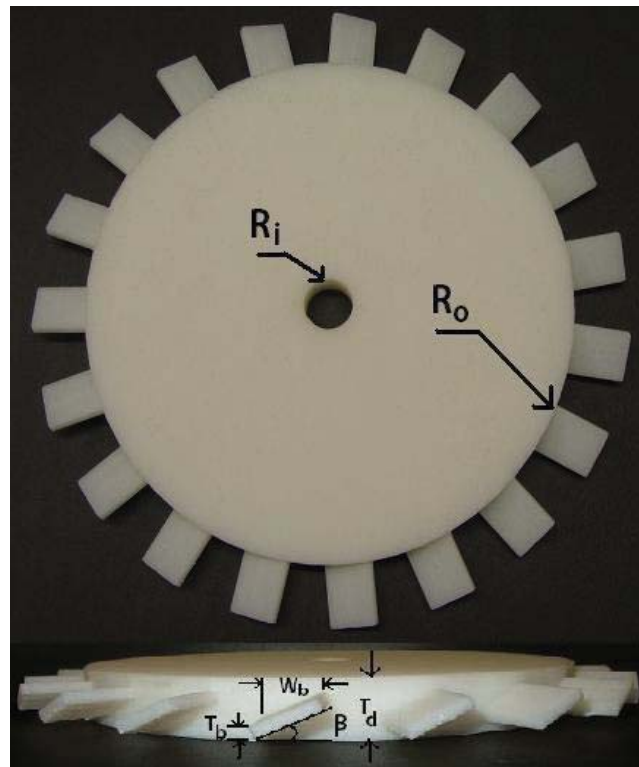


*Fig. 3.18 Actual 3D prototype IBR developed for EMA*





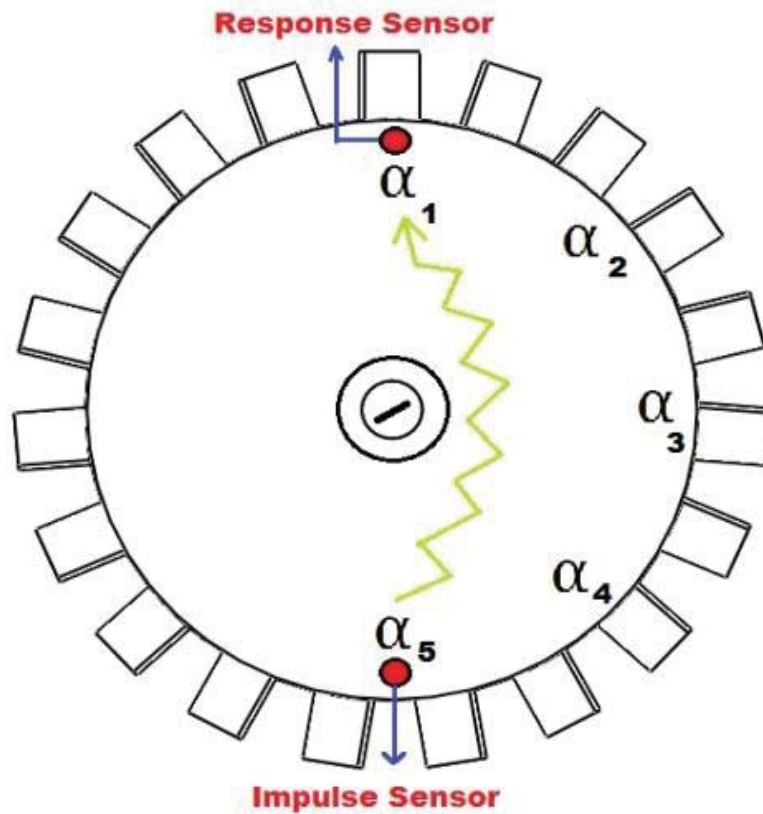


*Fig. 3.20 Input-output Measurement Locations for FRF*

### 3.7.2 EXPERIMENTAL INVESTIGATION

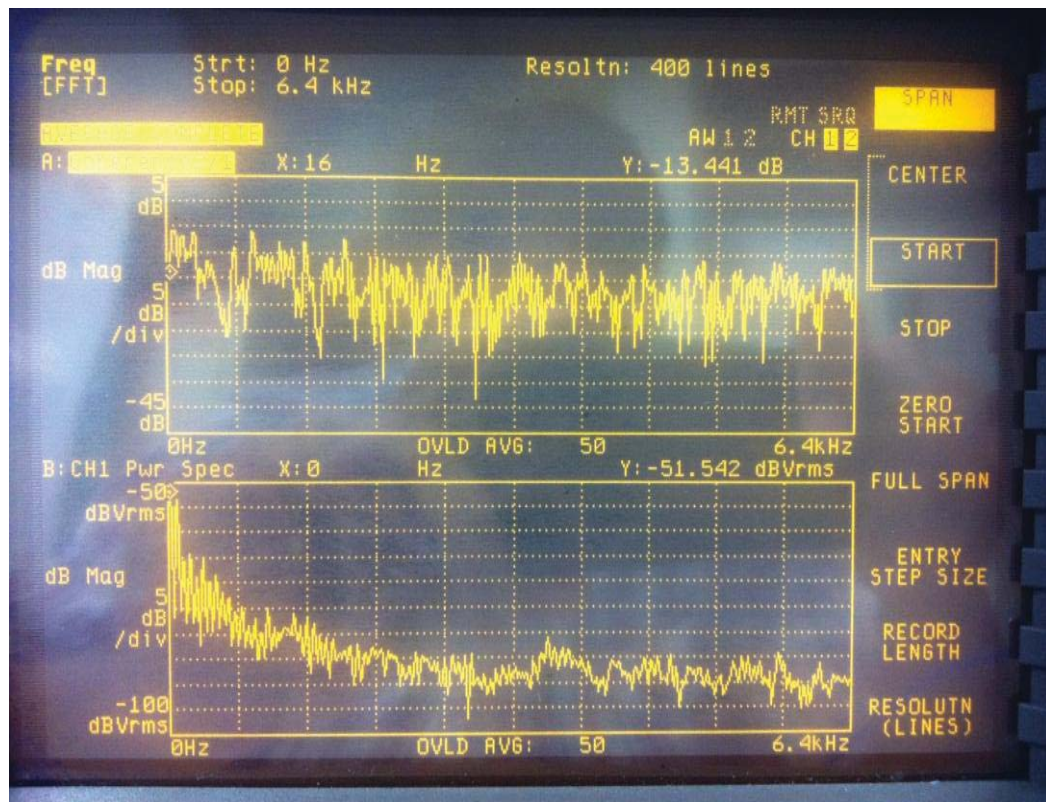
An experimental modal analysis has been carried out to determine the structural dynamics behaviour of the realized model. The most important measurement that is needed for modal analysis is frequency response function (FRF) which was done with the help of the FFT analyser. For accuracy of data to go through the FFT analyser; input-output measurement points for FRFs were most eminent. At the beginning of the experimental analysis the model was investigated by trial and error. By means of test runs the position and resolution of the measurement points and impact locations were optimized regarding the interval of one measurement and the achievable precision of the results. Since for mechanical structures, the dynamic responses (output) are the direct records of the sensors that are installed at several locations [4] five input-output measurement locations were selected to collect the final data as shown in fig. 3.20. Averaging of about 50 impacts was taken for the accuracy of results. As favoured by engineers and vibration experts, Hanning

windowing was selected in computation of Fourier transform in the dynamic signal analyser (D.S.A)

The selection of hammer tip can have significant impact on the requisite measurements. The hardness of the tip controls input excitation frequency. The tip needs to be selected such that all the modes of interest should be excited on the required frequency range. In conducted experiment, by selecting soft tip doesn't excite all the frequency range as evidenced by the roll off of the power spectra depicted in Fig. 3.21a. On the other hand, with hard hammer tip in Fig. 3.21b we have fairly good and relatively flat input excitation force function hence was used to carry on with the experiment.

A series of frequency response measurements is typically made between several excitation points and a single response point, or alternatively, between a single excitation point and several response points. The test structure was excited by placing output sensor on selected locations with single excitation point as shown in figure 3.22. it was observed that by selecting different response points the resonant frequency at 605 Hz changed phase, giving a clue that the nodal line lie between these two selection point. Although in fig. 3.23, one can observe so many different resonant peaks contaminating the result at recurring 60 Hz frequency. To eliminate this problem, 60 Hz notch filter were used to reduce the DC hum and to obtain clearer results as shown in Fig. 3.24. All the repetitive DC hum at 60 Hz were diminished and clearly showing the structure's resonant frequencies.

(a)



(b)

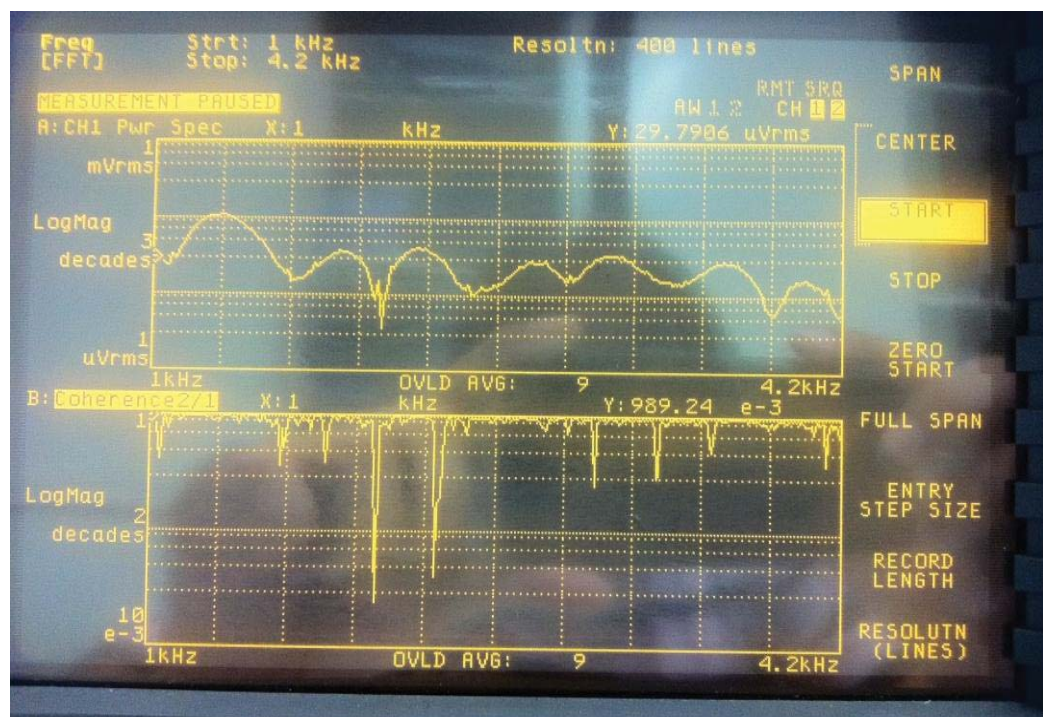


Fig. 3.21 Selection of Hammer tips for required FRF

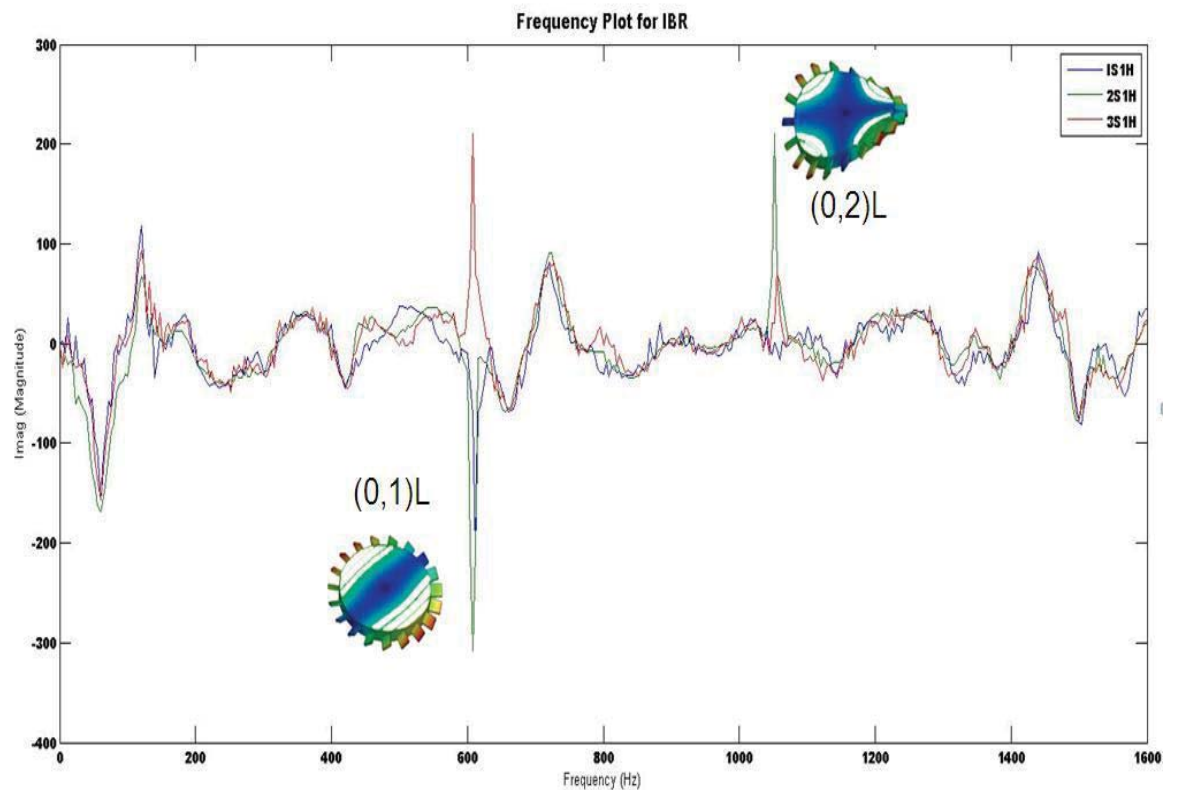


Fig. 3.22. Frequency response function plot at different Input-output measuring locations

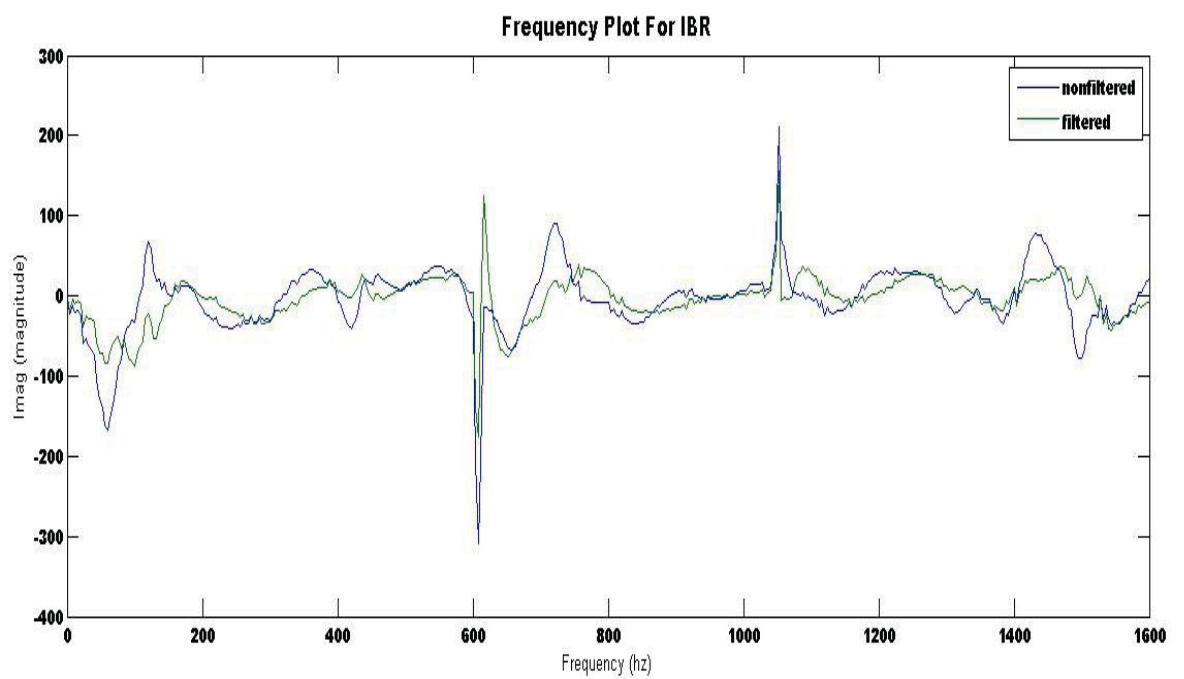


Fig. 3.23. Comparison b/w filtered and non-filtered frequency plot at 60Hz DC hum



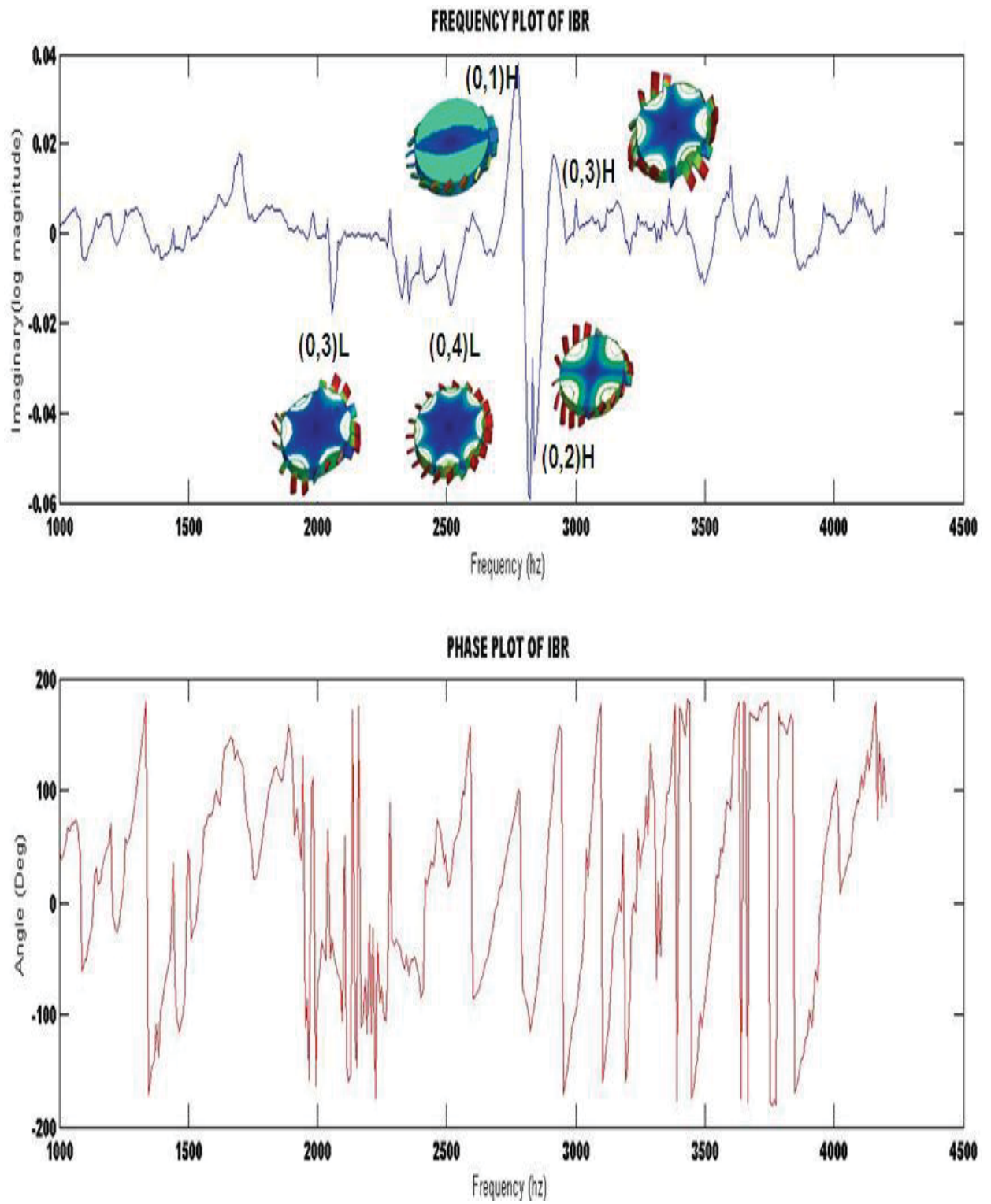


Fig. 3.24. Frequency and phase angle plot of replica mode through Experimental modal analysis

<b>Table 3.2. Natural Frequency Comparison of Replica Modes Through FEA, EMA and Chladni</b>				
<b>Mode no.</b>	<b>FEA Simulation</b>	<b>Experimental modal analysis (EMA)</b>	<b>Chladni's Pattern</b>	<b>% Error ( max)</b>
(0,1)L	603	612	604	2%
(0,2)L	1050	1057	1050	1%
(0,3)L	2055	2058	2054	1%
(0,4)L	2502	2509	2503	1%
(0,1)H	2778	2782	2778	1.5%
(0,2)H	2822s – 2850c	2828s- 2840c	2826	3%
(0,3)H	3140	3149	3143	3%

Observations were taken in the range 1000 Hz – 4300 Hz to capture most of replica modes depicted in fig. 3.24. In the graph, experimental modal analysis (EMA) illustrated clearly the replica modes observed in IBR by Finite Element Analysis (FEA) with respect to resonant frequency and phase angle. Mode (0, 2)<sub>H</sub> showing (0, 2)<sub>HSine</sub> and (0, 2)<sub>HCosine</sub> resonant peaks within 30 Hz range well predicted in the FEA is also notable. All the observations were recorded in Table 3.2.

### **3.8 CHLADNI'S PATTERN**

Chladni's study consisted of vibrating a fixed, circular plate with a violin bow and then sprinkling fine sand across it to show the various nodal lines and patterns. Although experimental methods and equipment have been much improved in the last 200 years, Chladni's law and original patterns are still regularly employed to study plate/disk vibrations. In this study we also adopted the classical method of Chladni's pattern for further verification of the new finding of replica modes.

### 3.8.1 EXPERIMENTAL SETUP

Fig. 3.25 shows the schematic diagram of the experimental set-up used for Chladni's patterns. Same 3D prototype of IBR with base clamps were used and precisely clamped on vibration damping table to carry out the experiment. As the prototyped IBR being thick; a number of piezoelectric actuators were glued in series on the base of IBR as shown in fig. 3.26 to completely shake the structure on different modal frequencies without noticeable damping. A commercial frequency generator was used to generate desired signals.

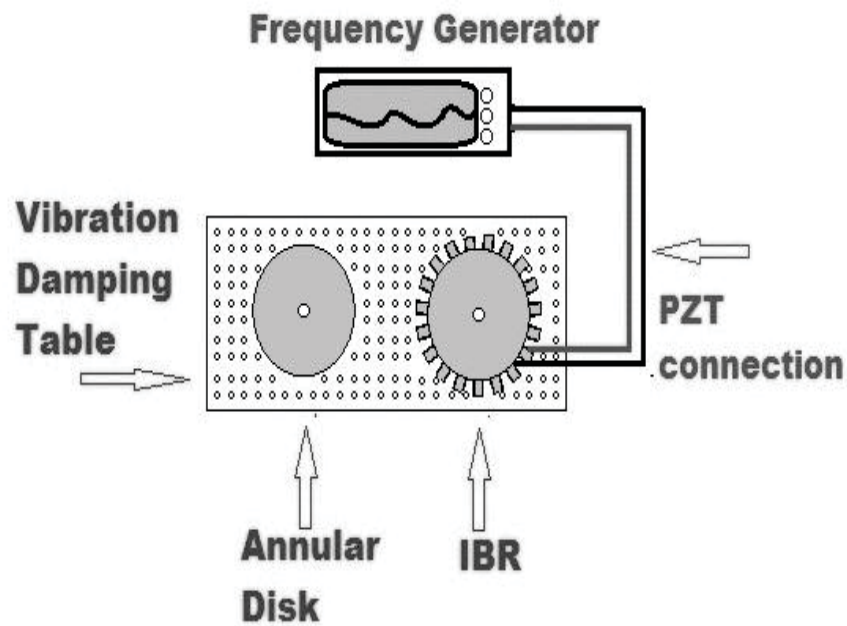


*Fig. 3.25 Schematic of Chladni's pattern experiment*

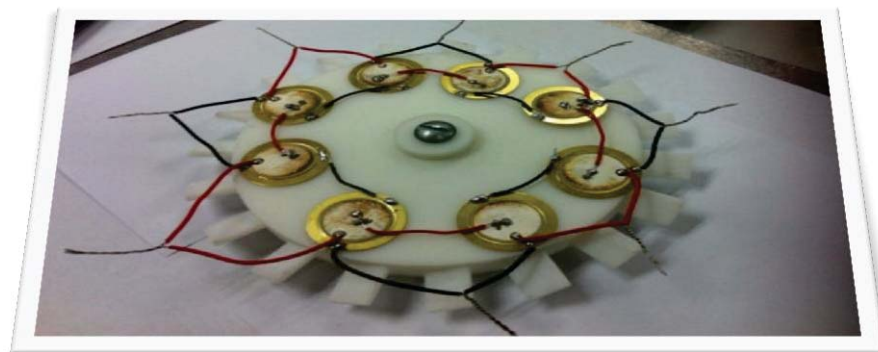


*Fig. 3.26 Series of PZT glued at IBR Prototype*

At each modal resonant frequency predicted by FEA simulation and generated by frequency generator; some fine colored sand was sprinkled across the IBR which settled along the various nodal lines and replica mode patterns were visible as depicted in figure 3.27. All resonant modes in the frequency range of our interest were discovered for each modal frequency. Results were recorded in table 3.2 for comparative study of the findings.

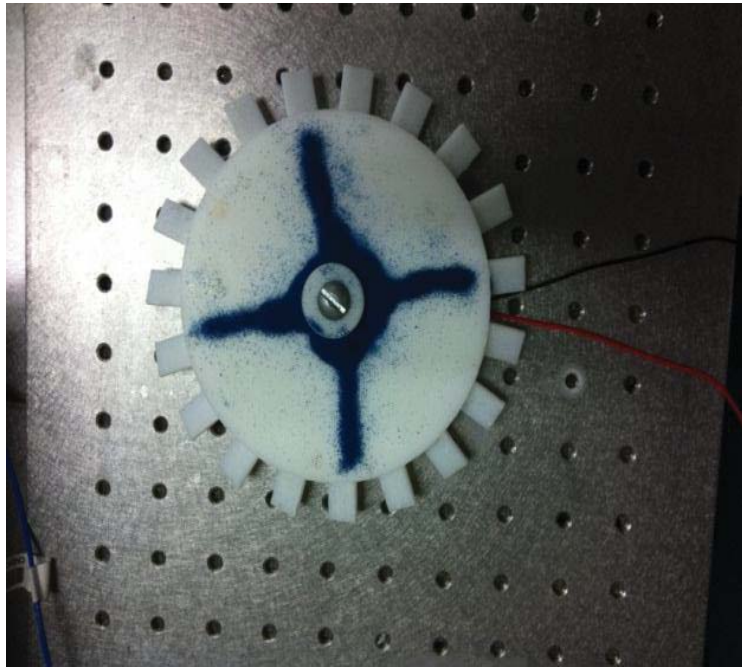


*Fig. 3.27 Mode  $(0, 2)_H$  depicted by Chladni's*

### 3.9 CONCLUSION

In this section of rotationally periodic structures, free vibrations of an integrated bladed rotor (IBR) are examined through finite element simulations and experimental studies. Parameter studies of varying blade angle and blade thickness have been conducted for identification of the best geometry design values for IBR's dynamics. Migration of natural frequencies and modal content of the model IBR structure have been observed and noted with the following conclusion remarks:

- (1) The appearance of replica mode,  $R(m, n)$ , has been observed in IBR structures



for repeated frequency doublets having nodal line  $n > 1$ . For each replica mode pair, integrated blades of low frequency component,  $P(m, n) L$ , vibrate in-phase with disk whereas for high frequency component,  $P(m, n) H$ , blades and disk vibrate out-of-phase with each other.

- (2) Nodal pattern as well as the associated Fourier content of low frequency replica component is found to be sensitive to change of blade angle while the pattern is observed fixed with respect to IBR structure.
- (3) Modulated stiffness wavenumber trend of Fourier harmonics is directly proportional to the order of polynomial curve with change in blade angle.
- (4) Merging of replica mode pair is observed with increasing blade angle while veering and clustering of high frequency replica modes are found when blade thickness is increased.
- (5) For all the replica modes, good agreement is found between the results of experimental modal analyses (EMA), Chladni's patterns technique and the Finite element analysis (FEA).

The aforementioned new findings can add to the literature, which also provide engineering implications in designing integrated bladed rotors subject to travelling wave and engine order excitations. The new finding of replica modes investigated in this chapter is accepted for publication as mentioned in [84-86]

In the next chapter, for thermal response on rotationally periodic structures, Hard disk drive has been selected. The research mainly focused on Disk Spindle Assembly (DSA) in a commercial HDD. Thermal expansion of DSA has been analyzed to find an approach to reduce the repeatable run-out error (RRO) of track following position error signal (PES) in high track per inch (TPI) hard disk drives.

## CHAPTER 4

### THERMAL RESPONSE OF ROTATIONALLY PERIODIC STRUCTURES

#### PRÉCIS

<b>Response selection:</b>	Thermal
<b>Model selection:</b>	Hard Disk Drive (HDD)
<b>Problem statement:</b>	Find a methodology to optimize and reduce the repeatable run-out error (RRO) of track following position error signal (PES) in high track per inch (TPI) hard disk drives caused by thermal expansion of Disk spindle Assembly (DSA) of HDD.

Thesis circulates around 3 major responses on rotationally periodic structures. Previous chapter covered free vibration response where Integrated bladed rotor (IBR) was taken as design component in RPS where effects on structure designs on free vibrations of integrated bladed rotor (IBR) has been conducted in that chapter. Migration of natural frequencies is characterized through parametric studies considering changes of blade angle and blade thickness on an underlying uniform axis-symmetric rotor. Recurring coupled repeated doublet modes, defined as replica modes, has been observed in this study by characterizing blade's vibrations in-phase or out-of-phase to disk's vibrations. Veering and cluster of replica modes' natural frequencies are observed with respect to the blade design parameters. Existence of replica modes has been verified via experimental studies. Also it's been observed that Fourier content for low frequency replica component is found to be sensitive and tune able to blade angle design.

On the other hand, this chapter discusses the thermal response of rotationally periodic structure. As discussed previously in section 1.3.2, Hard disk drive has been selected as a

RPS model with focus on Disk spindle assembly to reduce run-out errors due to thermal effects.

#### 4.1 INTRODUCTION

From the last few decades, the hard disk drive (HDD) has emerged as a key technological product of the computer age beginning. It consists of the main, magnetic disk-spindle assembly (DSA) system which greatly influences the dynamics of the performance of the HDD.

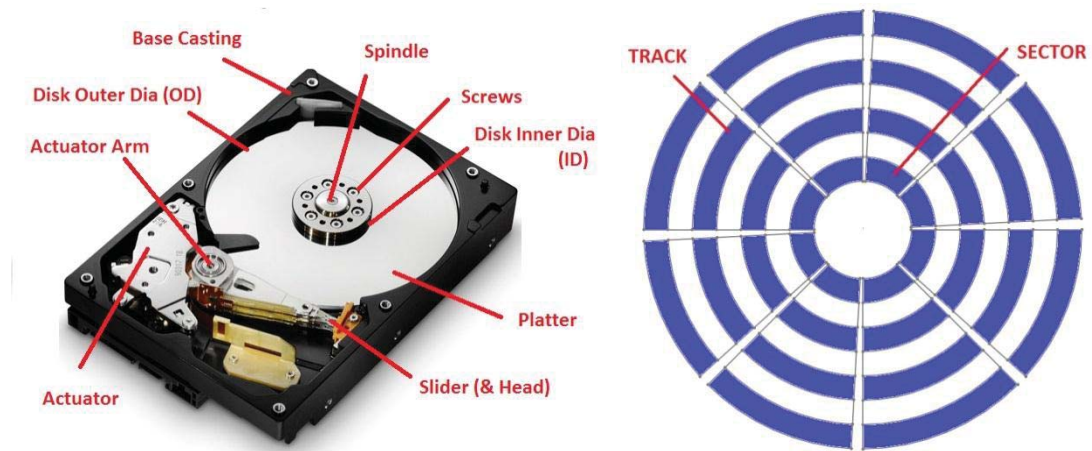


*Fig. 4.1(a) Mechanical components of a commercial HDD (b) Servo and data sectors on a magnetic HDD [22]*

The HDD as shown in Fig 4.1(a), has many mechanical parts and components such as the load/unload ramp, head suspension assembly (HSA) consisting of a rotary actuator, mechanical spindle assembly, flexible cable assembly (FCA), head gimbal assembly (HGA) and the voice coil motor (VCM). The hard disk has traditionally been observed as an electrical engineering device; however, it consists primarily of several mechanical parts. The disk spindle assembly (DSA) consists of several objects such as a disk clamp, small rotating motor, and single or some number of platters, many spacer rings, and screws to hold the disk onto the spindle motor. The DSA and its components often experience rotational forces which causes cyclic symmetric dynamic or axis symmetric dynamic features to the rotating axis of the spindle. In the HDD industry, the magnetic information held in a HDD is stored in data sectors upheld by servo factors created as quasi-concentric

tracks on the magnetic disk, Fig. 4.1(b). HSA interactions and DSA dynamics have been engineered carefully to minimize deviation and to ensure even writing of the servo tracks. HSA and DSA implementation is based on mechanical methods presented in several patented work [50-55] from disk drive's manufacturing process. A wide operating temperature has been engineered due to various applications of the HDD.

The positional error signals (PES) of a HDD are to be minimized by the prewritten tracks when the HDD is in operation. This is indicated by the deviation in the header from the center of the track which ensures data access is reliable [56], [1]. However as reported in [56], several real-time dynamic factors can cause an increase in the PES. In reality, disk spindle system changing aspects are susceptible to temperature in relation with recorded-in position error signals which on the other hand are insensitive to the surrounding temperature of the HDD. Since the device is electromagnetic in nature, all the mechanical components inside the DSA are susceptible to rise in temperature which practically may cause the factors of run-out errors. At elevated temperatures any mechanical component inside the disk spindle assembly is susceptible to heat [36]-[33] which in return cause repeatable run-out errors (RRO). The electromagnetic excitation related RRO dynamics is usually alleviated by the servo feed-forward [17], [23], [18] and actuator servo loop shaping methods [67], [66].

The magnetic disks are kept together by screws when being manufactured as shown in Fig. 4.1(a). The mechanism holding the disk together is depicted as rotationally periodic spring that fits over the ID of the HDD although the stiffness coefficient is susceptible to temperature. [19] and [41] have presented mechanical designs which allow greater engagement with the motor and the clamp of the Disk Spindle Assembly. This prevents disk slip because of vibrations and external shock and reduces spring load deviations between screws on the operating temperature. Kim *et al.* [38] has suggested in their design for an optimized clamp that concentration caused by stress due to fasteners can be rearranged on the disk to reduce elevated run-out errors near disk ID.

RRO would still exist in high amounts around the inner diameter disk region as shown from literature [17] and from patents [18], [20] and cannot be eliminated no matter how

optimized the disk clamp design is. Given the preference of higher recording density and capacity, the RRO PES inner diameter thermal sensitive problem can be seen as repeated radial deviance from the center of the track. This is one of the greater mechanical challenges for HDD designers and engineers. By studying the experimental PES RRO observations at different temperatures along with the driving mechanism is highly important and will be the main focus of this chapter of the thesis.

## **4.2 EXPERIMENTAL OBSERVATIONS**

Magnetic HDD have been assumed to be resistant to mechanical deformations. Discussion on the effects of screws in disk spindle assembly and thermal effects on RRO-PES on HDD has not been sufficient although much has been written on vibrations of magnetic disks and the disk spindle assembly systems [44], [71]. Experimental results mentioned in this section focus primarily on the DSA RRO problem.

Fig. 4.1(a) shows a commercial HDD which is exposed to the open to allow disk flatness measurements. The shape of the disk is actually deformed in the likeness of a saucer rather than being flat, Fig. 4.2(a). Fig. 4.2(b) [17] is based around the outer diameter of the disk (OD); the deformation of the disk produced two oscillations for every disk rotation with the frequency reading of 2X of the spindle assembly's rotational speed. The magnetic signal when attained by read/write elements from the surface of the disk leads to the same deformation effect as in 2X RRO PES.

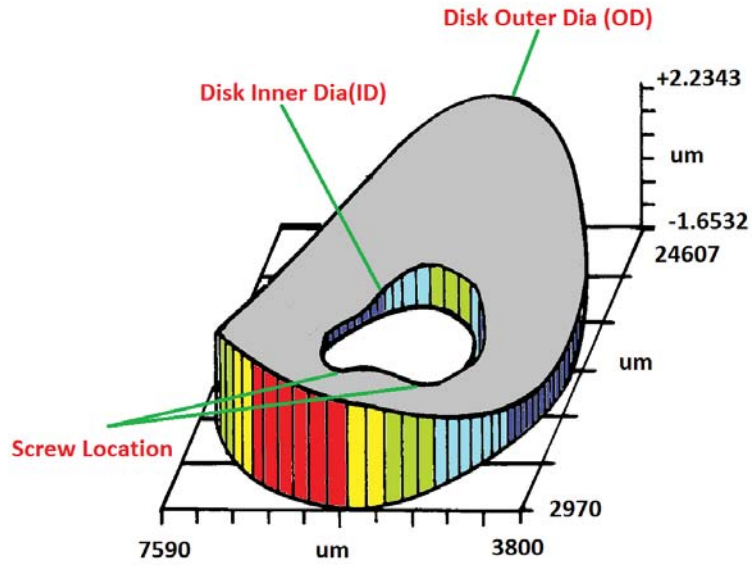


Fig. 4.2 (a) HDD deformed as a saucer against a disk flatness measurement [20]

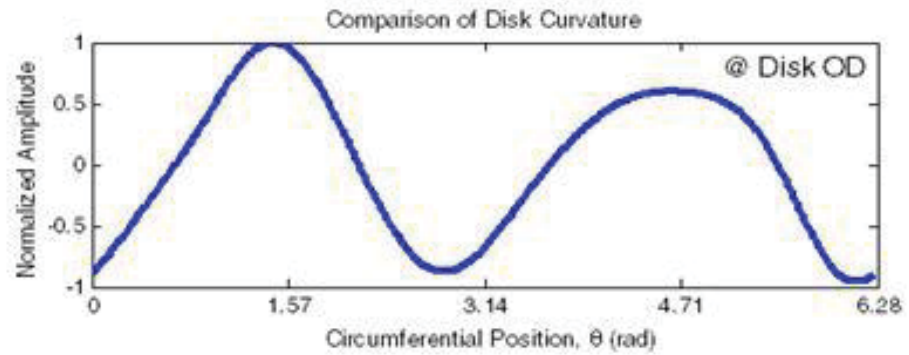


Fig. 4.2 (b) the subsequent displacement plot at outer diameter (OD) of spindle assembly [17]

RRO PES are produced when PES is synchronized further based on the DSA's spin speed. This synchronization takes place by taking the HDD slider as a sensor. For example, a 3-platter, 6-screw model commercially available HDD having an RRO PES spectra as shown in Fig. 4.3 [22] at disk (a) OD – outer diameter, (b) MD – middle diameter and (c) ID – inner diameter, respectively. The %TP is percent track pitch and the wide blue line is the scaled servo sensitive function whereas, the other hints of colour are the RRO spectrum obtained by every single read/write slider on the disk stack. RRO is index 0 on the surface of the disk and is placed close to the fasteners and disk clamp which is from the top read/write head whereas; the base of DSA is index 4. As seen from Fig. 4.3, there are few RRO harmonics which are very strongly dependent of location and as seen from the figure,

there are other harmonics which are not dependent of location. Harmonics which occur due to the electromagnetic excitations of the spindle are excluded and those of amplitudes 1X and 2X of the RRO harmonics are seen not to be dependent of the sliders location along the radial direction of the disk [17], [20].

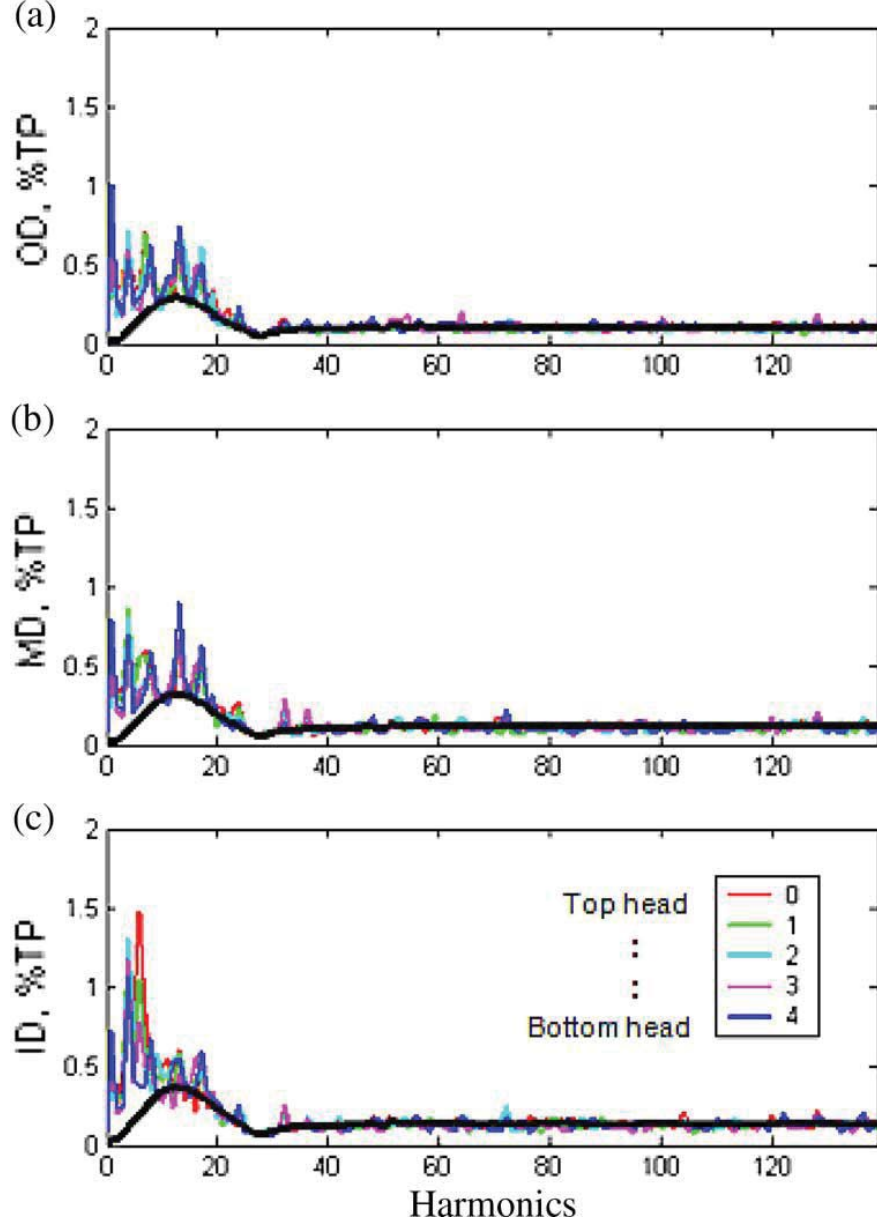


Fig. 4.3 RRO PES spectra examples as seen on disk (a) OD, (b) MD , and (c) ID [45]

As seen on Fig. 4.4 amplitudes of harmonics like 4X, 5X, 6X for example, increases towards disk ID which causes high position error in the HDD. Measurements of PES at high temperatures as reported in [17] and [20] that the equation which governs the  $k^{\text{th}}$  RRO harmonic having several ramping behaviour in the disk is written as:



$$|n \pm k| = NF, 2NF, 3NF, \dots \quad (1)$$

Here  $NF$  represents the number of fasteners and presently this is taken as  $NF = 6HDD$  and  $n \in \{1, 2, NF\}$  signifies the driving mechanisms from disk radius, disk distortion as a saucer, and restraining stress from fastenings, respectively.

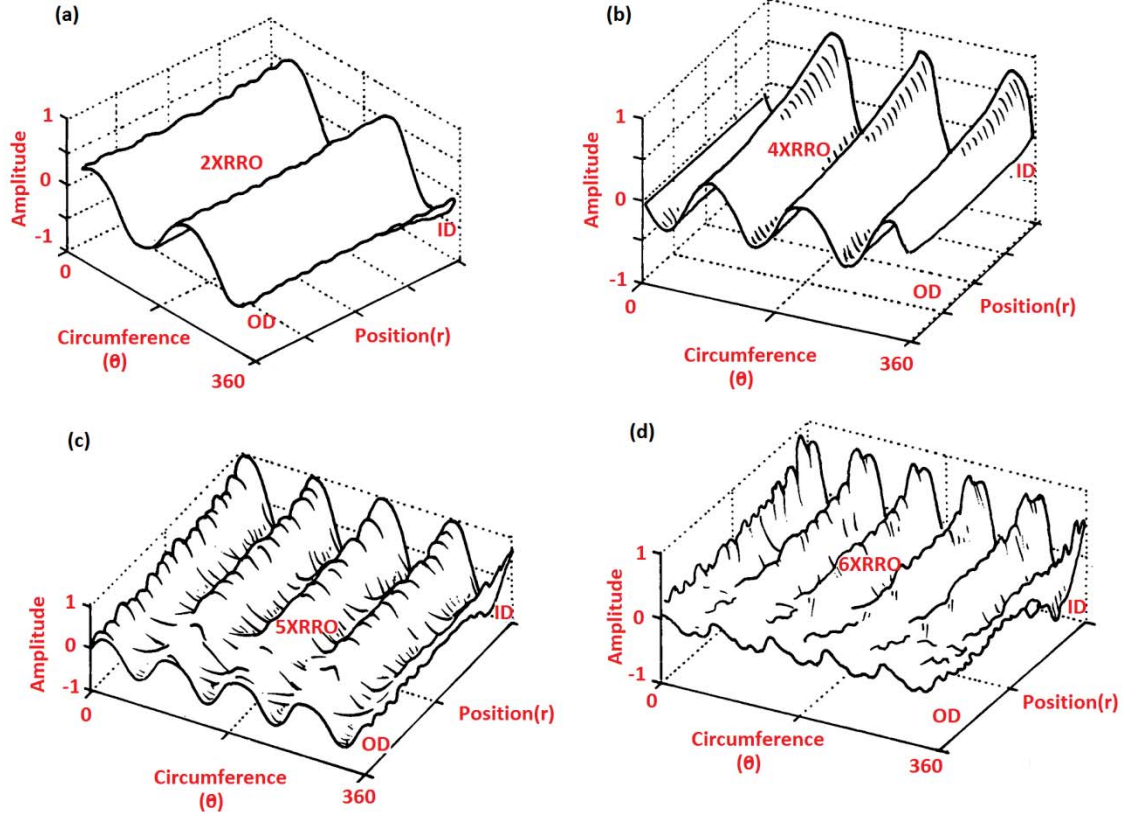


Fig. 4.4 Repeatable Run-out Diagrams from disk OD to ID for (a) 2X, (b) 4X, (c) 5X, and (d) 6X RRO harmonics [45]

In this case, the effect of disk slip with 1X RRO when  $n = 1$  can produce an amplitude ramping RRO harmonics for  $k$  values,  $k = 5, 7, 11, 13, \dots$ , etc. This disk deforms like a saucer at  $n = 2$  and has a constant amplitude 2X RRO PES as displayed in Fig. 4.4(a) [45]. The amplitude ramping RRO harmonics take place at  $k = 4, 8, 10, 14, \dots$ , etc. according to equation (1). When ' $n$ ' is replaced with  $NF$  in equation (1), then ' $k$ ' depicts fastener's harmonics used in the disk. All these three factors mentioned above are susceptible to temperature difference has already been reported in [17] and [20]. The next section of the chapter highlight the appearance of 2X of repeatable run-out errors through FEA and studied by increasing temperature of the HDD.



### 4.3 FINITE ELEMENT MODEL

Through computer-aided design software such as Solid Works, the commercial HDD is constructed using the geometric specifications of the disk-spindle assembly as shown in Fig. 4.5

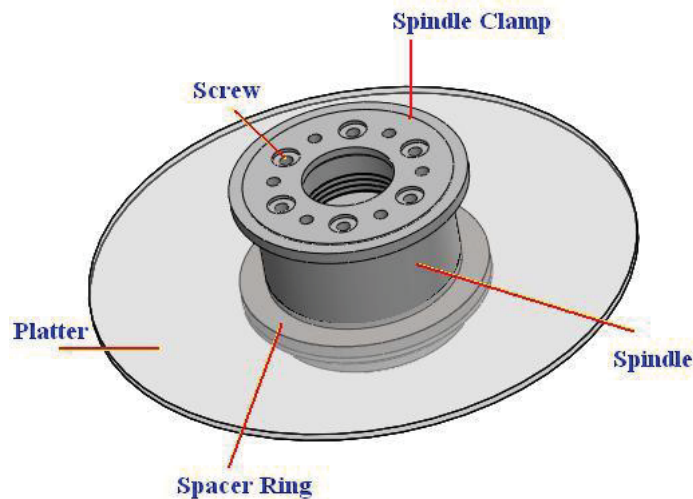


*Fig. 4.5 Finite Element Model of the Disk Spindle Assembly (DSA) of a HDD*

The magnetic HDD consists of spacer rings, spindle clamp, spindle hub structure all made of stainless steel, and the top and bottom surface of the disk is coated with a magnetic film made of a glass substrate. The position of the disk along the perpendicular axis of the DSA is studied by constraining a single disk through several spacer rings which are included in the system. All of spacer rings and the spindle clamp are aligned in a single line from the spindle hub from a gap of 0.1 mm. The solid parts are considered to be attached to isotropic materials. Although it is not possible to have perfect alignment in real life applications of the HDD, it is assumed that the disk will have 1% eccentricity over 0.1 mm underlying opening from the seeming of the hub structure with regards to the system solid model.

All solid forms in the system model are meshed by a four-node tetrahedral element. The spindle clamp has six screw holes attached and the spindle is clamped in the hub structure to two bearing locations. This creates a contact load which is transferred by holding the magnetic HDD through the spacer rings. Simulation for thermal analysis were performed

on the solid model system by uniformly increasing temperature at 25°C, 40°C, 60°C and 80°C, this increases the number of elements locally and globally with convergence assured. DSA is assembled in a clean environment for practical conditions at a temperature of 25°C. The radial displacement of the disk calculated to a temperature of 25°C which is done to study the change in temperature of the spindle hub and disk deformation.

#### **4.3.1 MODIFICATION IN FINITE ELEMENT MODEL**

The solid model of the disks outer diameter and its radial displacement is shown in Fig. 4.6(c) around 40° C temperature. Fig. 4.6(e) shows the resulting Fourier harmonics from which the only noticeable harmonic is the zeroth without any other harmonic observable. The finite element model assumes an even temperature distribution and isotropic conditions, the zeroth model, shows a uniform thermal amplification of the platter. This demonstrates the size of the platter increases at higher temperatures, compared to its original size at 25° C. Given that the disk was not aligned concentrically towards the spindle hub, the thermal expansion causes the outer surface of the spindle hub to come in contact with the disk. The 1X RRO, or the first harmonic as expected, is shown in Fig. 4.6(e).

However, the present thermal-elastic simulation shows that the saucer like disk deformation did not take place as shown in Fig. 4.2(a). Symmetry was achieved in the original design as shown in Fig. 4.6(a) by the screw holes and the load applied, creating a rotationally periodic structure. A cyclic symmetric structure is highly unlikely to happen because of handling and processing during assembling processes and manufacture. Alignment features such as notch shapes or chamfer in a HDD spindle system are inserted for bearing elements into the assumed axis-symmetric spindle hub. Looking at the imperfections in structure geometries and taking the alignment features into consideration, Fig. 4.6(b) shows a notch or cut-off which is purposely installed in the spindle hub. The cyclic symmetry is destroyed by the notch eventually leading to an asymmetric DSA model.

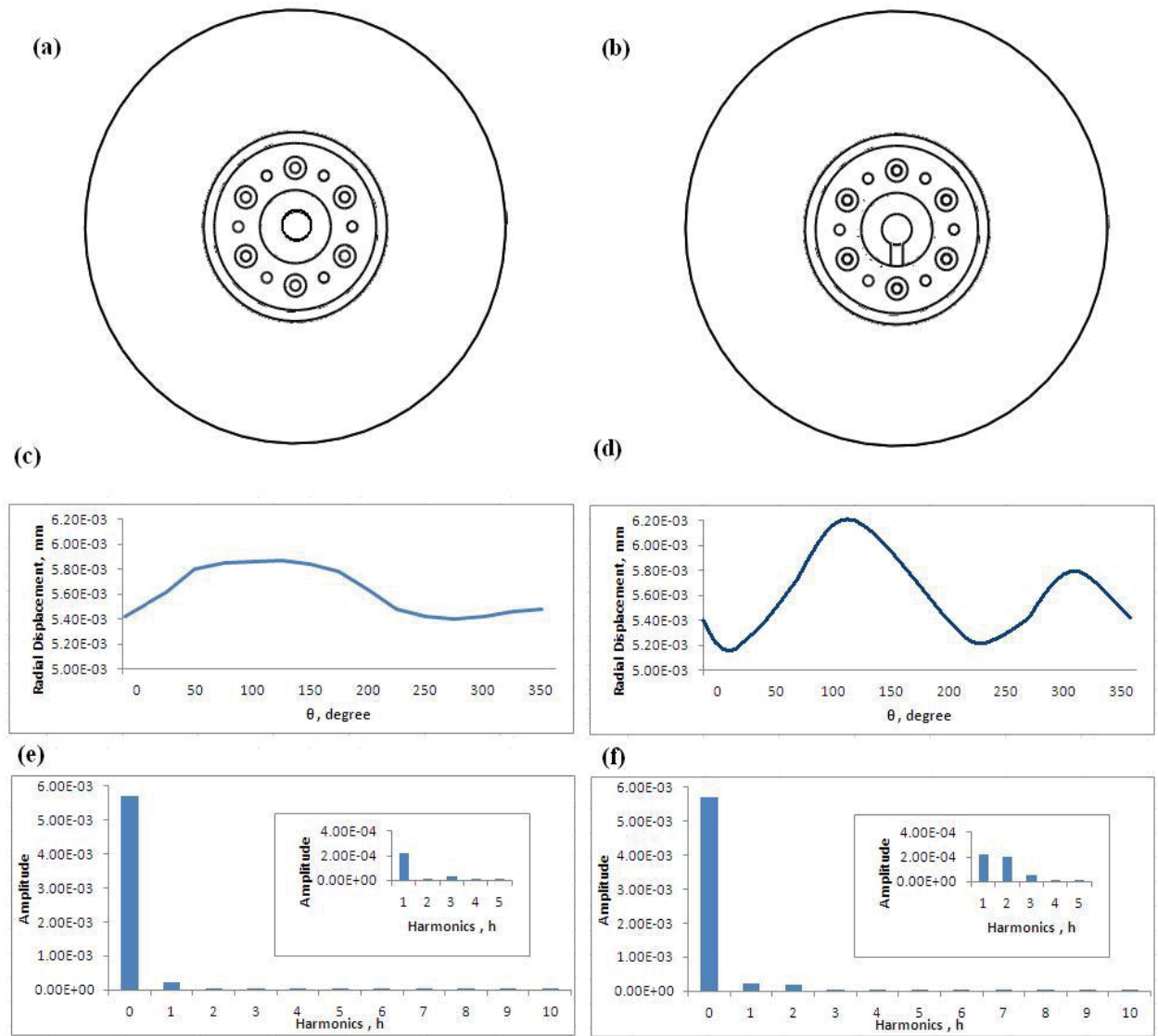


*Fig. 4.6. Comparison of (a) rotationally periodic and (b) non-periodic spindle assembly models and the corresponding disk radial deformation in (c) and (d), respectively. The resultant harmonics are shown in (e) and (f)*

After the implementation of asymmetric features due to rising temperature, the disk starts to bend into a saucer. Fig. 4.6(d) shows the disk OD radial displacement at 40°C constructed under the presence of the notch. The resulting Fourier subjects as presented in Fig. 4.6(f) keeps the same level of zeroth harmonic whereas, the second harmonic related to 2X RRO is very prominent. The disk profile when distorted as shown in Fig. 4.6(d) is in very good agreement to when it is measured directly from the disk, Fig. 4.2 (b). The following section will make use of the asymmetry DSA finite model.

### 4.3.2 INTERRELATION AT INCREASED TEMPERATURES

By observing from bird's-eye view of simulated DSA, it was observed that not only the disk bends like a saucer but because of the fasteners, also the spindle assembly shaped like a cooling tower which results in zero harmonics. As discussed earlier, the deformed spindle assembly will cause in producing 1X localized connection with disk internal diameter (ID), the reason behind this phenomena is apparently unconventional alignment with disk and the hub assembly.

In contrast, the new slot design introduced in the spindle assembly depicts in double localized connection between the disk and the hub which in return distort the disk like a saucer as shown in Fig. 4.7(d). For audience convenience, spacer rings and clamps have been hidden for a clear picture of deformed disk spindle assembly.

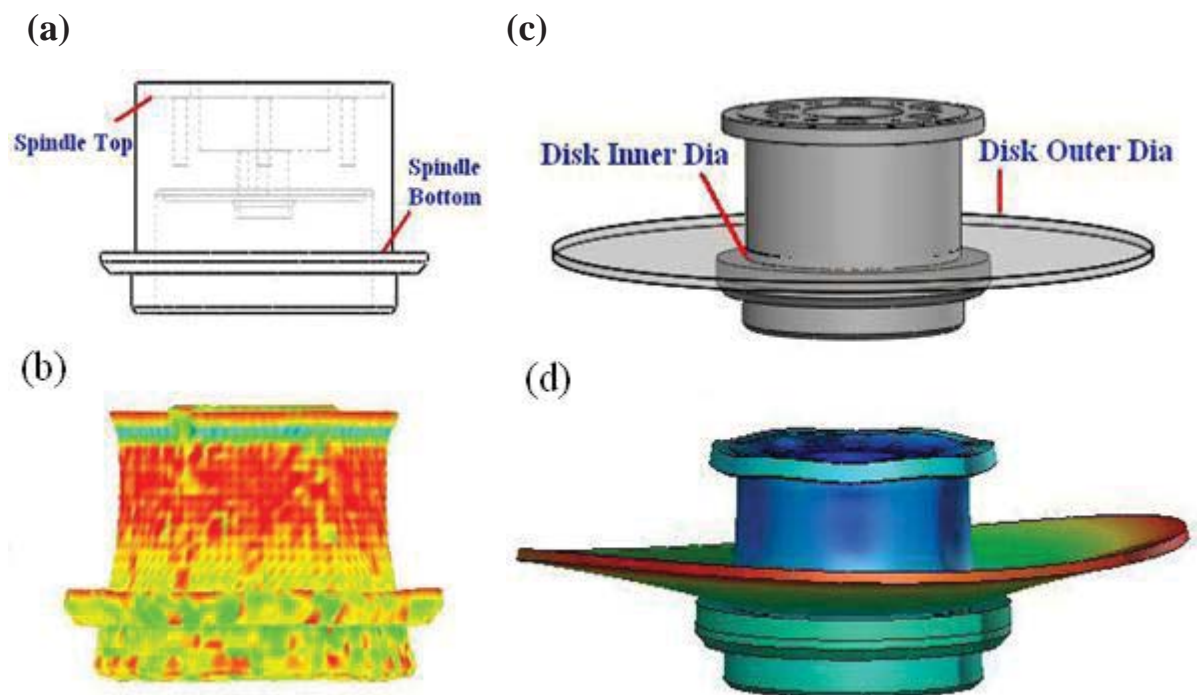


*Fig. 4.7 Side view of (a) Original and (b) deformed spindle hub structure at 80°C and (c) Original and (d) deformed DSA at 80°C*

It's quite clear in the Fig. 4.7, the waviness caused by the screws acting as point stiffness at 6 different locations, making the hub assembly results in 6X RRO in one complete revolution at disk inner dia. (ID). In HDD industry, the permanent magnets that used to actuate the coils are placed in the bottom portion of the spindle hub. From the simulation at elevated working temperature of an HDD, it's been observed that the hub expands from the bottom and shape up like a cooling tower as depicted in figure 4.7(b) and (d). Interestingly, by placing the disk platter quite near the bottom part of the spindle hub, we get increased 2X RRO as the hub deforms substantially near the bottom on increased temperature. This observation has significant effects in placing the magnetic disks. One of the solutions is to reconsider the design of the hub to minimize the distortion in the structure and to decrease the 2X RRO.

To consider the connection between master and slave RRO harmonics, an interrelation study has been carried out using the modified disk spindle assembly model. From the FEA study, it's been observed that the 2X RRO is causing the 4X and 8X RRO. In other words, 2X RRO are the master harmonics and 4X and 8X RRO are the slave harmonics, which can be clearly seen in Fig. 4.8(a) & (c). Similarly, 5X RRO and 7X RRO have been driven from 1X RRO as shown in fig. 4.8(b) & (d). Which is verified from [40]'s rule where we can replace Number of Features(NF) with 6 as total number of screws in this working model and ' $n$ ' will be replaced by either 2 or 1, which is conditional on the contact from either the disk saucer shaping or disk slip which in return cause the hub and disk contact. All together, the observed thermal-elastic phenomena in the disk spindle model are well-preserved. All the stress-strain relationship and deflection values return to original when the disk comes back to non-operational condition where the room temperature is back to 25° C. The current study is well supported from the experimental observations carried out in [17] on RRO's.

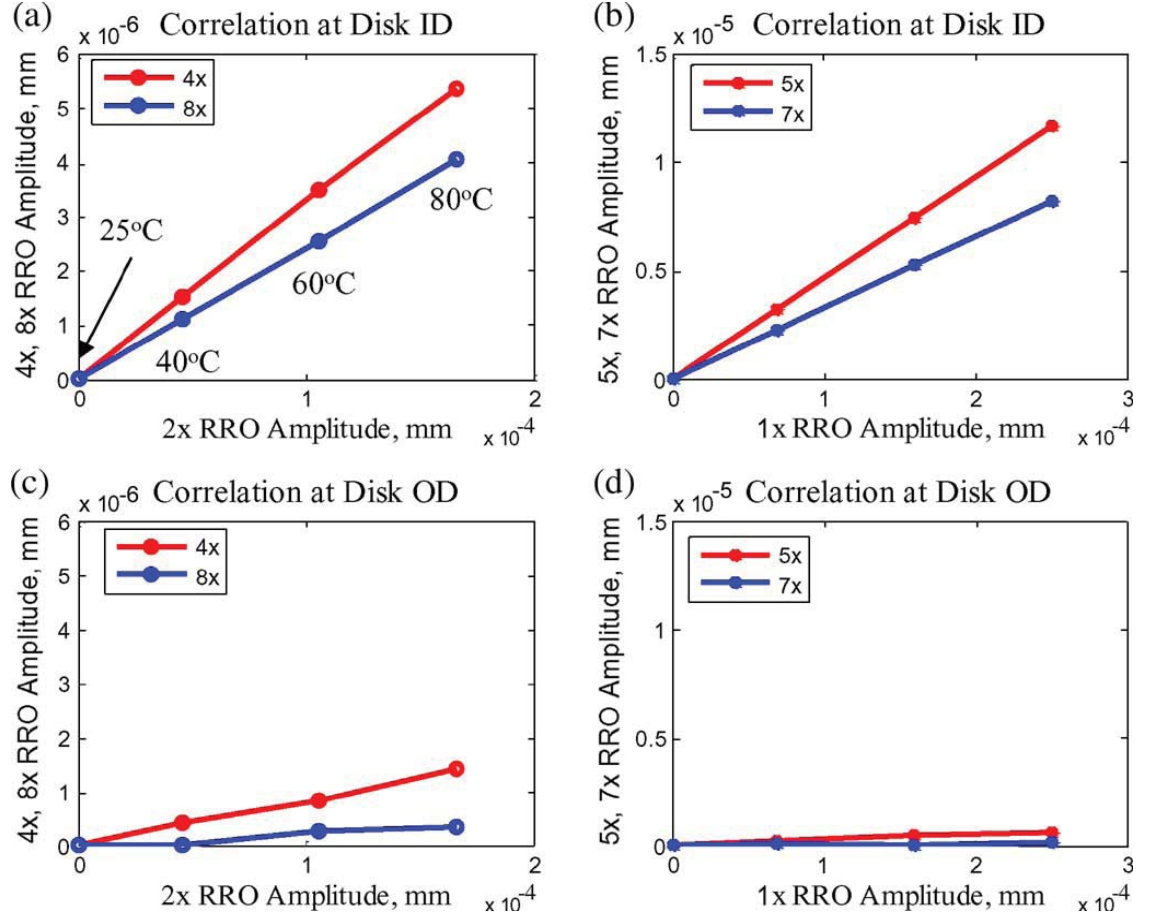


Fig. 4.8 FEA results of interrelationship of 2X with 4X and 8X RRO scales at disk internal and Outer Dia. in (a) and (c), respectively; Interrelationship of 1X with 5X and 7X RRO scales at disk internal and outer diameter, in (b) and (d), respectively. [45]

#### 4.4 PERTURBATION STUDY

Through experimental work [17] and [20], and interested by the FEA results, the DSA thermal expansion RRO problem is emulated by a perturbation model which is presented in this section.

Imperfections represented by notches and seen in terms of displacement and load, fasteners and screws can be seen as negative or positive features of stiffness. As mentioned before, the thermal-elastic problem by disk deformation is seen in the form of base harmonics from  $n = 1$  or 2, which represents temperature cycles. Hence, this model problem is viewed as disk vibration problem with the eigenvalues corresponding towards the thermal cycles.

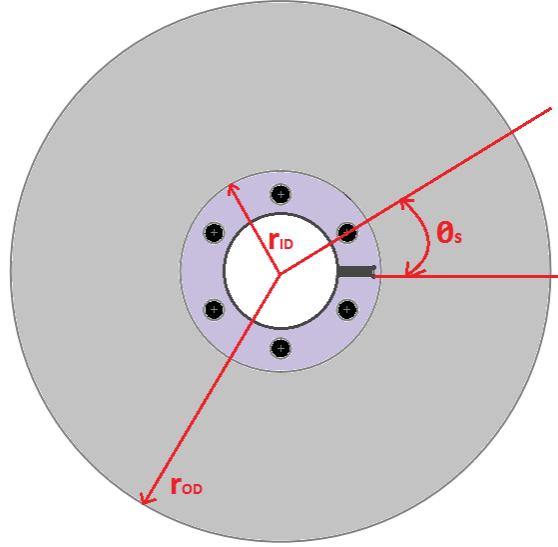


Fig.4.9 Elastic constraints of a disk clamped by six fasteners

The coordinate system with an  $r - \theta$  frame is applied with  $\theta = 0$  positioned at middle of one fasteners feature. Fig. 4.9, shows the free HDD platter disk without constraints that has  $NF = 6$  exactly. Positioned stiffness features that are located at common radial positions are represented by  $r_{ID}$ . At this position a fastener or a screw load occurs. From one of the screw location or point stiffness features, the location of the slim rectangular at  $\theta_s$  represents effect of slot which made the structure asymmetric. This is negative stiffness with respect to the deformation of the circular disk. The formulated equations are considered in a dimensionless form and the  $r_{OD}$ , the outer radius is a characteristic length and the time scaling factor is represented as  $\tau^{-1} = \sqrt{E/(1 - \nu^2)\rho r_{OD}}$ , where  $\rho$  represents the volumetric mass density of the magnetic disk,  $E$  is Young's modulus, and  $\nu$  is the Poisson ratio.

The EOM for the free, undamped classical disk can be written as

$$\mathbf{M} \mathbf{u}_{,tt} (r, \theta) + \mathbf{K} \mathbf{u} (r, \theta) = \mathbf{0} \quad (2)$$

This can be interpreted as a typical eigenvalue problem

$$\mathbf{K} \mathbf{U}_n = \lambda_n \mathbf{M} \mathbf{U}_n \quad (3)$$

The  $\lambda_n$  is the perturbed eigenvalue,  $\mathbf{M}$  is the self-ad joint stiffness and inertia operator,  $\mathbf{U}_n$  is the perturbed eigenfunction corresponding to the shape of the deformed disk and  $\mathbf{K}$  is the



self-adjoint stiffness operator. The NF and index  $n = 1, 2$  are the driving source being disk slip, screw/fastener and disk saucer shaping.

Using the perturbation method [23], the eigenvalue problem of the model can be approximated using a first order approximation where  $\lambda_n \approx \lambda_{n(0)} + \epsilon \lambda_{n(1)}$ ,  $U_n \approx U_{n(0)} + \epsilon U_{n(1)}$ ,  $K_n \approx K_{n(0)} + \epsilon K_{n(1)}$  are inserted into equation (2). The removal of cyclic symmetry is scaled to  $\epsilon \ll 1$ .

For a given classical plate we can describe:  $K^{(0)} = \nabla^4 \bullet$  and  $M = I \bullet$ , where the bi-harmonic operator is given as:  $\nabla^4 \bullet$  in  $r - \theta$  polar coordinate system. The identity operator is represented by  $\bullet$ . The stiffness distribution can be written as:

$$K^{(1)} = \frac{k_0}{r_{ID}} \sum_{i=1}^{NF} \delta \left( \theta - \frac{2\pi(i-1)}{NF} \right) \delta(r - r_{ID}) - \frac{K_s}{r_{ID}} \delta(\theta_s) \delta(r - r_{ID}) \quad (4)$$

Where  $k_0$  and  $k_s$  are dimensionless constants that describe the local intensities of stiffness due to screws or fasteners and notch, respectively and  $0 \leq \theta_s \leq \frac{2\pi}{NF}$  with  $\delta$  being the Dirac delta function [45].

By substituting equation (4) and the first-order approximation into equation (3),  $U_n^{(1)}$  can be represented with a linear combination of orthonormalized eigenfunctions from the axis of symmetry of the disk and with group term orders, these eigenfunctions of the thermal-elastic deformed can be stated as:

$$U = U_{n=1} + U_{n=2} + U_{n=NF} \quad (5)$$

$$U_{n=1} = U_{1(0)} + (a_0 + \sum_{k=1}^{\infty} (a_{1,k} \cos(k\theta) + b_{1,k} \sin(k\theta)))$$

$$k : \{|1 \pm k| = NF, 2NF, 3NF, 4NF, \dots\} \quad (6)$$

$$U_{n=2} = U_{2(0)} + (a_0 + \sum_{k=1}^{\infty} (a_{2,k} \cos(k\theta) + b_{2,k} \sin(k\theta)))$$

$$k : \{|2 \pm k| = NF, 2NF, 3NF, 4NF, \dots\} \quad (7)$$

And

$$U_{n=NF} = U_{NF(0)} + (a_0 + \sum_{k=1}^{\infty} (a_{NF,k} \cos(k\theta) + b_{NF,k} \sin(k\theta)))$$

$$k : \{|NF \pm k| = NF, 2NF, 3NF, 4NF, \dots\} \quad (8)$$



From equations, in (6) – (8) ,  $a$  and  $b$  represents the Fourier coefficients which are dependent on extra harmonics ( $k$ ) and driving harmonics ( $n$ ) which is represented in integer multiples  $n = 1, 2, NF$ . The experimental observations, equation (1), are confirmed from the previous equations (6) – (8). For  $NF = 6$  case, the disk is deformed in shape of a saucer due to mismatch in thermal expansion, at  $n = 2$ , with additional harmonics present at  $k = 4, 8$  for example.

#### 4.5 REDUCTION OF 2X RRO

The infirmity in spindle hub assembly is the major reason behind the distortion of the disk platter like a tea-saucer as displayed in Fig. 4.7 in sub-section 4.3.2. This infirmity can either be increased or decreased with the implication of a slot or a cut designed inside the disk spindle. This section will deal with the different design study carried out with the intention of reducing the effect of RRO caused by the deformation of spindle hub assembly on elevated temperature. Different spindle notch/slot designs were developed to represent bearing insertion feature or any imperfection caused during manufacturing processes to the DSA at notch angles of  $0^\circ$ ,  $15^\circ$ ,  $30^\circ$  and  $45^\circ$  with respect to the centre of the spindle screw as illustrated in Fig.4.10. It's been observed from nodal displacement plot at disk OD in Fig. 4.11 that the implication of the notch angle at different locations has some significant effects on the disk distortion with respect to elevated temperatures. More displacement is noticeable.

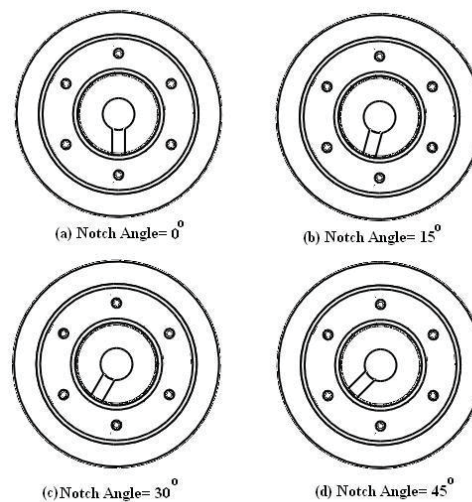


Fig. 4.10 Spindle hub designs with different slot angles

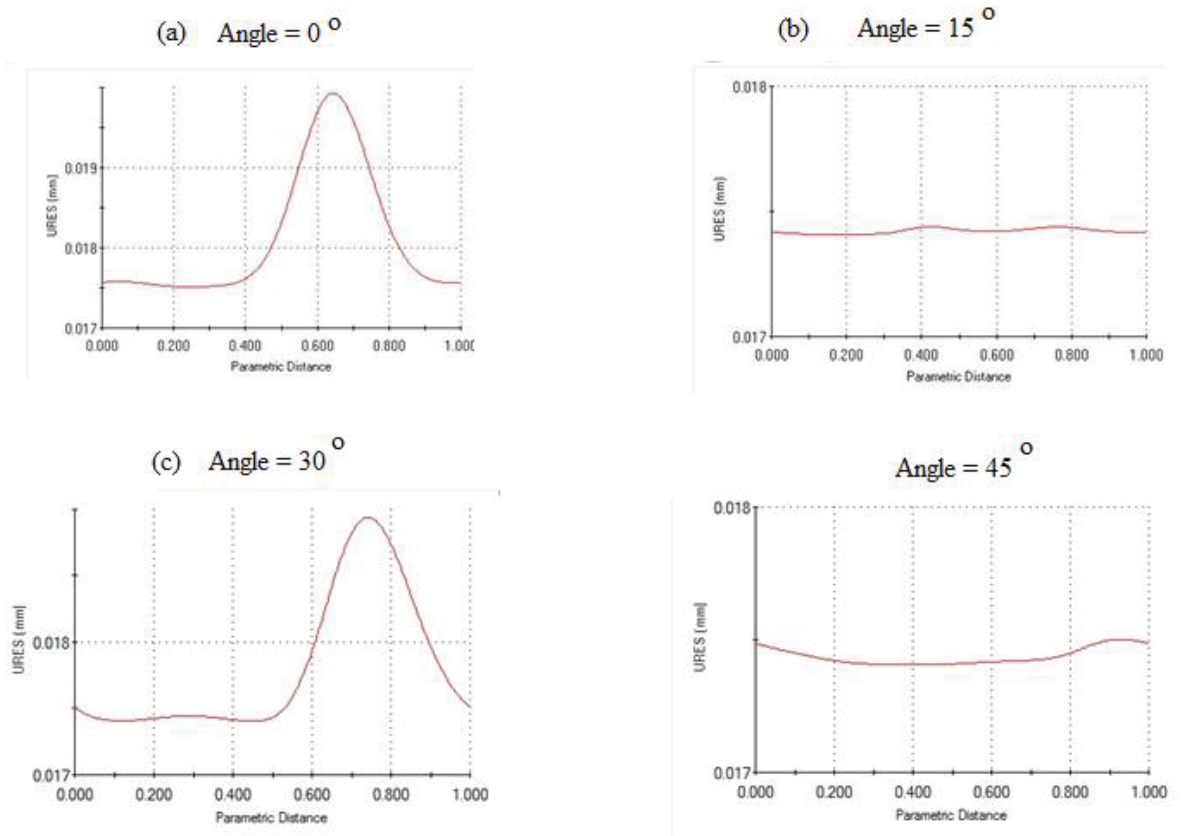


Fig. 4.11 FEA nodal displacement plots at Disk OD at 80° C on (a) 0° slot angle (b) 15 slot angle (c) 30° slot angle and (d) 45° slot angle

On the other hand, Fig. 4.12 displays RRO harmonic components at disk OD radial displacement as functions of ambient temperature and slot orientation. Large amplitudes for the RRO at 1<sup>st</sup> and 2<sup>nd</sup> harmonics are observed at the high temperature region at 80°C comparatively to room temperature at 25°C. It can also be observed that amplitudes of the 1st harmonic, caused by imperfection, and 2nd harmonic, caused by spindle hub potato-chipping, increase monotonically with temperature. In contrast, by changing the slot angle from 0 to 45°, a major reduction in harmonic amplitudes has been observed. Slot angle at 15° and 45° was reported acceptable positions for spindle notch as it reduced RRO more significantly or even completely eradicated comparative to other notch designs. In context of the findings, more slot angle designs can be generated for reducing the 2X RRO by using the following equation:

$$\theta s = \frac{\pi}{2 \times i \times NF}, i = 1, 2, 3, \dots \dots \dots (9)$$

Where,  $NF$  = Number of fasteners, and  $\theta s$  = notch/slot angle.

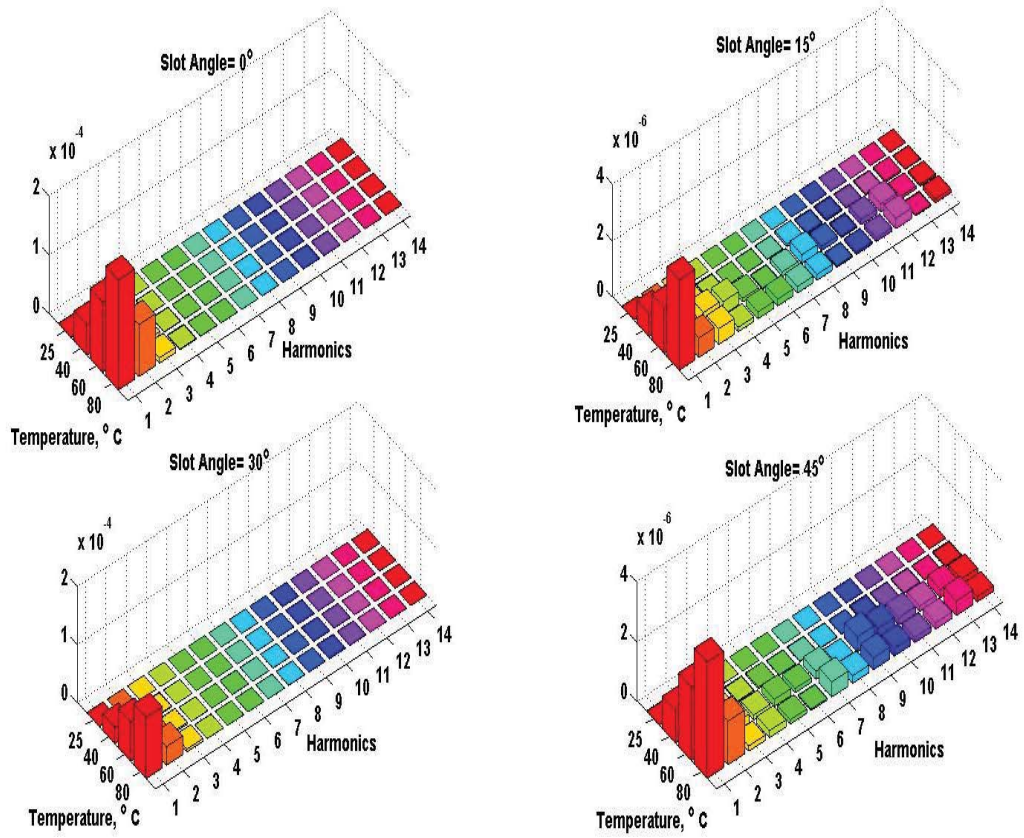


Fig. 4.12 RRO harmonics of OD radial displacement (mm) at different temperature and slot angle designs

This finding of creating imperfection in spindle hub design to reduce the RRO has significant inferences in mechanical integrity and design of the hub assembly. For example, design engineers can use the slot feature at desired location to purposely generate imperfection which can act as a method of lubrication or enclosure for ball bearings.

In the next chapter, the periodicity in rotationally periodic structures has been investigated through shock wave response. Again for simplicity and ease of availability, hard drives have been adopted as the key research model in RPS, and its head gimbal assembly (HGA) been taken as the motivation of the research. The main focus of next chapter is to analyze the shock wave effect on the periodicity of the rotationally periodic structure.

## CHAPTER 5

### SHOCK WAVE RESPONSE OF ROTATIONALLY PERIODIC STRUCTURES

#### PRÉCIS

<b>Response selection:</b>	Shock stress
<b>Model selection:</b>	Hard disk drive (HDD)
<b>Problem statement:</b>	De-bonding of head gimbal assembly and suspension in Hard disk drives via Shock stress

This thesis circulates around 3 major responses on rotationally periodic structures. Previous chapter covered thermal response where HDD's DSA was taken as design component in RPS. With the view toward understanding the underlying physics and to minimize the corresponding repeatable run-out (RRO) of track following position error signal (PES) in high track per inch (TPI) magnetic disk drives, analytical representation of thermal expansion mismatch between disk and spindle hub structure formulated in form of operators and finite element analysis (FEA) are employed. Parameter studies with analysis taken at different operational temperatures suggest that RRO can be minimized significantly when location of spindle notch is properly located. RRO harmonics resulted from the thermal expansion mismatch and structure misalignments are studied and concluded with simple algebraic expression related to number of fasteners used in disk-spindle assembly.

On the other hand, this chapter discusses the shock stress response of rotationally periodic structure. As discussed previously in section 1.3.3, hard disk drive has been selected as a RPS model with focus on head gimbal assembly and suspension of HDD to eliminate head de-bonding phenomena due to shock wave.

## 5.1 INTRODUCTION

Hard disk drives (HDD) are composed of tiny components that hold an immense degree of sensitivity. Increasing demands of HDD with shrinkage of data track widths requires precision in design, in consideration of all aspects of possible failures either physically or logically. Major drive failure most likely is caused by shock impulse.

All shocks carry the potential of causing the drive to fail or data loss. The most disruptive events are those with high shock levels and short duration. Hence the study to overcome these errors is eminent in the design of HDD.

Several literature could be found regarding shock dynamics in head disk interface. Jang and Seo [34] developed a finite-element model with mode superposition to analyze the shock response of a HDD with FDBs, a head-suspension-actuator with pivot bearings and air bearings, and a base plate with complicated geometry and proposed method that predicts the peak value of the vibration due to shock composed of a spinning disk-spindle system. Lim and Yang [43] integrated MEMS actuator with HGA and investigated 1000 G of shock amplitude and reported larger maximum stress level in non-operational HDD model compared to operational HDD model. Bhargava and Bogy [4] examined air bearing response and proposed a procedure to compute the normal loads and moments applied to the slider. Feliss, Murthy, and Talke [27] reported that the thicker the cover plate, the better is the shock response. They also suggested modification in suspension to prevent slapping motion of the head/suspension against the disk. In recent work, Zheng and Murthy [75] investigated dimple response and suggested a large diameter and high dimple preload to reduce the contact stress and shock performance of the suspension. Li *et al* [42] examined relative displacement between the dimple and gimbal and reported as it follows acceleration of the suspension, with a minimum effect of friction coefficient on the relative displacement. Yap *et al* [77] considered discontinuity and nonlinearities between components in a HDD when subjected to shock excitation while Rai and Bogy [63] examined contact dynamics between the HGA and ramp under operational vibration cases. In addition to the aforementioned approaches Shu and Yap [81] studied the effect of clamping conditions on shock response of HDD and reported the shock response of the

drive will decrease when the disk is more tightly clamped. Lately, K. Kim, S. Kim and N.C. Park [39] compared thermally assisted magnetic recording head gimbal assembly (TAMR HGA) with conventional HGA and reported TAMR HGA to withstand more shock but have higher risk of contact between media and slider. This chapter, on the other hand presents a head gimbal assembly (HGA) design approach that would be able to reduce certain impact stress at head component caused by non-operational shocks on a HDD. This study has engineering implications in mechanical design to ensure reliability of the head gimbal assembly in HDDs.

## **5.2 EXPERIMENTAL OBSERVATIONS**

HDD are assumed to be sturdy but because of their technical conditions they have a high risk of drive failure. They contain electromechanical components that might be damaged by external conditions e.g. thermal and shock stress. Although a broad research has been done on non-operational shock analysis but not much has been carried out in HGA de-bonding phenomena by external shock stress wave. To fix an idea and for completeness of describing motivation of the HGA de-bonding problem, experimental measurements are presented and discussed in this section.

For the experimental analysis, an enterprise HDD was tested on a linear shock test machine as shown in Figure 5.1. This set-up was composed of accelerometers, FFT analyser, and a linear drop tester. All accelerometers were calibrated before test. Before continuing to the experimental observations, three accelerometers were installed at fixture, rail and base positions respectively and sanity check was carried out to ensure the accuracy of the test. Shock direction was agreed to be perpendicular to the base cover. Figure 5.2 shows comparison of measured shock pulse at different locations. Shock response at fixture and rail were very similar which concluded that rail/fixture attachment was good.



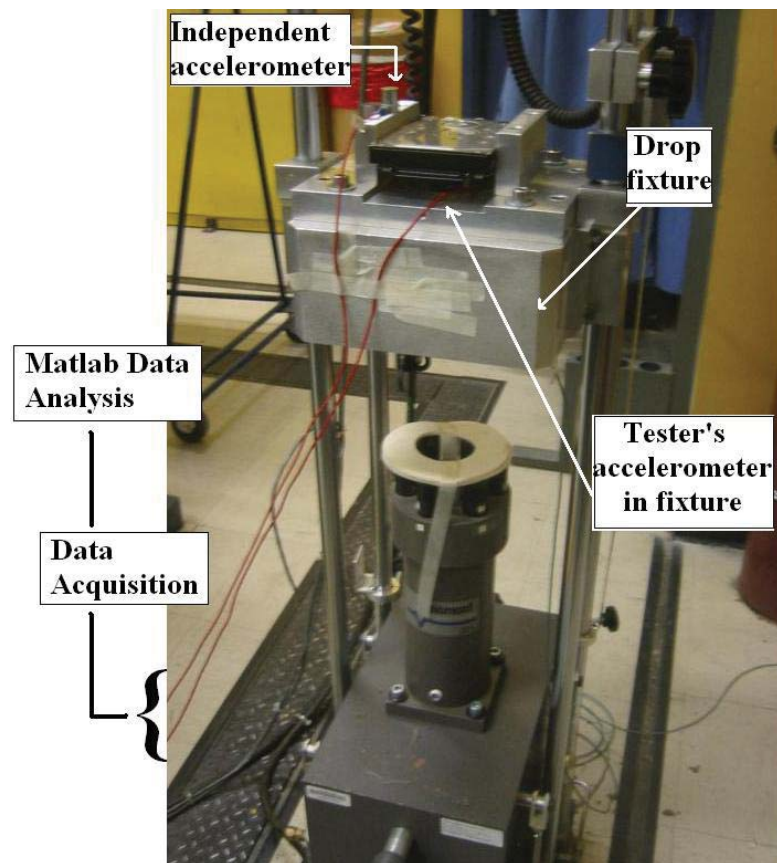


Fig. 5.1 Experimental setup for drop test analysis

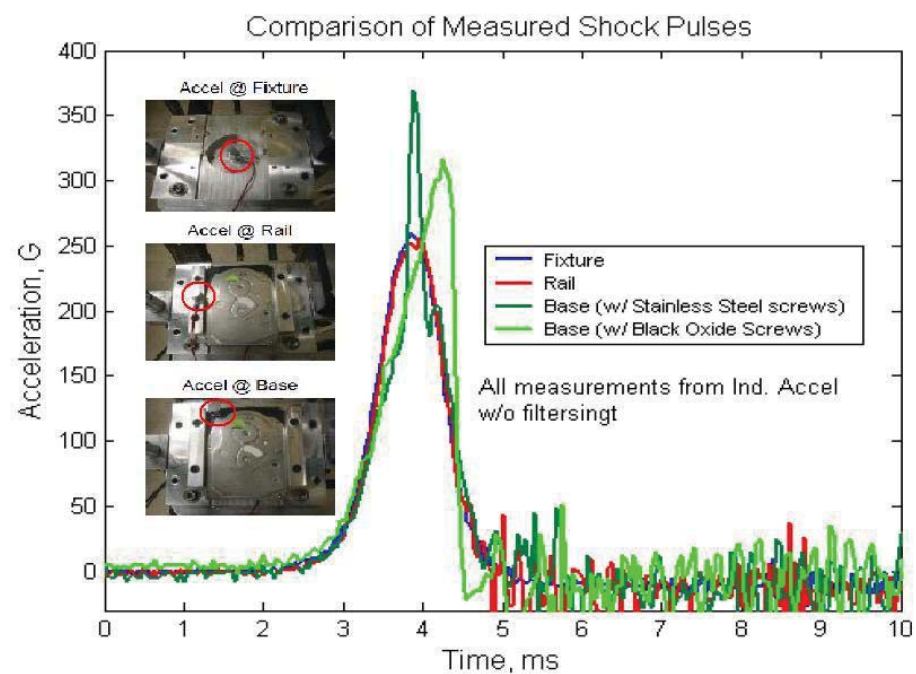


Fig. 5.2 Sanity check of drop fixture

Although it was spotted that the screws used to hold the file to rail, played an important role for G level amplification. Base with black oxide screws were used for stable shock pulse. An independent accelerometer and a tester accelerometer were installed at rail and HDD base respectively. The drop fixture was released from a certain height under the gravity pull to acquire the alleged shock G levels. The shock pulse signal was analysed using the Lansmont software. The assembled suspension with different configuration of accelerometer was excited under 250 G level. Different shock pulse signals were analysed until they reached steady state of desired G level and shock duration. The drop test statistic is shown in table 5.1(a). Independent accelerometer's output correlated very well to tester's accelerometer output as depicted in figure 5.3. This graph satisfied that the desired G level had been transmitted to the designated spot under HGA.

The HDD specimen was dismantled after the impact from the drop fixture and was unscrewed for non-operational shock analysis. No motor spin or head load/unload was allowed after shock test. Microscopic observations were carried out for any noticeable damage. HGA pictures were taken before and after drop as shown in Fig. 5.4. It was observed that head was de-bonded from flexure which could be the reason of significant failure of HDD. Table 5.1(b) statistics shows about 8.5% of internal HGA were facing the de-bonding phenomena in non-operational shock conditions

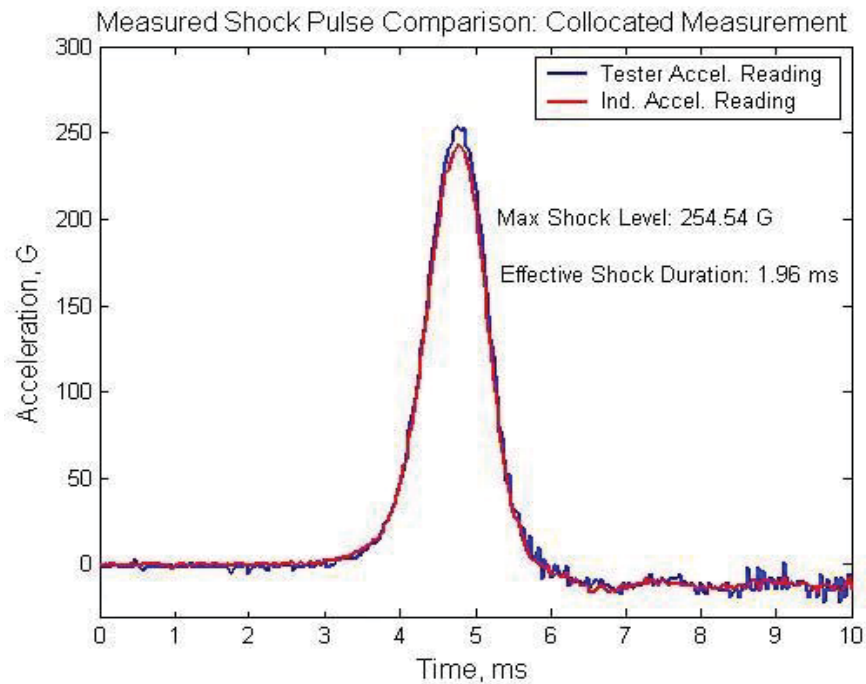




Fig. 5.3 independent and tester accelerometer stability diagram

**Table 5.1**

(a) Drop Test Statistics

Based on N=48 recorded Test	Shock Level (G)	Shock duration (ms)
AVG	253.07	2.08
Max	263.91	2.2
Min	239.78	1.97

(b) Qualitative observation of Flexure De-bond

Visual de-bonded vs Total heads	
Internal HGA	10/118 = 8.5%

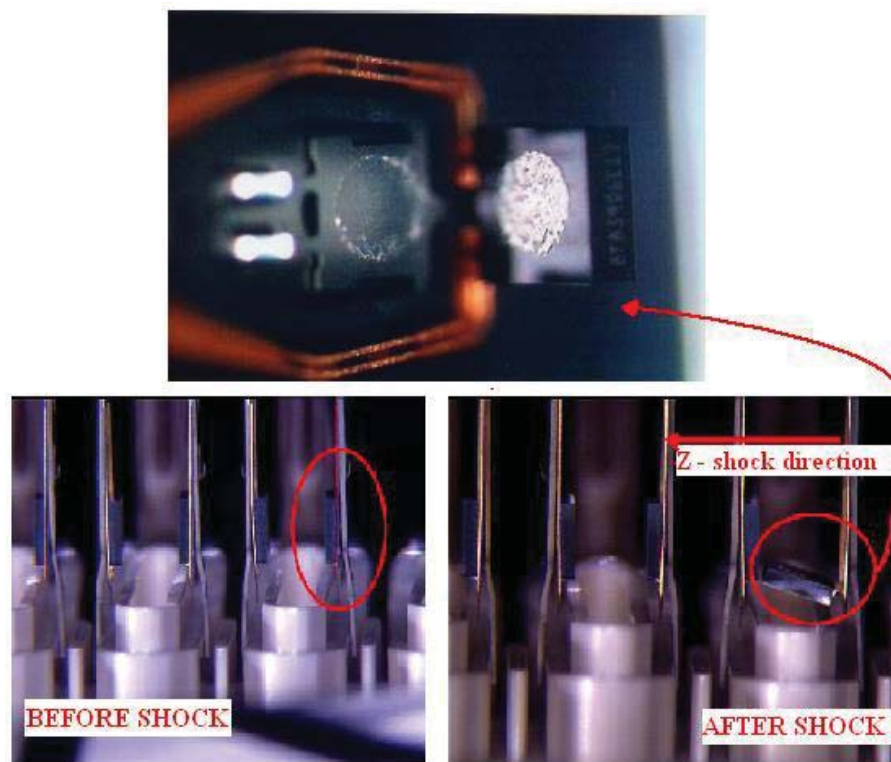
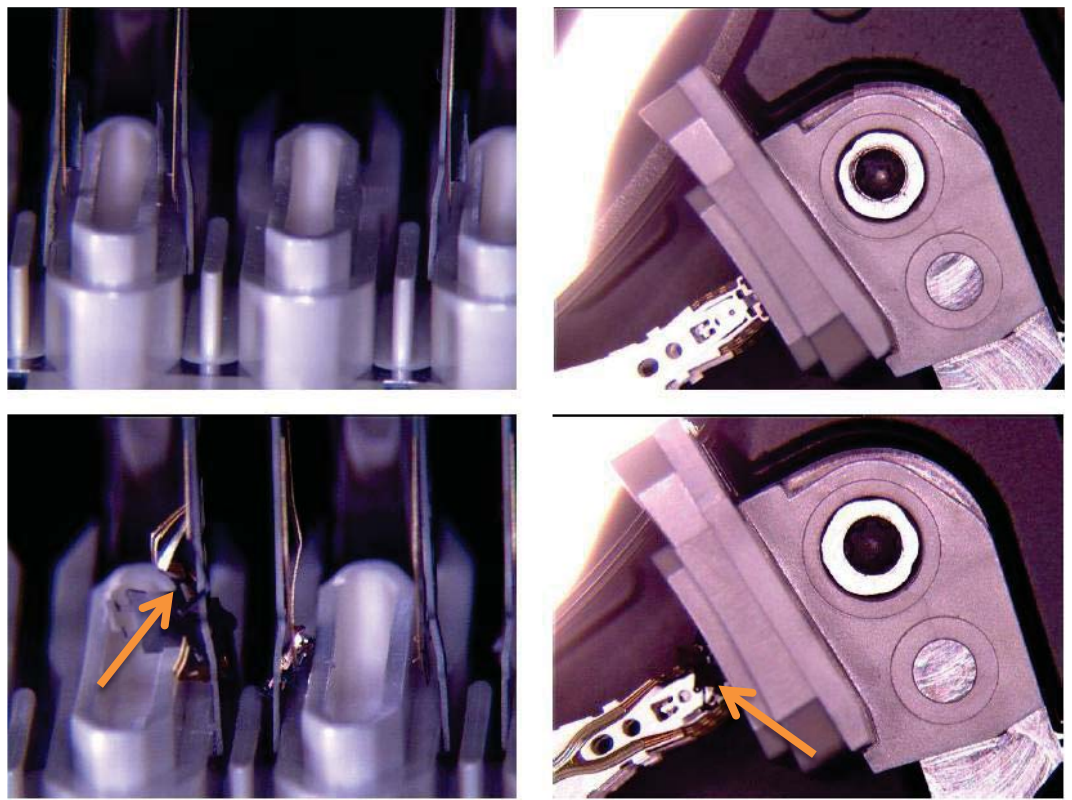


Fig. 5.4 De-bonding of flexure @250G and 2ms

This small de-bonding effects air bearing which results in head crash after unloading and leads to total mechanical failure of HDD as depicted in fig. 5.5. This strong observation of de-bonding phenomena between head gimbal assembly (HGA) and suspension as illustrated in fig. 5.4 and fig. 5.5 of a commercial 3.5-inch enterprise HDD under non-operational 250G shock test leads to revisit design of HGA/suspension with objective placed on withstanding shocks between the head slider and the suspension. In the following section, strengthening of HGA to overcome de-bonding will be studied and discussed through HGA finite element studies at different shock impulse.



*Fig. 5.5 Photograph of small and large de-bonding resulting mechanical failure*

### 5.3 FINITE ELEMENT MODEL

A fully populated 3D finite element model using geometric specifications of a head gimbal assembly (HGA) obtained from an enterprise HDD was constructed by using commercial SolidWorks software as shown in Fig. 5.6. Material properties of base casting, gimbal assembly and spindle motor have been taken as stainless steel while ramp and disk has been taken as ABS plastic and glass, respectively. To reduce computational effort, reduced mass and stiffness matrices are used in the simulation with suppression of those given by disk spindle motor assembly (DSA). HGA is rested and parked at ramp in the model to mimic realistic non-operational condition. Interaction between the ramp and HGA surfaces which were likely to come in contact was taken as bonded with no-penetration. The shock energy imposed on the HGA was transmitted from the pivot point of actuator. Drop test analyses were conducted to generate shock impulse provided by SolidWorks simulation module

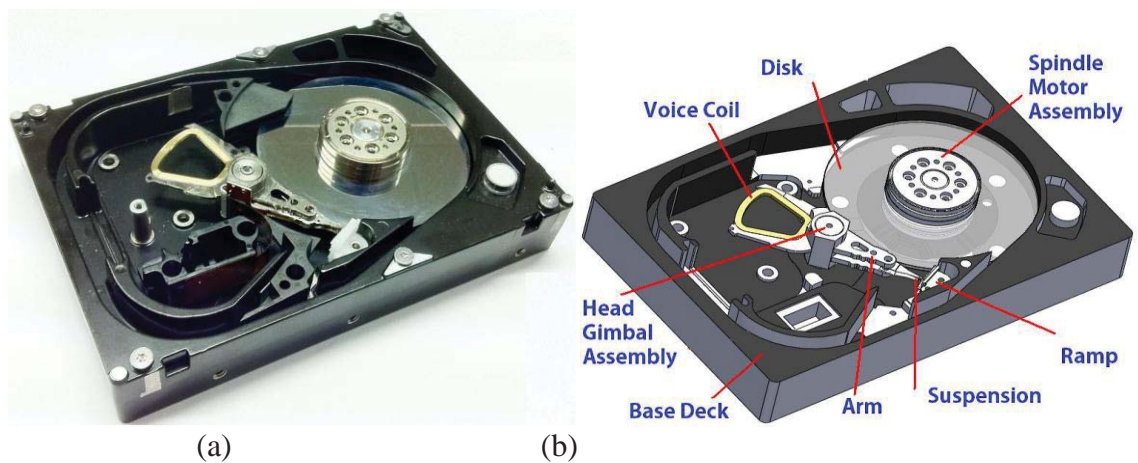


*Fig. 5.6 Photograph of dismantled enterprise HDD (a) and the corresponding finite element model in (b)*

Shock measurements have been taken from the centroid of the HDD, and assumed to be oriented parallel to the rigid floor. The default angle of the floor at which HDD dropped was taken normal to gravity. Several different HGA designs as illustrated in Fig. 5.7 were developed for parametric study.

Four critical vertex points were taken on HGA to record shock responses when tested with

different design parameters and drop heights. These vertexes were denoted as upper arm joint vertex ( $U_{JV}$ ), upper arm head vertex ( $U_{HV}$ ), lower arm joint vertex ( $L_{JV}$ ), and lower arm head vertex ( $L_{HV}$ ) as shown in Fig. 5.8, respectively. Drop test has been simulated at 4 different heights, namely 0.5m, 1m, 2m, and 3m. In other words, the non-operation shock has peak level at 50G, 100G, 200G and 300G, respectively

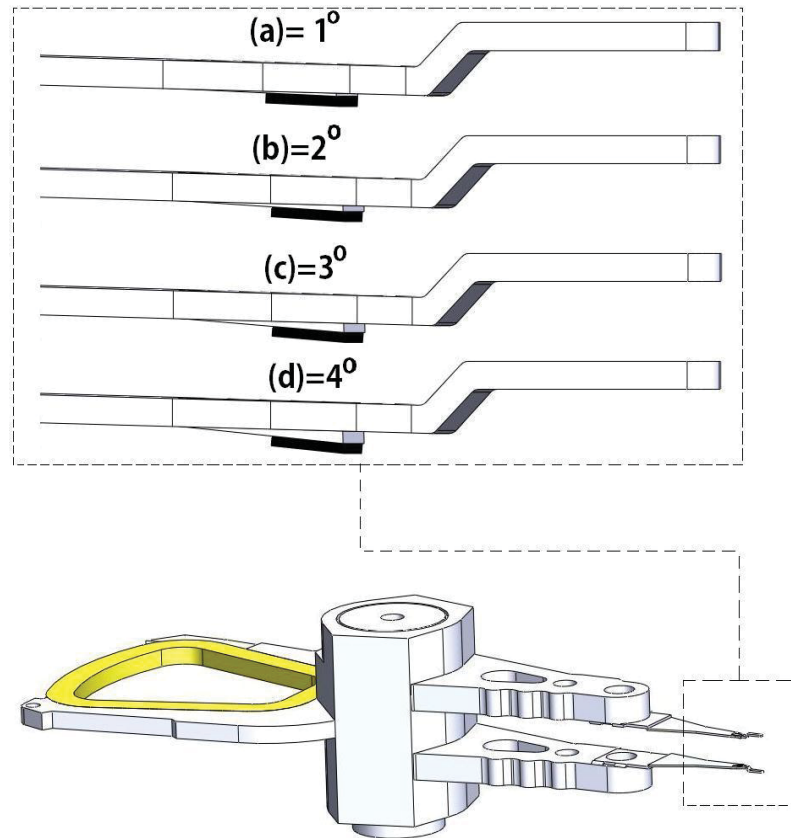


*Fig. 5.7 HGA designs with different flexure angle,  $\alpha$  at (a)  $1^\circ$ , (b)  $2^\circ$ , (c)  $3^\circ$ , and (d)  $4^\circ$*

#### 5.4 MINIMIZATION OF SHOCK EFFECT

As an illustrative example, von Mises stress history plot for all four critical vertex points were shown in Fig. 5.8 after the HDD hits the concrete floor when it is dropped 1m above the floor. The oscillations simply represent aftershock responses in which maximum stress level is of engineering importance.

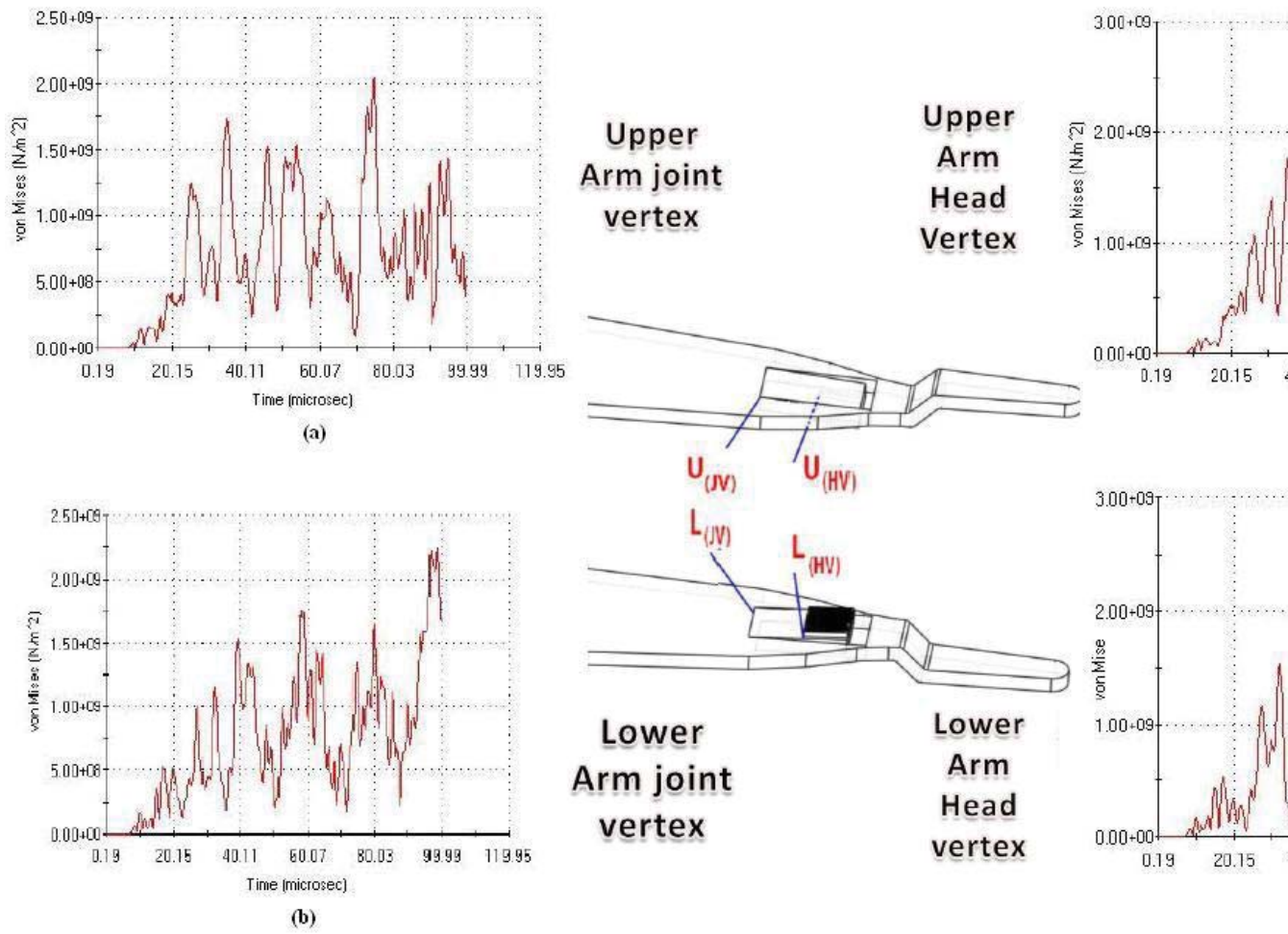


Fig. 5.8 HGA impact stress history plot of four critical vertex points with flexure angle at  $\alpha=1^\circ$



Fig. 5.9 shows maximum stress at critical vertex points with respect to drop heights. It can be clearly seen that upper and lower arm head vertexes ( $U_{HV}$  and  $L_{HV}$  cases) are vitally exposed to shock. At 250G which is equivalent to 2.5m drop height, it seemed to face terminal stress exceeding bonding strength between the slider and the suspension. This explains and agrees with the experimental observations as shown in Fig. 5.4 in which the slider is de-bonded from the suspension at the upper and lower arm vertex points when it is subject to 250G non-operational shock.

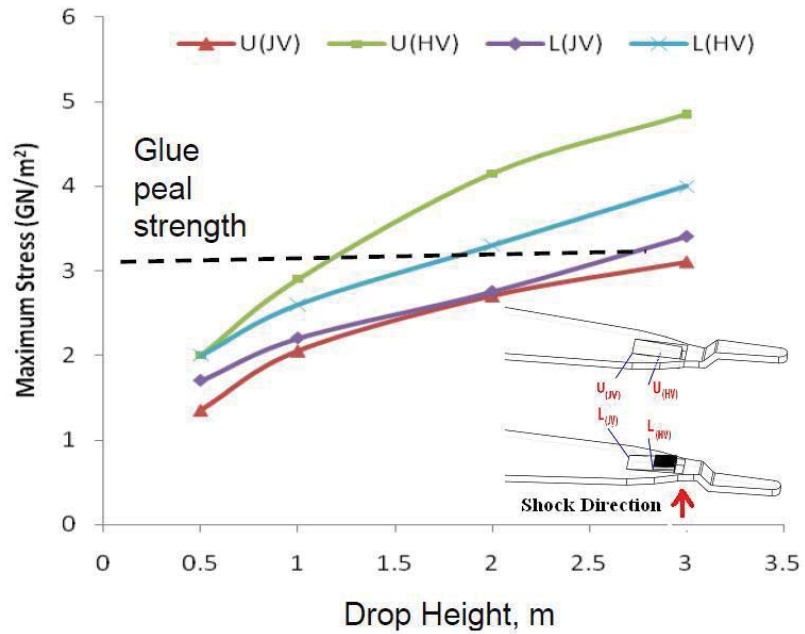


Fig. 5.9. Maximum impact stress around HGA critical vertex points as function of drop heights with  $\alpha=1^\circ$

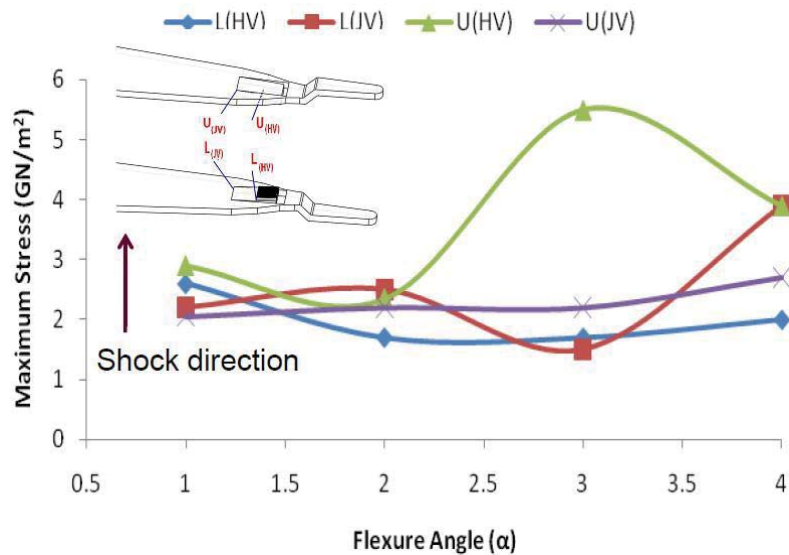
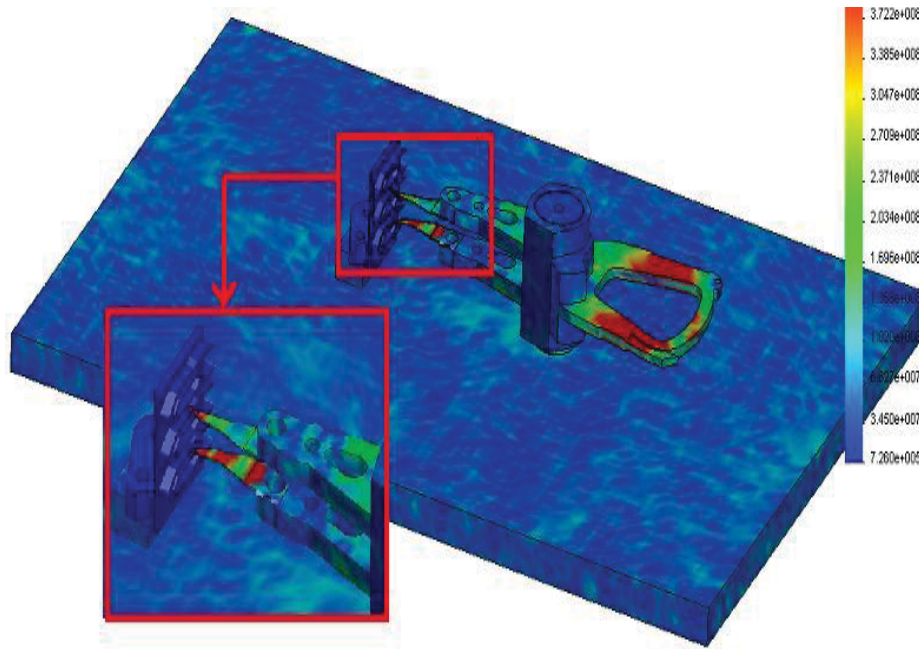


Fig. 5.10. Maximum impact stress around HGA critical vertex points as function of flexure angles at 200G/2m drop height



*Fig. 5.11 Simulated HGA with Stress concentration regions*

A simulated picture of HGA is depicted in fig. 5.11. Since being tiny with high degree of sensitivity; the HGA holds high stress concentration regions. Figure 5.11 show that a small impact can cause more stress at these regions then other parts of HDD.

By changing the flexure angle  $\alpha$ , quite interesting phenomena was observed as shown in Fig. 10 in which the shock level 200G, i.e. drop height is 2m from ground. It is noted that upper arm head vertex ( $U_{HV}$ ) and lower arm joint vertex ( $L_{JV}$ ) seemed to form a wave shape with respect to flexure angle  $\alpha$ . Whereas for lower arm head vertex ( $L_{HV}$ ) and upper arm joint vertex ( $U_{JV}$ ), the transition is smooth and stays in stress limit, which obviously can be modelled by 2<sup>nd</sup> order polynomials. With the present commercial HGA/suspension design, it is found that flexure angle at 2 degree can provide relative less non-operating shock stresses on all critical vertex points.

## 5.5 CONCLUSION

In this section of the thesis, experimental and finite element studies were performed to understand resistance of HDD head gimbal assembly to non-operational shocks from which concluding remarks can be summarized as:

1. Non-operational shock causes severe impact at head gimbal assembly (HGA) which could force leader head to de-bond from suspension.
2. By changing flexure angle, one can significantly reduce shock stress at critical vertex in HGA.
3. Flexure angle at 2 degree is reported to withstand less stress concentration with respect to non-operational shocks.
4. Numerical simulation results from the present study agreed very well with experimental observations which can serve as design tool to enhance reliability of HGA at product development stage.

The analysis on the design of HGA to withstand shock impulse in this chapter has been accepted for publication as mentioned in [83, 87]



## CHAPTER 6

### CONCLUSION

#### 6.1 SUMMARY

There are numbers of technological applications for rotationally periodic structures spread throughout the market. All of these structures have common axis-symmetrical base with periodic features either in shape of evenly spaced bolts, clamping or additional built-in features. As for the reason of such periodic features the vibratory or thermal response becomes contaminated and produces additional wavenumber in the structure's circumference. The doctoral research targeted the vibratory, thermal and shock response via design, analysis and testing of rotationally periodic structures with careful selection of RPS models through wide range of applications.

This thesis very briefly describes the basics and importance of rotationally periodic structures in engineering and natural world. After carefully studying the broad variety of RPS, newly developed integrated bladed rotors and hard disk drives is chosen to carry forward the research. The set research goals have been successfully dominated in vibratory, thermal and shock response in rotationally periodic structures with new findings of replica modes in integrally bladed rotors (IBR), a reduction to total elimination of thermal expansion mismatch in hard disk spindle assembly (DSA) and new design to withstand shock and enhance reliability of head gimbal assembly (HGA) in HDD respectively.

In brief, for vibratory response of rotationally periodic structures, effects on structure designs on free vibrations of integrated bladed rotor (IBR) have been conducted in this research. Migration of natural frequencies is characterized through parameter studies considering changes of blade angle and blade thickness on an underlying uniform axis-symmetric rotor. The appearance of replica mode,  $R(m, n)$ , has been observed in IBR structures for repeated frequency doublets having nodal line  $n > 1$ . For each replica mode pair, integrated blades of low frequency component,  $P(m, n)L$ , vibrate in-phase with disk whereas for high frequency component,  $P(m, n)H$ , blades and disk vibrate out-of-phase

with each other. A spring mass model was developed and equations of motion have been established. Nodal pattern as well as the associated Fourier content of low frequency replica component is found to be sensitive to change of blade angle while the pattern is observed fixed with respect to IBR structure. Veering and cluster of replica modes' natural frequencies are observed with respect to the blade design parameters. Existence of replica modes has been verified via experimental studies. For all the replica modes, good agreement is found between the results of experimental modal analyses (EMA), Chladni's patterns technique and the finite element analysis (FEA).

In thermal response of RPS, radial repeatable run-out caused by component thermal expansion mismatches in a disk-spindle assembly (DSA) was examined. System models for disk-spindle assembly were constructed by considering realistic conditions of alignment eccentricity and structure imperfection. Thermal –elastic finite element analyses were performed for the system at elevated temperatures. It is concluded that the 2X RRO pertaining disk's deformation as potato chip is caused by spindle hub's thermal expansion to an oval shape whereas 1X RRO is caused by thermal expansion contact due to disk/hub eccentric alignment. Furthermore, it was supported by perturbation model and found that additional harmonics  $k$  satisfies the algebraic equation  $|n \pm k| = NF, 2NF, 3NF, \dots$  were strongly related to driving harmonics  $n = 1, 2$ , and  $NF$  which correspond to physical disk slip contact, disk deformation to a potato chip, and constraining loads from screws and fasteners, respectively. Amplifying structure imperfection and destroying its cyclic symmetry, it is also found from finite element studies that 2 x RRO caused by thermal expansion of DSA can be completely eliminated by properly placing notch feature inside the underlying cyclic symmetric spindle hub.

For shock wave response on the periodicity of RPS, head gimbal assembly (HGA) of HDD was taken as research focus. By experimental observations and drop test technique, it was observed that non-operational shock causes severe impact at head gimbal assembly (HGA) which could force leader head to de-bond from suspension. Different design modifications were adapted to withstand shock waves. It was observed that by changing flexure angle in HGA, shock stress can be reduced. FEA simulation results have been presented to verify the findings.

## 6.2 LIMITATIONS

The thesis-based research contains several limitations due to the shortage of the resources. The following issues for the integrated bladed rotor with evenly-spaced blades have been identified in this study.

1. The manufacturing of the integrally bladed rotor – Integrally bladed rotor was tried to manufacture using stainless steel disk and welded blades at the end to mock as an integrally bladed rotor. But because of the manhandled job most blades seemed to be mistuned which affect the accuracy of the results. Instead of manufacturing proper rotor, the rapid prototype technology is used to manufacture the cyclic symmetric bladed rotor in order to reduce time and cost consumption. The size and material were the major trade-offs which may have caused the preciseness of the result but were close enough to do the experiment. Although, there were very few deviations exhibiting between the blades but still it is more likely to affect the mode shape and also some modulation in natural frequency. Therefore, it is recommended that the accurately manufactured integrally bladed rotor should be replaced in order to solve these problems and ensure the precise performance.
2. Piezoelectric driving system – In carrying out Chladni's experiment, the function generator and ring of piezoelectric actuators were employed as the driving sources. In order to fulfil the optimal actuation, plural buzzers were employed to achieve this purpose. However, it changed the mass property and it was likely to affect the structure responses. The prototyped IBR was made of PU material which was likely to damp the driving effect, with this setting; it was tricky to get accurately visible nodal lines on required frequencies due to the lack of the equipment and design. Moreover, it is unlikely to obtain the optimal result without optimum actuation output. Hence, it is recommended that a shaker driving system with high voltage power amplifier should be developed to drive the actuators and an accurately manufactured IBR should be replaced from a 3D printed model.

3. Transition of research models – For thermal response on rotationally periodic structure and key example taken as integrally bladed rotor, it was inevitable to continue because of the manufacturing limitations and polyurethane material, it was impossible to perform a thermal test on prototypical IBR at high temperatures. Therefore, a hard disk drive spindle system has been selected to carry out the research further for thermal as well as shock analysis.

### **6.3 FUTURE WORK**

Some directions of future work have been highlighted in the following section on the new finding of replica modes in integrally bladed rotors:

#### **6.3.1 FORCED VIBRATION RESPONSE ON REPLICA MODES**

The new finding of replica modes has been analyzed through free vibration response in the thesis. The response study does not address the force vibration response on integrally bladed rotors. Further work can be done by applying some forced response in terms of air pressure or real life asymmetrical clamping effects could be considered as unwanted force vibrations. In the real application, turbine blades are curve-shaped, which also causes the aerodynamically vibration problems and should be considered in the integrally bladed rotor's forced response analysis. Consequently, inclusion of those considerations in the vibration model would provide a more accurate and real presentation than the model discussed in this thesis. These effects generate a situation under which multiple sections of rotational periodicity can affect and change the structure's vibration characteristics. The trends of replica modes under force vibration can be analysed and compared with the present study.

#### **6.3.2 DAMPING OF REPLICA MODES**

The free vibration response study considered in the thesis was adapted with no damping effect. The new finding of replica modes can be analyzed and a damping technique can be introduced to damp both higher and lower frequency sine cosine replica modes by just

applying damping to one mode shape. For instance one can design a rotational plate with actuated air nozzle effect to damp certain modal frequencies. This can provide engineering implications in designing integrated bladed rotors subject to travelling wave and engine order excitations.

### **6.3.3 MISTUNING EFFECT ON REPLICA MODES**

A perfect and idealized model of integrated bladed rotor was assumed in this thesis. However in the real world, asymmetry of the structure can cause extra harmonics which results in modulating the structures frequency. Small imperfections are inevitable in the manufacturing process of turbine blades and therefore some mistuning is always present in bladed disk. It is usually found that in mistuned blades excessively large vibrations occur when compared to perfectly tuned systems. Although the subject of mistuning is beyond the scope of this thesis but extra stiffness and inertia is also of practical importance. Replica modes can be analyzed by intentionally mistuning a blade to mock as reality which might possibly reduce certain contamination waves.

## REFERENCES

- [1] **K. G. Ashar**, “Magnetic Disk Drive Technology”. New York: IEEE Press, 1997.
- [2] **R.H. Aungier**, “Turbine Aerodynamics: Axial-Flow and Radial-Flow Turbine. Design and Analysis,” ASEM Press, ISBN 0-7918-0241-8, New York, NY, USA, 2006. . Imai, “Fluid dynamics mechanism of disk flutter by measuring the pressure between disks”, IEEE Transactions on magnetic, vol. 37, no.2, 2001.
- [3] **R. J. Barber**, "Implications of thermoelastic instabilities for the design of brakes", Jnl. Tribology., v. 107, pp. 206–210. 1985.
- [4] **Bhargava**, P., Boggy, D.B., (2007) “Numerical simulation of operational-shock in small form factor hard disk drives,” *Journal of Tribology*, Vol. 129.
- [5] **P. Bisegna**, G. Caruso ,” Optimization of a passive vibration control scheme acting on a bladed rotor using an homogenized model”, Structural and multidisciplinary optimization, vol. 39: page 625-636. 2009.
- [6] **H. Bittner**, I.Y. Shen, “ Tamming disk spindle vibrations through aerodynamic bearings and acoustically tuned-mass dampers”, IEEE trans. Magn., vol. 35. No. 2, pp.827-832. 1999.
- [7] **J. Byrne**, R.F. Hall and B.E. Powell, “Influence of LCF Overloads on Combined HCF/LCF Crack Growth,” International Journal of Fatigue, Vol. 25, Issue 9-11, pp. 827-834, 2003.
- [8] **J.Y. Chang**, J.A. Wickert, “Measurement and Analysis of Modulated Doublet Mode Response in Bladed Disks,” Journal of Sound and Vibrations, Vol. 250, pp.379-400, 2002.
- [9] **J.Y. Chang**, J.A. Wickert, “Response of Modulated Doublet Mode to Travelling Wave Excitation,” Journal of Sound and Vibrations, vol. 242(1), pp.69-83, 2001.
- [10] **J.Y. Chang** and J.Y. Shen, "Repeatable Run-out Harmonics Induced By Disk Clamp In Magnetic Disk Storage Devices," ASME 14th Annual Conference on Information Storage and Processing Systems, Santa Clara, CA, USA, June 14-16, 2004.

- [11] J.Y. **Chang**, C.A. Gimenez, R.P. Harshberger, and J.Y. Shen, "Method and System For Optimizing Servo Track Writing Motor Current Profile to Reduce Written-In High Frequency Repeatable Runout Track Mis-Registration," United States Patent, US 7,133,244 B1, November 7, 2006.
- [12] J.Y. **Chang**, J.A. Wickert, "Measurement and Analysis of Modulated Doublet Mode Response in Bladed Disks," Journal of Sound and Vibrations, Vol. 250, pp.379-400, 2002.
- [13] J.Y. **Chang**, J.A. Wickert, "Response of Modulated Doublet Mode to Travelling Wave Excitation," Journal of Sound and Vibrations, vol. 242(1), pp.69-83, 2001.
- [14] J.Y. **Chang**, C. A Gimenez, R. P. Harshberger, and J. Y. Shen, "Method and System for Optimizing Servo Track Writing Motor Current Profile and Reduce Written-in High Frequency Repeatable Runout Track Mis-Registration," U.S. Patent US7133244, 2006.
- [15] J.Y. **Chang**, C. A Gimenez, R. P. Harshberger, and J. Y. Shen, "Method and System for Optimizing Servo Track Writing Motor Current Profile and Reduce Written-in High Frequency Repeatable Runout Track Mis-Registration," U.S. Patent US7345842, 2006.
- [16] J. Y. **Chang**, "Mitigation of track following repeatable runout in high TPI hard disk drives through servo and mechanical designs", IEEE trans. Magn., Vol. 45, no. 11, pp 5010 – 5015, 2009.
- [17] J. Y. **Chang** and J. Ralay, "Repeatable Runout Compensation Methods and Apparatus for Data Storage Devices," U.S. Patent US6937424, 2005.
- [18] A. S. **Chang**, T. C. Fu, A. K. Hanlon, S. A. Hassen, T. Jefferson, K. Shida, J. Y. Shen, and S. Y. Wong, "Hard Disk Drive With Disk Clamp Inner Wall Engaging Bearing Sleeve Outer Wall," U.S. Patent US6961216, Nov. 2005.
- [19] J. Y. **Chang**, "Method and Apparatus for Determining Modulated Amplitude Ramping RRO harmonics in Multi-Screw Clamped Disk/Spindle Assembly," U.S. Patent US6992853, Jan. 2006.
- [20] J. Y. **Chang** and J. A. Wickert, "Response of Modulated Doublet Modes to travelling wave excitation" J. Sound Vib., vol. 242, no. 1, pp. 69 – 83, 2001.



- [21] J.Y. **Chang**, 2011 “Thermal Analysis of Disk-Spindle Repeatable Run-out in Spindle Data Storage Devices”, IEEE Transaction on mechanics, Vol. 47, pp. 1855-1861.
- [22] B. M. **Chen**, T. H. Lee, and V. Vengataramanan, Hard Disk Drive Servo Systems, London, U. K.: Springer-Verlag, 2002.
- [23] G. **Dalpiaz**, ” Early detection of fatigue cracks in gears by vibration analysis techniques” *Österreichische Ingenieur - und Architekten - Zeitschrift (ÖIAZ)* 135, 312-317,1990.
- [24] G. **Dalpiaz**, A. Rivola , R. Rubini, “ Gear fault monitoring: comparison of vibration analysis techniques”, Third international conference on acoustical and vibratory surveillance methods and diagnostic techniques, senlis, france, vol. 2, pp-623-637, 1998.
- [25] R. M. **Ehrlich** and F. A Zayas, “ Disk Drive Write Method,” U. S. Patent US7721049 , 2010.
- [26] **Feliss**, B., Murthy, A.N., and Talke F.E. (2007) “Microdrive operational and non-operational shock and vibration testing,” *Microsystem Technology*, Vol. 13, pp. 1015-1021.
- [27] T. C. **Fu**, R. Lenicheck, S. Malek, U. Kim and S. Y. Wong, “ Apparatus and System for Centering Media Disks on the Hub of a Spindle Motor in a Hard Disk Drive,” U.S. Patent US7283325, Oct. 2007.
- [28] C. **Fukushima**, K. K. Kambla, and M. M. Yu, “ Read Write Offset Error Correction Using Geometric Reference in Self Servo Write Process,” U. S. Patent US7586709, 2009.
- [29] Tony **Giampalo**, “The Gas Turbine Handbook: Principles and Practices”<sup>2<sup>nd</sup></sup> Edition, pp. 178, 2003.
- [30] J.H. **Griffin** and C.-H. Menq, “Friction Damping of Circular Motion and Its Implications to Vibration Control,” ASME Journal of Vibration and Acoustics, Vol. 113, Issue 2, pp. 225-229, 1911.
- [31] H. **Inoue**, ”Analysis of brake judder caused by thermal deformation of brake discs” , SAE Technical Paper Series, no. 865131. 1986.

- [32] G. H. **Jang**, S. J. Park, and S. H Lee, “ Electromechanical analysis of a HDD/ spindle motor considering electromagnetic, thermal analysis , hydrodynamic bearing and rotor dynamics,,: IEEE Trans. Magn., Vol41, pp. 1608-1611, May 2005.
- [33] G. H. **Jang**, “Analysis of a hydrodynamic bearing of a HDD spindle motor at elevated temperature ,” ASME J. Tribol., Vol 126, No. 2, pp. 353-359, April 2004.
- [34] G. H. **Jang**, C. H. Seo, (2007) “Finite-Element Shock Analysis of an Operating Hard Disk Drive Considering the Flexibility of a spinning Disk-Spindle, a Head-Suspension-Actuator, and a Supporting Structure” *IEEE Trans. Magn.* VOL. 43, NO. 9.
- [35] K.H. **Jeong**, B.K. Ahn, S.C. Lee, Modal analysis of perforated rectangular plates in contact with water, *Structural Engineering and Mechanics* 12 pp.189–200, 2001.
- [36] J.C. **Ji**, N. Zhang, ”Suppression of the primary resonance vibrations of a forced nonlinear system using a dynamic vibration absorber, *Journal of sound and vibration* 329, page 2044-2056. 2010.
- [37] **Kenyon**, J.A. and Griffin, J.H.: *Forced Response of Turbine Engine Bladed Disks and Sensitivity to Harmonic Mistuning*. International Gas Turbine and Aeroengine Congress and Exhibition, 125(1):113–120, 2003.
- [38] H. **Kim**, I.Y. Shen, ”Vibrations of Spinning Rotationally Periodic Rotor,” Proceedings to the ASME 2007 international design engineering technical conferences & computers and information in engineering conferences IDETC/CIE, 4-7 September 2007, Las Vegas, USA.
- [39] M. **Kim**, J. Moon, J.A Wickert, ”Spatial Modulation of Repeated Vibration Modes in Rotationally Periodic Structures”, *Journal of Vibrations and Acoustics*, Vol. 122, pp. 62-68, 2000.
- [40] S. **Kim**, G. Han, H. Son, 1998,” A study of Characteristics of disk vibration and rotating airflow in magneto optical disk drives”, *IEEE transactions on consumer electronics* Vol.44, No. 3, August 1998.
- [41] H. **Kim**, I.Y. Shen, ”Vibrations of Spinning Rotationally Periodic Rotor,” Proceedings to the ASME 2007 international design engineering technical conferences & computers and information in engineering conferences

IDETC/CIE, 4-7 September 2007, Las Vegas, USA.

- [42] M. **Kim**, J. Moon, J.A Wickert, "Spatial Modulation of Repeated Vibration Modes in Rotationally Periodic Structures", *Journal of Vibrations and Acoustics*, Vol. 122, pp. 62-68, 2000.
- [43] U. **Kim** and D. K. Lieu, "Magnetic field calculation in permanent magnet motors with rotor eccentricity: Without notching effect," *IEEE Trans. Magn.* Vol 34, pp 2243 – 2252 , July. 1998.
- [44] K. H. **Kim**, S. Kim, N. Park, Y. Park , K. Park, (2011), "Operating Shock Analysis of a Thermally Assisted Magnetic Recording Head Gimbal Assembly Considering the Thermal Effects During Writing to Record the Data", ", *IEEE trans. Magn.* , Vol. 47, No. 7, July 2011.
- [45] W. **Kim**, W. S. Kim and J. Chang, "Optimal disk clamp design to minimize stress variation of disks in a hard disk drive," *J. Mech Sci. Technol.*, vol. 23 no 10. pp. 2645 – 2651 , 2009.
- [46] K-H. **Koh** and J.H. Griffin, "Dynamic Behavior of Spherical Friction Dampers and Its Implication to Damper Contact Stiffness," *ASME Journal of Engineering Gas Turbines and Power*, Vol. 129, Issue 2, pp. 511-521, 2007.
- [47] B. B. **LIM**, J . P. YANG, S . X. CHEN, J . Q. MOU , Y. LU , (2002),"Shock Analysis of MEMS Actuator Integrated with HGA for Operational and Non-operational HDD" *Asia-pacific magnetic recording conference (APMRC)*.
- [48] J. S. **McAllister**, "Characterization of disk Vibrations on aluminium and alternate substrates," *IEEE Trans. Magn.*, Vol. 33, no. 1 , pp. 968 – 973, 1997.
- [49] P.D. **McFadden**, "Detecting fatigue cracks in gear by amplitude and phase demodulation of the meshing vibration", *ASME J. of Vibration, Acoustics, Stress, and Reliability in Design* 108, 165-170. 1986.
- [50] **Mignolet**, M.P.; Rivas-Guerra, A.J. and Delor, J.P.: *Identification of Mistuning Characteristics of Bladed Disks From Free Response Data—Part I*. *Journal of Engineering for Gas Turbines and Power*, 123(2):395–403, 2001.
- [51] R.N. **Mubarak**, J.Y. Chang, "Identification of Replica Modes in Integrally Bladed Rotors," *Applied Mechanics and Materials* Vols. 110-116 (2012) pp 2348-2353

Trans Tech Publications, Switzerland doi: 10.4028 / www.scientific.net/ AMM.110-116.2348 (2011).

- [52] R.N. **Mubarak**, J.Y. Chang, “Modal Bifurcation in Integrally Bladed Rotors,” Proceedings of the 2011 *ASME* International Mechanical Engineering Congress and Exposition (IMECE’11), IMECE2011-62461, Denver, CO, *USA*, November 11-17, 2011.
- [53] R.N. **Mubarak** and J.Y. Chang, 2012, “Non-Operational Shock Analysis and Design of Head Gimbal Assembly in Spinning Data Storage Devices”, *Microsystem Technologies* vol. 18, pp. 1463–1468 DOI 10.1007/s00542-012-1572-3.
- [54] R.N. **Mubarak** and J.Y. Chang, 2011, “Identification of Replica Modes in Integrally Bladed Rotors,” *Applied Mechanics and Materials* Vols. 110-116 (2012) pp 2348-2353 Trans Tech Publications, Switzerland.  
doi:10.4028/www.scientific.net/AMM.110-116.2348 (2011).
- [55] R.N. **Mubarak** and J.Y. Chang, 2011, “Modal Bifurcation in Integrally Bladed Rotors,” Proceedings of the 2011 *ASME* International Mechanical Engineering Congress and Exposition (IMECE’11), IMECE2011-62461, Denver, CO, *USA*, November 11-17, 2011.
- [56] R.N. **Mubarak** and J.Y. Chang, 2011, “Identification of Replica Modes in Integrally Bladed Rotors,” Proceedings of 2011 2nd International Conference on Mechanical and Aerospace Engineering, Bangkok, *Thailand*, July 29-31, 2011.
- [57] R.N. **Mubarak** and J.Y. Chang, 2011, “Parametric Study on Effect of Non-operational Shock on Head Gimbal Assembly in Hard Disk Drives,” Proceedings of the 21th *ASME* International Conference on Information Storage and Processing Systems (ISPS’11), SH05, pp. 67-69, Santa Clara, CA, *USA*, June 13-14, 2011.
- [58] R.N. **Mubarak** and J.Y. Chang, 2010, “Free Vibration Study of Integrated Bladed Rotor (IBR) Through Finite-Element Simulations,” BB08-010, Proceeding of the 27th Chinese Society of Mechanical Engineers Annual Conference, Vol. B, p.586-591, Taipei, *Taiwan*, December 10-11, 2010.
- [59] R.N. **Mubarak**, A. Afridi, and J.Y. Chang, 2010, “A Thermal Analysis of Disk-Spindle Assembly on RRO in Computer Hard Disk Drives,” Proceedings of the

- Asia-Pacific Magnetic Recording Conference 2010 (APMRC'10), Invited Paper, BB-1, *IEEE* ISBN: 978-981-08-6059-1, *Singapore*, November 10-12, 2010.
- [60] B.J. **Olson**, S. W. Shaw, "Vibration absorbers for a rotating flexible structure with cyclic symmetry: nonlinear path design, *Nonlinear Dynamic* vol. 60: 149-182. 2010.
- [61] R. G. **Parker**, P. J. Sathe, , "EXACT SOLUTIONS FOR THE FREE AND FORCED VIBRATION OF A ROTATING DISK^SPINDLE SYSTEM", *Journal of Sound and Vibration* 223(3), 445±465, 1999.
- [62] S.N. **Patwardhan** and S. C. Smith, " Correcting a Track Pitch Error With a Subsequent Servo-Write Pass," U.S. Patent US7667920, 2010.
- [63] **Rai**, R., Bogy D. B., (2010), "Parametric study of operational shock in mobile disk drives with disk-ramp contact," *Asia-Pacific Magnetic Recording Conference (APMRC)*, *Singapore*.
- [64] R.B **Randall**, "A new method of modelling gear faults" *Journal of Mechanical Design* 104, 259-267. 1982.
- [65] **Rao**, "Mechanical Vibrations", 4thEdition. 2004.
- [66] **Ren**, Wei-Xin. "Experimental and Analytical Modal Analysis of Steel Arch Bridge. *Journal of structural Engineering ASCE*, 2004.
- [67] A. H. **Sacks**, M. Bodson, and M. Messner, "Advanced methods for repeatable runout compensation [disk drives]," *IEEE Trans. Magn.*, Vol. 31, pp. 1031 – 1036 , Mar. 1995.
- [68] T. **Semba**, F. Y. Huang, and M. T. White, "Integrated servo/mechanical design of HDD actuators and bandwidth estimation," *IEEE Trans. Magn.* , vol. 39, pp. 2588 – 2590, Sep. 2003.
- [69] I.Y. **Shen**, "Vibrations of Rotationally Periodic Structures", *Journal of Sound and Vibrations*, Vol. 172, pp.459-470, 1994.
- [70] I.Y. **Shen**, C. P. R. Ku, " A nonclassical vibration analysis of a multiple rotating disk and assembly" *Journal of Applied Mechanics*, Vol. 46, pp. 165-174.1997.
- [71] L. **Shrinkle**, D. Hu, P. Crill, and M. Yee, " Magnetic Head Tester Using Magnetic Disk With Pre-Written Servo," U. S. Patent US7580218 , 2009.

- [72] D. **Shu**, F.F. Yap, B. Gu, B. Shi, D. W. Djamri, (2011), “Effect of Disk Clamping Conditions on the Operational Shock Response of Hard disk Drives”, *IEEE trans. Magn.* , Vol. 47, No. 7 pp.3738-3743.
- [73] **Sinha**, A. and Chen, S.: *A Higher Order Technique to Compute the Statistics of Forced Response of a Mistuned Bladed Disk Assembly*. Journal of Sound and Vibration, 130(2):207 – 221, 1989, ISSN 0022-460X.
- [74] J. **Slavič**, M.D. Bryant and M. Boltežar , "A new approach to roughness-induced vibrations on a slider.", Journal of Sound and Vibration, Volume 306, Issues 3-5, 9 October 2007, Pages 732-750. 2007.
- [75] M. **Tatewaki**, N. Tsuda , T. Maruyama, “An Analysis of Disk Flutter in Hard Disk Drives in Aerodynamic Simulations”, IEEE Transactions on magnetic, vol. 37, no.2,2001.
- [76] J.G. **Tseng**, J. A. Wickert, Split Vibration Modes in Acoustically-Coupled Disk Stacks”, Transaction of ASME, Vol. 120, January 1998.
- [77] J.G. **Tseng**, J. A. Wickert,” On the vibration of bolted Plate and Flange Assemblies” Transaction of ASME, Vol. 116, Page 468-473,1994.
- [78] L.F. **Wagner**, J.H. Griffin,” A continuous analog model for grouped-blade vibration”, Journal of sound and vibration. Vol. 165: pp.421-438. 1993.
- [79] **Wagner**, J.T.: *Coupling of Turbomachine Blade Vibrations Through the Rotor*. ASME Journal of Engineering for Power, 89:502–512, 1967.
- [80] D. **Wang**, C. Zhou, J. Rong, “Free and Forced Vibrations of Repetitive Structures,” International Journal of Solids and Structures, Vol.40, 5477-5494, 2003.
- [81] S. **Wang** and A. M. Taratorin, Magnetic Information Storage Technology, London, UK.: Academic, 1999.
- [82] **Wei**, S.T. and Pierre, C.: *Localization Phenomena in Mistuned Assemblies with Cyclic Symmetry Part I: Free Vibrations*. Journal of Vibration Acoustics Stress and Reliability in Design, 110(4):429–438, 1988.
- [83] “Disc Brakes”, **Wikipedia**, the Free encyclopaedia, accessed from: [http://en.wikipedia.org/wiki/Disc\\_brake](http://en.wikipedia.org/wiki/Disc_brake), Access date: 1<sup>st</sup> Feb, 2011.

- [84] T. L. **Wu**, I. Y. Shen, F. Okamoto, and T. Asada, “ Vibration of 1.8 in Hard disk drive spindle motors at various ambient temperatures,” *IEEE Trans. Magn.*, vol. 43, no. 9, pp. 3716 – 3720, 2007.
- [85] Y.J. **Yan**, P.L. Cui, h. N. Hao, ”Vibration mechanism of a mistuned bladed-disk”, *Journal of Sound and Vibration*, Vol.317, pages 294-307. 2008.
- [86] **Yap** F.F., Harmoko H., Liu M., and Vahdati N., (2007), “Modeling of hard disk drives for shock and vibration analysis - consideration of nonlinearities and discontinuities,” *Nonlinear Dynamics*, Vol. 50, pp.717-731.
- [87] **Zheng**, H., Murthy A.N., (2010) “Effect of suspension design on the non-operational shock response in a load/unload hard disk drive,” *Microsystem Technology*, Vol. 16, pp.267-271.
- [88] **Li**, L., Zheng, H., Fanslau E.B., and Talke F.E., (2011), ”A numerical study of the dimple/gimbal interface in a hard disk drive,” *Microsystem Technology*, published online first.



## **APPENDICES**

- I) Matlab code for Fourier Analysis on IBR
- II) Matlab Code for suppressing 60Hz DC hum
- III) Matlab code for Fourier analysis on Disk Spindle Assembly

## APPENDIX A

### MATLAB CODE FOR FOURIER ANALYSIS ON IBR

```
clear all
close all

function DFT=ProfileDFT(data,H,flag)
SID=length(data);
x=0:(SID-1);

stopH=H;

if flag == 0
    startH=0;Fourierdata=zeros(H+1,4);
else
    startH=stopH;Fourierdata=zeros(1,4);
end

for k=startH:stopH
    f1i=data.*cos(k*2*pi.*(x')/SID);
    f2i=data.*sin(k*2*pi.*(x')/SID);

    if flag == 0
        if k == 0
            ai(k+1,1)=sum(f1i)/SID;
        else
            ai(k+1,1)=sum(f1i)/SID*2;
        end
        bi(k+1,1)=sum(f2i)/SID*2;
        ci(k+1,1)=sqrt(ai(k+1)^2+bi(k+1)^2);
    else
        if k == 0
            ai(1,1)=sum(f1i)/SID;
        else
            ai(1,1)=sum(f1i)/SID*2;
            bi(1,1)=sum(f2i)/SID*2;
            ci(1,1)=sqrt(ai(1)^2+bi(1)^2);
        end
    end
end
```

```

        ai(1,1)=sum(f1i)/SID*2;
    end
    bi(1,1)=sum(f2i)/SID*2;
    ci(1,1)=sqrt(ai(1)^2+bi(1)^2);
end
end
Fourierdata(:,1)=(startH:stopH)';
Fourierdata(:,2)=ai;
Fourierdata(:,3)=bi;
Fourierdata(:,4)=ci;

DFT=Fourierdata;

T=80;
A=0;
H=10;
X=load(['Disk_OD_x' num2str(T) '_' num2str(A) 'd.txt']);
Y=load(['Disk_OD_y' num2str(T) '_' num2str(A) 'd.txt']);

R=sqrt(X(:,2).^2+Y(:,2).^2);

temp=size(R);

for i=0:temp-1
    q(i+1,1)=i*2*pi/temp(1,1);
end

figure
subplot(211)
plot(q*360/2/pi,R)
XLIM([0 360])
ylim([0.0166 0.0178])
xlabel('\theta, degree')
ylabel('Radial displacement, mm')

subplot(212)
test=ProfileDFT(R,H,0);

```

```
bar(test(:,1),test(:,2:4));  
axis normal  
xlabel('Harmonics, h')  
ylabel('Amplitude')  
Legend('Cosine - A_h', 'Sine - B_h', 'Magnitude - C_h')
```

## APPENDIX B

### MATLAB CODE FOR SUPPRESSING 60HZ DC HUM

```
x= load(['1F2S num2str(T) '_' num2str(A) '1.txt']);
x=[];
y=y.';
z=y;
u=x;
%plot(y,x)

% FS = 8192;
%FS=3000;
%F0 = 60;

%FIR Notch filter

FG = 570;
FGAINdB = 5;
FGAIN = 10^(FGAINdB/20);
w0 = 2*pi*F0/FS;
wg = 2*pi*FG/FS;
GH = abs(1 - 2*cos(w0)*exp(-1i*wg) + exp(-1i*2*wg));
G = FGAIN/GH;
h = [1 -2*cos(w0) 1];
%figure
freqz(G*h,1,[], FS);

titlestr = ['FIR Notch Filter for ' num2str(F0) 'Hz'];
title(titlestr)

out=filter(G*h,1,x);
plot(y,out,'r',z,u,'b')
legend('filtered graph','original graph')
subplot(2,1,2)
plot(y,out)
plot(z,u)
```

```

%IIR

r=0.79;
bg = abs(1 - 2*cos(w0)*exp(-1i*wg) + exp(-1i*2*wg));
ag = abs(1 - 2*cos(w0)*exp(-1i*wg) + (r^2)*exp(-1i*2*wg));
GH = bg/ag;
G = FGAIN/GH;

b = [1 -2*cos(w0) 1];
a = [1 -2*cos(w0) (r^2)];

%figure
freqz(G*b,a,1024, FS);
titlestr = ['IIR Notch Filter for ' num2str(F0) 'Hz and r = ' num2str(r)];
title(titlestr)
output2=filter(G*b,a,x);
plot(y,output2)

%%%%%%%%%%%%%%%%%%%%%%%%%%%%%%%%%%%%%%%%%%%%%%%%%%%%%%%%%%%%%%%%%%%%%%%% Notch Filter
Fs = 1200;          % sampling freq [Hz]
Fn = Fs/2;          % Nyquist  freq [Hz]
W0 = 60;            % notch frequency [Hz]
w0 = W0*pi/Fn;      % notch frequency normalized
BandWidth = 100;    % -3dB BandWidth [Hz]
B = BandWidth*pi/Fn; % normalized bandwidth
k1 = -cos(w0); k2 = (1 - tan(B/2))/(1 + tan(B/2));
b = [1+k2 2*k1*(1+k2) 1+k2];
a = [2 2*k1*(1+k2) 2*k2];

%figure(1);
%freqz(b,a);
%title('sampling frequency 200Hz, notch @ 20HzHz, notch bandwidth 5Hz');
% z : your signal
zfiltered=filter(b,a,x);
plot(z,u,y,zfiltered)
legend('nonfiltered', 'filtered')

```

## APPENDIX C

### MATLAB CODING FOR DISK SPINDLE ASSEMBLY THERMAL STUDY FOURIER ANALYSIS

```
clear all
close all
T=[25 40 60 80];
A=[00 15 30 45];
H=15;

for t=1:length(T)
    for a=1:length(A)
        %
        % Load FEM data: Hub_B cases
        %
        x_temp = load(['Hub_B_x' num2str(T(t)) '_' num2str(A(a)) 'd.txt']);
        y_temp = load(['Hub_B_y' num2str(T(t)) '_' num2str(A(a)) 'd.txt']);
        Hub_B(:,t,a)=sqrt(x_temp(:,2).^2+y_temp(:,2).^2);
        temp=ProfileDFT(Hub_B(:,t,a),H,0);
        Hub_B_Ai(:,t,a)=temp(:,2);
        Hub_B_Bi(:,t,a)=temp(:,3);
        Hub_B_Ci(:,t,a)=temp(:,4);
        clear x_temp y_temp temp;
        %
        % Load FEM data: Hub_T cases
        %
        x_temp = load(['Hub_T_x' num2str(T(t)) '_' num2str(A(a)) 'd.txt']);
        y_temp = load(['Hub_T_y' num2str(T(t)) '_' num2str(A(a)) 'd.txt']);
        Hub_T(:,t,a)=sqrt(x_temp(:,2).^2+y_temp(:,2).^2);
        temp=ProfileDFT(Hub_T(:,t,a),H,0);
        Hub_T_Ai(:,t,a)=temp(:,2);
        Hub_T_Bi(:,t,a)=temp(:,3);
        Hub_T_Ci(:,t,a)=temp(:,4);
        clear x_temp y_temp temp;
        %
        % Load FEM data: Disk_OD cases
        %
```



```

x_temp = load(['Disk_OD_x' num2str(T(t)) '_' num2str(A(a)) 'd.txt']);
y_temp = load(['Disk_OD_y' num2str(T(t)) '_' num2str(A(a)) 'd.txt']);
Disk_OD(:,t,a)=sqrt(x_temp(:,2).^2+y_temp(:,2).^2);
temp=ProfileDFT(Disk_OD(:,t,a),H,0);
Disk_OD_Ai(:,t,a)=temp(:,2);
Disk_OD_Bi(:,t,a)=temp(:,3);
Disk_OD_Ci(:,t,a)=temp(:,4);
clear x_temp y_temp temp;
%
% Load FEM data: Disk_ID cases
%
x_temp = load(['Disk_ID_x' num2str(T(t)) '_' num2str(A(a)) 'd.txt']);
y_temp = load(['Disk_ID_y' num2str(T(t)) '_' num2str(A(a)) 'd.txt']);
Disk_ID(:,t,a)=sqrt(x_temp(:,2).^2+y_temp(:,2).^2);
temp=ProfileDFT(Disk_ID(:,t,a),H,0);
Disk_ID_Ai(:,t,a)=temp(:,2);
Disk_ID_Bi(:,t,a)=temp(:,3);
Disk_ID_Ci(:,t,a)=temp(:,4);
clear x_temp y_temp temp;
end
end
% % for h=0:H
% range=[1:H];
% range_ticklabel=range-1;

% for h=1:H
range=[2:H];
range_ticklabel=range-1;

figure(1)
for i=1:length(A)
    subplot(2,2,i)
    bar3(Hub_T_Ci(range,:,i)); %view(20,32);
    set(gca,'XTickLabel',range_ticklabel)
    xlabel('Harmonics')
    set(gca,'YTickLabel',T); ylabel('Temperature, ^o C')
    title(['Slot Angle= ' num2str(A(i)) '^o'])
end

```

```

subplot(221); H=text(5,20, 'Top Hub Radial Displacement');
set(H,'FontSize', 20);

figure(2)
for i=1:length(A)
    subplot(2,2,i)
    bar3(Hub_B_Ci(range,:,i)); % view(20,32);
    set(gca,'XTickLabel',range_ticklabel)
    xlabel('Harmonics')
    set(gca,'YTickLabel',T); ylabel('Temperature, ^o C')
    title(['Slot Angle= ' num2str(A(i)) ' ^o'])
end
subplot(221); H=text(5,20, 'Bottom Hub Radial Displacement');
set(H,'FontSize', 20);

figure(3)
for i=1:length(A)
    subplot(2,2,i)
    bar3(Disk_ID_Ci(range,:,i)); % view(20,32);
    set(gca,'XTickLabel',range_ticklabel)
    xlabel('Harmonics')
    set(gca,'YTickLabel',T); ylabel('Temperature, ^o C')
    title(['Slot Angle= ' num2str(A(i)) ' ^o'])
end
subplot(221); H=text(5,20, 'Disk ID Radial Displacement');
set(H,'FontSize', 20);

figure(4)
for i=1:length(A)
    subplot(2,2,i)
    bar3(Disk_OD_Ci(range,:,i)); % view(20,32);
    set(gca,'XTickLabel',range_ticklabel)
    xlabel('Harmonics')
    set(gca,'YTickLabel',T); ylabel('Temperature, ^o C')
    title(['Slot Angle= ' num2str(A(i)) ' ^o'])
end
subplot(221); H=text(5,20, 'Disk OD Radial Displacement');
set(H,'FontSize', 20);

```

**%%Hub Top**

clear all

close all

T=80;

A=30;

H=15;

X=load(['Hub\_T\_x' num2str(T) '\_' num2str(A) 'd.txt']);

Y=load(['Hub\_T\_y' num2str(T) '\_' num2str(A) 'd.txt']);

R=sqrt(X(:,2).^2+Y(:,2).^2);

temp=size(R);

for i=0:temp-1

    q(i+1,1)=i\*2\*pi/temp(1,1);

end

figure

subplot(211)

plot(q\*360/2/pi,R)

XLIM([0 360])

xlabel('\theta, degree')

ylabel('Radial displacement, mm')

subplot(212)

test=ProfileDFT(R,H,0);

bar(test(:,1),test(:,2:4));

axis normal

xlabel('Harmonics, h')

ylabel('Amplitude')

Legend('Cosine - A\_h', 'Since - B\_h', 'Magnitude - C\_h')

**%%Hub Base**

```

clear all
close all

T=60;
A=30;
H=15;
X=load(['Hub_B_x' num2str(T) '_' num2str(A) 'd.txt']);
Y=load(['Hub_B_y' num2str(T) '_' num2str(A) 'd.txt']);

R=sqrt(X(:,2).^2+Y(:,2).^2);

temp=size(R);

for i=0:temp-1
    q(i+1,1)=i*2*pi/temp(1,1);
end

figure
subplot(211)
plot(q*360/2/pi,R)
XLIM([0 360])
xlabel('\theta, degree')
ylabel('Radial displacement, mm')

subplot(212)
test=ProfileDFT(R,H,0);
bar(test(:,1),test(:,2:4));
axis normal
xlabel('Harmonics, h')
ylabel('Amplitude')
Legend('Cosine - A_h', 'Sine - B_h', 'Magnitude - C_h')

%%Disk ID

clear all
close all

```

```

T=80;
A=0;
H=10;
X=load(['Disk_ID_x' num2str(T) '_' num2str(A) 'd.txt']);
Y=load(['Disk_ID_y' num2str(T) '_' num2str(A) 'd.txt']);

R=sqrt(X(:,2).^2+Y(:,2).^2);

temp=size(R);

for i=0:temp-1
    q(i+1,1)=i*2*pi/temp(1,1);
end

figure
subplot(211)
plot(q*360/2/pi,R)
XLIM([0 360])
xlabel('\theta, degree')
ylabel('Radial displacement, mm')

subplot(212)
test=ProfileDFT(R,H,0);
bar(test(:,1),test(:,2:4));
axis normal
xlabel('Harmonics, h')
ylabel('Amplitude')
Legend('Cosine - A_h', 'Since - B_h', 'Magnitude - C_h')

%% DISK OD

clear all
close all

T=80;
A=0;
H=10;
X=load(['Disk_OD_x' num2str(T) '_' num2str(A) 'd.txt']);

```

```

Y=load(['Disk_OD_y' num2str(T) '_' num2str(A) 'd.txt']);

R=sqrt(X(:,2).^2+Y(:,2).^2);

temp=size(R);

for i=0:temp-1
    q(i+1,1)=i*2*pi/temp(1,1);
end

figure
subplot(211)
plot(q*360/2/pi,R)
XLM([0 360])
ylim([0.0166 0.0178])
xlabel('\theta, degree')
ylabel('Radial displacement, mm')

subplot(212)
test=ProfileDFT(R,H,0);
bar(test(:,1),test(:,2:4));
axis normal
xlabel('Harmonics, h')
ylabel('Amplitude')
Legend('Cosine - A_h', 'Sine - B_h', 'Magnitude - C_h')

```

## LIST OF PUBLICATIONS

### Journal Papers

- I) **R.N. Mubarak** and J.Y. Chang, 2012, “Non-Operational Shock Analysis and Design of Head Gimbal Assembly in Spinning Data Storage Devices”, *Microsystem Technologies* vol. 18, pp. 1463–1468 DOI 10.1007/s00542-012-1572-3
- II) **R.N. Mubarak** and J.Y. Chang, 2011, “Identification of Replica Modes in Integrally Bladed Rotors,” *Applied Mechanics and Materials* Vols. 110-116 (2012) pp 2348-2353 Trans Tech Publications, Switzerland doi:10.4028/www.scientific.net/AMM.110-116.2348 (2011)

### Conference Papers

- III) **R.N. Mubarak** and J.Y. Chang, 2011, “Modal Bifurcation in Integrally Bladed Rotors,” *Proceedings of the 2011 ASME International Mechanical Engineering Congress and Exposition (IMECE’11)*, IMECE2011-62461, Denver, CO, **USA**, November 11-17, 2011.
- IV) **R.N. Mubarak** and J.Y. Chang, 2011, “Identification of Replica Modes in Integrally Bladed Rotors,” *Proceedings of 2011 2nd International Conference on Mechanical and Aerospace Engineering*, Bangkok, **Thailand**, July 29-31, 2011.
- V) **R.N. Mubarak** and J.Y. Chang, 2011, “Parametric Study on Effect of Non-operational Shock on Head Gimbal Assembly in Hard Disk Drives,” *Proceedings of the 21th ASME International Conference on Information Storage and Processing Systems (ISPS’11)*, SH05, pp. 67-69, Santa Clara, CA, **USA**, June 13-14, 2011.
- VI) **R.N. Mubarak** and J.Y. Chang, 2010, “Free Vibration Study of Integrated Bladed Rotor (IBR) Through Finite-Element Simulations,” BB08-010, *Proceeding of the 27th Chinese Society of Mechanical Engineers Annual Conference*, Vol. B, p.586-591, Taipei, **Taiwan**, December 10-11, 2010.



- VII) **R.N. Mubarak**, A. Afridi, and J.Y. Chang, 2010, “A Thermal Analysis of Disk-Spindle Assembly on RRO in Computer Hard Disk Drives,” Proceedings of the Asia-Pacific Magnetic Recording Conference 2010 (APMRC’10), Invited Paper, BB-1, *IEEE* ISBN: 978-981-08-6059-1, *Singapore*, November 10-12, 2010.